Crack propagation in rubber-like materials

2005 J. Phys.: Condens. Matter 17 R1071

(http://iopscience.iop.org/0953-8984/17/44/R01)

INSTITUTE OF PHYSICS PUBLISHING JOURNAL OF PHYSICS: CONDENSED MATTER

J. Phys.: Condens. Matter **17** (2005) R1071–R1142 doi:10.1088/0953-8984/17/44/R01

TOPICAL REVIEW

Crack propagation in rubber-like materials

B N J Persson[1,2], O Albohr[3], G Heinrich[4] and H Ueba[2]

[1] IFF, FZ-Jülich, 52425 Jülich, Germany
[2] Departments of Electronics, Toyama University, Gofuku, Toyama 930-8555, Japan
[3] Pirelli Deutschland AG, 64733 Höchts/Odenwald, Postfach 1120, Germany
[4] Leibniz Institut für Polymerforschung, Hohe Strasse 6, D-01069, Dresden, Germany

Received 25 April 2005, in final form 9 September 2005
Published 17 October 2005
Online at stacks.iop.org/JPhysCM/17/R1071

Abstract

Crack propagation in rubber-like materials is of great practical importance but still not well understood. We study the contribution to the crack propagation energy (per unit area) G from the viscoelastic deformations of the rubber in front of the propagating crack tip. We show that G takes the standard form $G(v, T) = G_0[1 + f(v, T)]$ where G_0 is associated with the (complex) bond-breaking processes at the crack tip while $f(v, T)$ is determined by the viscoelastic energy dissipation in front of the crack tip. As applications, we discuss the role of crack propagation for adhesion, rolling resistance and sliding friction for smooth surfaces, and for rubber wear.

(Some figures in this article are in colour only in the electronic version)

Contents

1. Introduction

The propagation of cracks in rubber is fundamental for many important applications, e.g., rubber wear [1] and pressure sensitive adhesives [2]. The failure of rubber products by crack propagation often results in catastrophic events involving large loss of life and capital, e.g., when a tyre explodes (see figure 1), or when a rubber O-ring seal fails (see figure 2). In other applications the failure by crack propagation may be less devastating but still a nuisance, e.g., the ageing of wiper blades (see figure 3) or the failure of rubber adhesives by interfacial crack propagation (see figure 4).

The strength of adhesion and cohesion of elastomer can be characterized by the amount of energy G required to advance a fracture plane by one unit area. Note that G includes not only the energy necessary to break the bonds at the crack tip, but all the energy 'dissipated' in the vicinity of the crack tip during crack propagation. For rubber-like materials this also includes the viscoelastic energy dissipation which may occur several micrometres away from the crack tip. If U is the potential energy supplied by the internal strain energy and external forces, $G = -\mathrm{d}U/\mathrm{d}A$, where A is the (nominal) crack surface area. Experiments [3–6] and theory [7–11, 13–18] have shown that G depend on the crack-tip velocity v and on the temperature T, and that

$$G(v, T) = G_0 [1 + f(v, T)] \tag{1}$$

where $f \to 0$ as $v \to 0$. Thus, G_0 is a threshold value below which no fracture occurs. The measured value of G (for non-crystallizing rubbers; see section 3.8) at extremely low crack velocities and high temperatures, when viscous effects in the rubber are minimized, is of the order of $\sim$50 J m^{-2} (or $\sim$3 eV Å^{-2}) and can be identified as G_0. At high crack velocities G may be up to 10^4 times higher. For simple hydrocarbon elastomer, and if the crack-tip velocity is so low that the temperature increase at the crack tip can be neglected, the effect of temperature can be completely accounted for by applying a simple multiplying factor, denoted by a_T, to the crack velocity v, i.e., $f(v, T) = f(a_T v)$. Moreover, values of a_T determined experimentally are equal to the Williams–Landel–Ferry [19] function determined from the

Figure 1. Catastrophic crack propagation in rubber, resulting in an exploded tyre.

Figure 2. A crack in an over-compressed rubber O-ring.

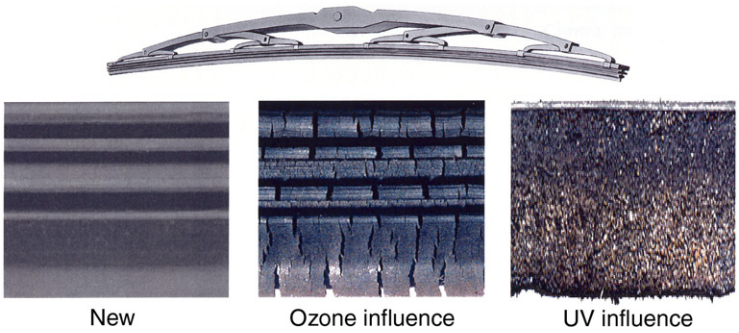

Figure 3. Ageing of a wiper blade (left) by ozone (middle) and ultraviolet radiation (right).

temperature dependence of the bulk viscoelastic modulus. This proves that the large effects of crack velocity and temperature on crack propagation in rubber materials are due to viscoelastic processes in the bulk.

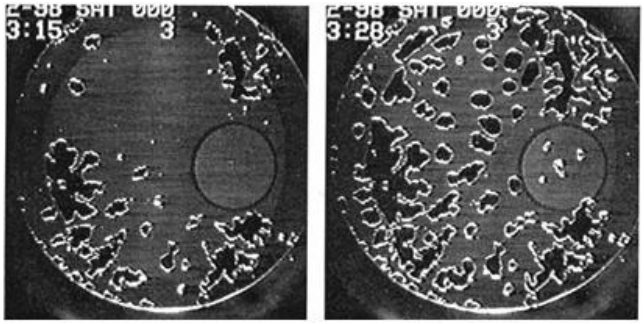

Figure 4. Bonding of a flat glass surface to a flat substrate by a thin film ($\sim$100 μm) of a rubber tack compound. The two snap-shot pictures show the formation and propagation of interfacial cracks at the rubber–substrate interface during (vertical) separation of the surfaces. Adapted from [61].

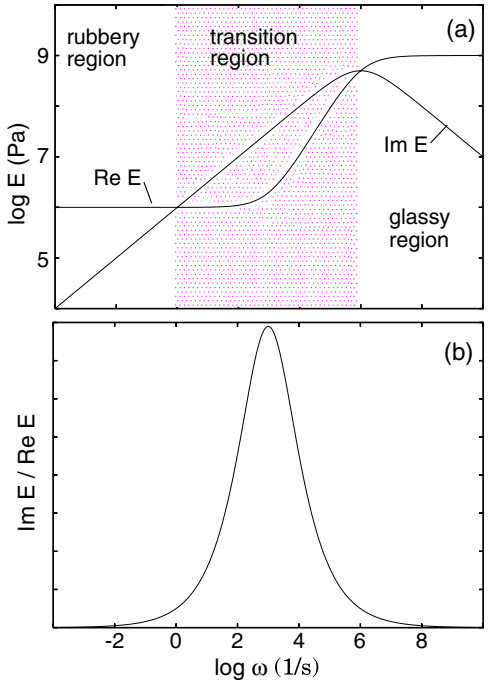

Figure 5. (a) The viscoelastic modulus $E(\omega) = E_1 + \mathrm{i}E_2$ of a typical rubber-like material, and (b) the loss tangent E_2/E_1. The latter quantity is maximal at some frequency ω_2 (schematic).

In order to understand the physical origin of expression (1) it is necessary to know the general structure of the viscoelastic modulus $E(\omega)$ of rubber-like materials. In figure 5 we show the real $E_1 = \mathrm{Re}\ E$ and the imaginary part $E_2 = \mathrm{Im}\ E$ of $E(\omega)$ and also the loss tangent E_2/E_1. At 'low' frequencies the material is in the 'rubbery' region where $\mathrm{Re}\ E(\omega)$ is relatively small and approximately constant. At very high frequencies the material is elastically very stiff (brittle-like). In this 'glassy' region $\mathrm{Re}\ E$ is again nearly constant but much larger (typically by three to four orders of magnitude) than in the rubbery region. In the intermediate frequency range (the 'transition' region) the loss tangent is very large and it is mainly this region which

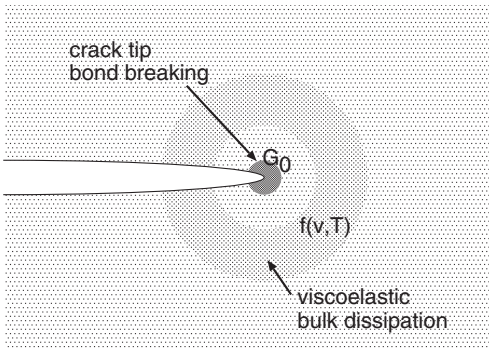

Figure 6. The crack propagation energy G is a product of a term G_0 derived from the bond breaking at the crack tip, and a term $f(v, T)$ derived from the bulk viscoelastic energy dissipation in front of the tip.

determines, e.g., the friction when a tyre is sliding on a road surface [20]. In what follows we will refer to the peak in the loss tangent curve (see figure 5(b)) as the viscoelastic loss peak.

The physical origin of the dynamical modulus $E(\omega)$ for rubber-like materials is related to stress-aided, thermally activated flipping of polymer segments between different configurations. If τ denotes the typical flipping time, then for $\omega \gg 1/\tau$ there is no time for thermally activated rearrangement of the polymer chain segments to occur, and the rubber response will be that of a hard glassy material. However, when $\omega \ll 1/\tau$, thermally activated rearrangements of the rubber polymer chains will occur adiabatically, resulting in a soft rubbery response. In fact, $E(\omega, T)$ will be a function of the form $E = E(\omega\tau)$, where τ depends on temperature according to a thermally activated process. Usually, one writes $\tau = \tau_0 a_T$, where τ_0 is temperature independent, and where a_T is (approximately) given by the WLF function proposed by Williams *et al* [19]:

$$\log a_T = \frac{C_1(T - T_g)}{C_2 + T - T_g}$$

where C_1 and C_2 are two constants and where T_g is the glass transition temperature of the rubber.

The energy dissipation at a crack in a viscoelastic solid has two contributions; see figure 6. The first is associated with the innermost region at the crack tip (the so-called crack tip process zone; the dark area at the crack tip in figure 6), and involves highly non-linear processes (e.g., cavity formation, stringing, chain pull-out (for polymers), and bond breaking) and is described phenomenologically via the term $G_0 = 2\gamma_0$. (Note: for rubber-like materials γ_0 is much larger than the surface energy γ.) This contribution to $G(v)$ cannot be accurately calculated theoretically, and is taken as an input (determined experimentally) in the theory. The second contribution (described by the factor $f(v, T)$) comes from the viscoelastic dissipation in the polymer in the linear viscoelastic region in front of the tip. If the *loss function* $\mathrm{Im}[1/E(\omega)]$ is maximal at some characteristic frequency ω_1, then this dissipative region will be centred a distance $r \sim v/\omega_1$ from the crack tip. For a fast moving crack this may be very far away from the crack tip. This contribution is calculated by the theory [7–11, 13, 14], and it has recently been shown [13, 14] that the exact form of the crack-tip process zone is not important for the calculation of the viscoelastic contribution to G.

In this article we discuss the nature of G for viscoelastic solids. We first briefly review the standard theory of cracks in elastic and viscoelastic solids. Most of the results presented below are based on the energy-balance approach to crack propagation. In this approach one

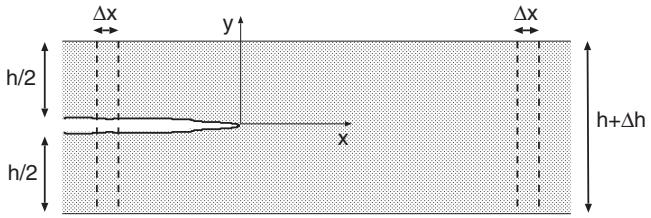

Figure 7. A crack in an infinitely wide (in the x-direction) elastic plate. The plate has the thickness h. The surfaces $y = \pm h/2$ are clamped and separated by the distance Δh.

first calculates the viscoelastic energy dissipation in the vicinity of a crack tip, and then uses it to derive a general expression for $G(v) = 2\gamma_{\rm eff}(v)$. This approach is much simpler than the treatment presented in most earlier studies, and results in a simple analytical formula for $G(v)$. Furthermore, the theory can be easily generalized to include other effects such as the influence of the tip flash temperature on the crack propagation.

The crack-propagation theory is applied to several important problems, namely adhesion, rolling resistance and sliding friction for smooth surfaces, and to rubber wear. Adhesion and rubber friction for smooth surfaces are important, e.g., for wiper blades and seals, and for pressure sensitive adhesives. Rubber wear is of great practical importance, e.g., tyre wear. When a rubber block is slipping on a hard substrate with surface roughness, rubber abrasion is usually due to fatigue, involving slowly propagating cracks.

2. Crack propagation in elastic solids

We present a brief discussion about cracks in elastic solids. Some information about this topic is necessary in order to understand the more complex topic of cracks in viscoelastic solids. We consider first the particular simple case of a crack in an infinite elastic slab, and then summarize the most important results from the general theory of cracks in elastic solids.

Crack in elastic slab

Consider an elastic slab with thickness h as in figure 7. Assume that a crack occurs in the middle of the slab as illustrated in figure 7. Assume now that the solid walls at $y = \pm h/2$ are clamped in the vertical direction, but free to slip in the parallel direction, and separated by the distance Δh. This corresponds to a plane stress situation, but similar results are obtained for plane strain. For an ideal elastic solid the crack is stable (i.e., it will not increase or decrease in size with increasing time) when the displacement Δh is so large that the elastic energy stored in a vertical slice (width Δx) of the elastic solid well in front of the crack tip is equal to the surface energy stored in a similar slice well to the left of the crack tip. The latter energy per unit length of the crack line equals

$$U_{\rm surf} = 2\gamma\Delta x,$$

where γ is the surface energy, and where the factor of two comes from the two crack surfaces. If σ is the tensile stress far away from the tip in front of the tip, then we have $\sigma = E\epsilon$, where $\epsilon = \Delta h/h$ and E is the Young's modulus. Thus, the elastic energy per unit length of the crack

$$U_{\rm el} = \frac{1}{2}h\Delta x\sigma\epsilon = \frac{1}{2E}h\Delta x\sigma^2.$$

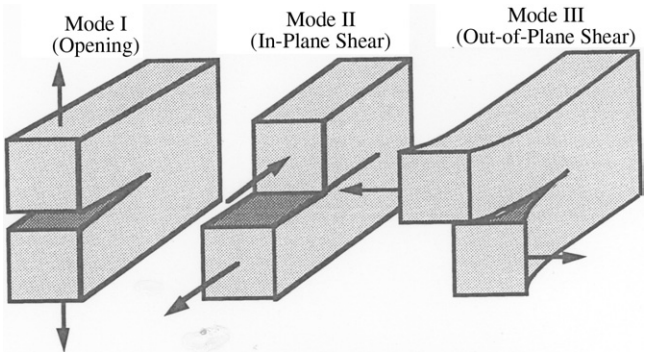

Figure 8. The three 'normal modes' of loading that can be applied to a crack.

Putting $U_{\text{surf}} = U_{\text{el}}$ gives $\sigma = \sigma_0$ where

$$\sigma_0 = \left(\frac{4E\gamma}{h}\right)^{1/2} \tag{2}$$

which is the famous Griffith criterion [21] for the stability of a crack. In this case the energy per unit area necessary to propagate the crack (very slowly) is $G = 2\gamma$. If $\sigma = \sigma_0$ the crack is stable and stationary, while for $\sigma > \sigma_0$ it will propagate as an *opening* crack. If $\sigma < \sigma_0$ it will propagate as a *closing* crack.

Equation (2) can also be derived by considering the stress in the vicinity of the crack tip. We have (see appendix A) [22]

$$\sigma(\mathbf{x}) \approx \left(\frac{h}{|\mathbf{x}|}\right)^{1/2} \sigma_0 \tag{3}$$

where $\mathbf{x} = (x, y)$. In a simple solid, the stress necessary to break a bond at the crack tip is of order $\sigma \approx E$. Thus, from (3) with $|\mathbf{x}| \approx a_0$ (where a_0 is an atomic distance) we get

$$\left(\frac{h}{a_0}\right)^{1/2} \sigma_0 \approx E.$$

Using the well known relation (which is valid for 'simple' solids) $a_0 \approx \gamma/E$ in this equation gives, to within a factor of order unity, the same expression as derived above, equation (2).

General results

The analytical theory of cracks, which is based on the theory of elasticity applied to a homogeneous and isotropic elastic continuum, predicts three different crack 'normal modes' schematically illustrated in figure 8. A general situation can be considered as a mixture of these three cases. The stress field close to a crack tip is of the form (see appendix A) [22, 23]

$$\sigma_{ij} = \frac{K}{(2\pi r)^{1/2}} f_{ij}(\phi) \tag{4}$$

where the angular function $f_{ij}(\phi)$ takes a universal form, which however differs for the three modes of loading. The energy per unit area to propagate a crack is denoted by $G(v)$ and is related to the *stress intensity factor* K via the equation (see appendix A) [22, 23]

$$G = K^2/E. \tag{5}$$

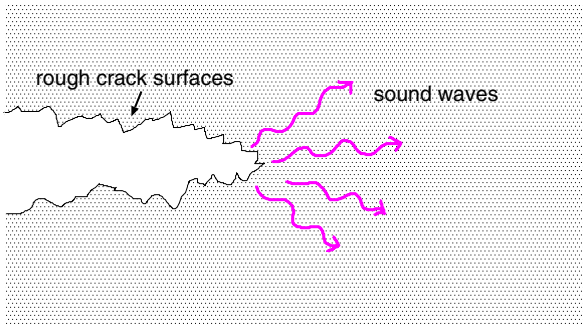

Figure 9. In an ideal brittle solid, the crack propagation energy $G(v)$ will increase with the crack-tip velocity v due to emission of sound waves and due to the creation of surface roughness.

This equation is valid for plane stress; for plane strain E must be replaced by $E/(1-\nu^2)$, where ν is the Poisson ratio. Equation (5) can be proved by considering the work necessary to close the crack over some short distance close to the crack tip [22, 23].

For a slowly moving crack in an ideal elastic solid $G = 2\gamma$, where γ is the surface energy of the created surfaces, and where the factor of two results from the fact that two surfaces are created during crack propagation. Thus, for the elastic slab we can also write (2) as

$$\sigma_0 = \left(\frac{2EG}{h}\right)^{1/2}.$$

Combining this with (5) gives $K = \sigma_0(h/2)^{1/2}$. Substituting this result in (4) gives, as expected, equation (3) to within a factor of order unity.

The crack propagation energy $G(v)$ will in general depend on the velocity v of the crack tip. This is easy to understand from the following very general argument: for the elastic slab configuration shown in figure 7 nothing stops us from elongating the slab so that much more elastic energy is stored in front of the crack tip than is necessary to create the planar crack surfaces (which require 2γ per unit area of crack propagation). Within the elastic continuum model there are only two ways this 'extra' energy can be 'dissipated': either by emission of elastic (sound) waves from the crack-tip region, or by the creation of rough crack surfaces (see figure 9), thus increasing the surface energy stored on the created crack surfaces. In reality, for brittle-like materials both effects usually occur. In fact, crack-tip instabilities (resulting in rough crack surfaces) often occur already before the crack-tip velocity has reached half the shear sound wave speed, and this often limits the crack-tip speed to about half of the shear sound velocity [24]. Phonon emission from the crack tip will occur at all non-zero crack-tip velocities. Within the elastic continuum mechanics theory it has been shown that the intensity of the emitted sound waves diverges as the crack-tip velocity approaches the shear wave speed, thus limiting the crack-tip velocity to be below the shear sound velocity [22].

In most real materials, the crack propagation energy $G(v)$ will be much larger than the ideal surface energy 2γ even for very small crack-tip velocities. Thus many materials, in particular metals and glassy polymers, undergo large plastic deformation before the stress is so high that the atomic bonds can be broken, and close to the crack tip a large plastically deformed region will usually occur. The work of plastic deformation will strongly increase the energy G necessary to propagate a crack, and for metals and glassy polymers G may be 10^3 times (or more) larger than the surface energy 2γ. Similarly, for viscoelastic solids such as rubber, large viscoelastic energy dissipation may occur close to the crack tip, which may enhance G by a factor of 10^3 or more. In what follows we will address this contribution to $G(v)$ for

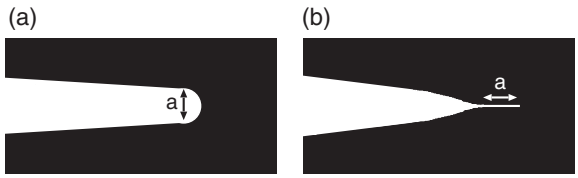

Figure 10. The singular stress region at a crack tip in continuum mechanics can be removed either by (a) tip blunting (tip diameter a), or (b) by introducing a lateral region (linear size a) over which the bond breaking occurs. The latter is the so-called Barenblatt process zone.

viscoelastic solids, and show how it depends on the crack-tip velocity, the temperature and the nature of the solids.

3. Crack propagation in viscoelastic solids

We first present a qualitative discussion about the nature of crack propagation in viscoelastic solids, and then summarize the basic equations. We consider both fast (catastrophic) crack propagation, and slow crack propagation involved in fatigue failure. For fast crack propagation, a large temperature increase may occur close to the crack tip and we discuss how this influences the crack tip propagation. We discuss the limitations of the theory, and compare the theoretical results to experimental data.

3.1. Qualitative discussion

Classical fracture mechanics, which is based on continuum mechanics, predicts a stress singularity at a crack tip, $\sigma \sim r^{-1/2}$, where r is the distance from the crack tip. However, any real material will yield when the stress becomes high enough. In an ideal brittle material such as mica, the relation $\sigma \sim r^{-1/2}$ may hold until $r \sim a$ is of the order of a lattice constant a. However, in most materials the $\sigma \sim r^{-1/2}$ relation will break down at much larger distances r. The spatial region in the vicinity of a crack tip where the relation $\sigma \sim r^{-1/2}$ is no longer valid is called the *crack-tip process zone*.

The crack propagation energy G will, in general, depend on the exact nature of the processes occurring in the crack-tip process zone. Since these bond-breaking processes may be highly complex, e.g., involving cavity formation and stringing, the crack propagation energy can in general not be calculated theoretically but must be deduced from experimental data. Only in the limiting case of ideal brittle solids (e.g., mica) will the crack propagation energy $G \approx 2\gamma$ be (nearly) equal to the energy per unit area, 2γ, to break the atomic bonds at the (atomically sharp) crack tip, which is known for many solids, e.g., it can sometimes be calculated using electronic structure methods [25].

The standard model used to describe the crack-tip process zone is due to Barenblatt [26]. He assumed that the bond breaking at the crack tip occurs by stretching the bonds orthogonal to the crack surfaces until they break at some characteristic stress level σ_c. The process zone extends a distance a in front of the crack tip as indicated by the horizontal white line in figure 10(b). This model was first applied to crack propagation in viscoelastic solids by Schapery [8] and later by Greenwood and Johnson [9], Barber *et al* [10], and Hui *et al* [11]. In [13, 14] a simpler treatment was presented, where the cut-off was introduced in a more ad hoc manner, which may be roughly interpreted as a blunting of the crack tip as in figure 10(a). It was also shown that the exact way the cut-off is introduced is unimportant, and in reality the

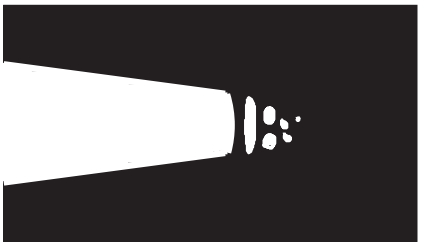

Figure 11. The crack-tip process zone in most materials is very complex, involving, e.g., cavity formation, stringing, chain pull-out (for polymers), and bond breaking.

process zone is much more complex than assumed in the theory; see figure 11. In general, the cut-off should be introduced in such a way as to simplify the analytical calculations as much as possible, and for crack propagation in viscoelastic solids we believe that the cut-off procedure used in [13, 14] results in the simplest formalism.

The paper by Barber *et al* studies crack propagation in viscoelastic solids using the Barenblatt model. This model results in a very complex set of equations, but the authors nevertheless were able to extract the high velocity behaviour of G, which agrees exactly with the limiting behaviour found in [13, 14]. This limiting behaviour was also obtained in the work by Greenwood and Johnson [9]. This shows that the exact way the short-distance cut-off is introduced is unimportant. Only the factor G_0 in (1) depends on the crack-tip process zone, but for polymers this quantity cannot be calculated accurately at present, and G_0 must be deduced directly from experimental data.

In reality, G_0 will also depend somewhat on the crack-tip velocity (and the temperature) (see below and appendix C) albeit more weakly than the factor $f(v, T)$. The reason is that because of thermal effects, cavity formation, stringing, chain pull-out and the bond breaking all depend on the speed with which the surfaces are separated at the crack tip and on the temperature.

The increase in the crack propagation energy $G(v, T)$ with the crack propagation velocity v can be understood as follows [7, 13]. Neglecting inertia effects, the stress tensor satisfies

$$\sigma_{ij,j} = 0. \tag{6}$$

In addition, the stress tensor must satisfy certain compatibility conditions, which, as long as the relation between the stress and strain is linear, and the material homogeneous and isotropic, are independent of the constitutive relation between the stress and the strain. For the plane stress or strain case, which interests us here (where the stress tensor is independent of z), the compatibility equation becomes

$$\nabla^2(\sigma_{xx} + \sigma_{yy}) = 0. \tag{7}$$

Note that (6) and (7) constitute three independent equations for three unknown quantities, namely σ_{xx}, σ_{yy} and σ_{xy}. It follows that the stress distribution in the vicinity of a crack tip has the universal form $\sim r^{-1/2}$ independent of the detailed form of the constitutive relation between stress and strain as long as the relation is linear and the material homogeneous and isotropic; i.e., it is also valid for a viscoelastic solid.

Next, let us prove that during crack opening

$$\lim_{v\to\infty} G(v) = G_0 E_\infty / E_0. \tag{8}$$

This relation is not valid during crack closing. The stress in the vicinity of the crack tip is of the form

$$\sigma = K(2\pi r)^{-1/2} \tag{9}$$

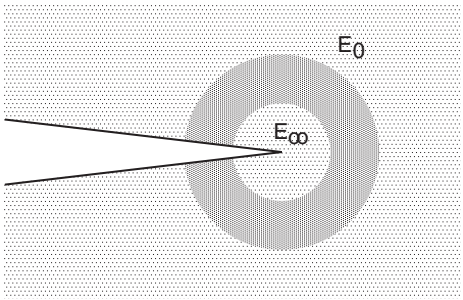

Figure 12. When a crack propagates fast in a viscoelastic solid, one can distinguish between three separate spatial regions: (a) an inner region, where the perturbing frequencies $\omega = v/r$ (where r is the distance from the crack tip) are so high that the rubber response corresponds to the hard glassy region characterized by the (high frequency) elastic modulus E_∞, (b) an outer region, where the perturbing frequencies are so small that the rubber responds with its zero-frequency modulus E_0, and (c) an intermediate region, where the full complex viscoelastic modulus $E(\omega)$ enters, and where the bulk viscoelastic energy dissipation occurs (schematic).

where the *stress intensity factor* K is proportional to the external applied stress. Assume that the crack tip propagates with a velocity v. The deformation rate of the viscoelastic solid at a distance r from the crack tip is characterized by the frequency $\omega = v/r$. Now, the smallest possible r is the crack-tip radius a (which cannot be smaller than an atomic diameter). Hence the highest possible frequency will be v/a. For very low velocity this frequency will be in the rubbery region of the viscoelastic spectra $E(\omega)$ and in this case the solid will behave purely elastically everywhere with the elastic modulus $E_0 = E(0)$. In this case there will be no dissipation in the bulk and the crack propagation energy $G = G_0$.

Next consider very high crack velocity v. Thus, for small enough r the frequency ω will be so high that the rubber response will correspond to the glassy region where the elastic modulus is $E(\omega) \approx E_\infty$. On the other hand, when r is large enough the frequency $\omega = v/r$ will correspond to the rubbery region where $E(\omega) \approx E_0$. At intermediate distances $E(\omega)$ is complex and this 'dissipative' region is indicated by the dark grey area in figure 12. Now, let us consider the crack propagation energy G, which for an elastic medium is related to the stress intensity factor K via equation (5):

$$G = K^2/E.$$

We first apply this formula to the inner region at the crack tip. In this case $G = G_0$ and $E = E_\infty$, giving

$$G_0 = K^2/E_\infty. \tag{10}$$

When we study the system at a lower *magnification* we do not observe the inner region and the dissipative region but only the outer region. In this case we must include in the crack propagation energy the energy dissipation in the rubber in the transition region (dark grey area in figure 12). Thus, G will now be larger than G_0. Since $E = E_0$ in the outer region, we get

$$G = K^2/E_0. \tag{11}$$

Combining (10) and (11) gives

$$G(\infty) = G_0 E_\infty/E_0.$$

Since for rubber-like materials E_∞/E_0 is of order 10^3 or more, the viscoelastic dissipation in the material in front of the tip will enormously enhance the crack propagation energy $G(v)$

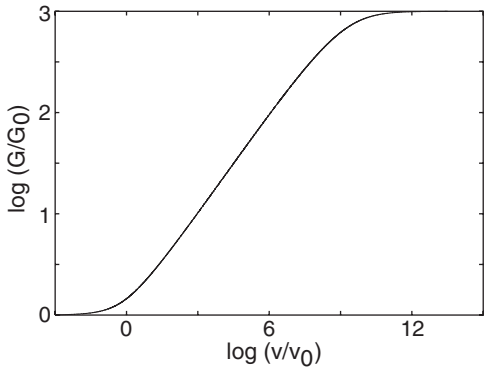

Figure 13. The qualitative form of the relation between the fracture energy G and the crack velocity v. The curve has been calculated (see [13]) without taking into account the increase in the temperature at the crack tip. This temperature effect only becomes important for relatively high crack-tip velocities; see [14]. For styrene–butadiene copolymer rubber the reference velocity v_0 is (at room temperature) typically of order 10^{-9} m s^{-1}, and the low-velocity crack propagation energy $G_0 \approx 30$ J m^{-2}.

for large v. This is the major reason for the extremely high tear strength (or toughness) of rubber-like materials. Figure 13 shows the qualitative form of the relation between the fracture energy G and the crack-tip velocity v [13].

3.2. Analytical results

The results presented below have been obtained using the energy loss method. Thus, energy conservation demands that the flow of elastic energy into the crack, Gv, must be equal to the fracture energy term $G_0 v$ plus the bulk viscoelastic dissipation term P:

$$Gv = G_0 v + P.$$

The viscoelastic energy 'dissipation' (conversion of mechanical energy to heat) can be obtained using

$$P = \int \mathrm{d}^3x \, \dot{\epsilon}_{ij} \sigma_{ij}$$

where $\dot{\epsilon}_{ij}$ is the local strain rate and σ_{ij} the local stress tensor; the integral involves the region close to the crack tip where the stress has the singular form (4). We note that the expression for P above in general includes the time derivative of the stored elastic energy. However, when only the singular $\sim r^{-1/2}$ stress and strain contributions are included in the integral, there is no time dependence of the stored elastic energy and the integral gives the 'dissipated' energy. In order for P to be finite, one must introduce a (velocity dependent) cut-off radius $a(v)$, which can be interpreted as the radius of the crack tip. One can show that P does not depend on the detailed way this cut-off is introduced, as long as $a(v)$ increases with the crack-tip velocity v in such a way that the stress at the crack tip does not exceed the critical value σ_c for bond breaking. The details of the calculations are presented in [13, 14].

The crack propagation energy G is usually written in the form (1), but here we write $G_0 = G_0^* g(v, T)$ so that

$$G(v, T) = G_0^* g(v, T) \, [1 + f(v, T)] \, , \tag{12}$$

where $f \to 0$ and $g \to 1$ as $v \to 0$. The theory of [13] shows that

$$1 + f(v, T) = a(v, T)/a_0, \tag{13}$$

where $a(v, T)$ is the crack-tip radius for a crack which propagates with the velocity v, while a_0 is the crack-tip radius for a very slowly propagating crack. The function $a(v, T)/a_0$ is determined by (see appendix B and references [13, 14])

$$\frac{a_0}{a} = 1 - \frac{2}{\pi} E_0 \int_0^{2\pi v/a} \mathrm{d}\omega \, \frac{F(\omega)}{\omega} \, \mathrm{Im} \, \frac{1}{E(\omega)}, \tag{14a}$$

which also can be written as

$$\frac{a_0}{a} = 1 - \kappa \frac{\int_0^{2\pi v/a} \mathrm{d}\omega \, \frac{F(\omega)}{\omega} \, \mathrm{Im} \, \frac{1}{E(\omega)}}{\int_0^{\infty} \mathrm{d}\omega \, \frac{1}{\omega} \, \mathrm{Im} \, \frac{1}{E(\omega)}}, \tag{14b}$$

where $\kappa = 1 - E_0/E_\infty$ and where

$$F(\omega) = \left[1 - (\omega a/2\pi v)^2\right]^{1/2}.$$

If we represent $E(\omega)$ in the form

$$\frac{1}{E(\omega)} = \frac{1}{E_\infty} + \int_0^{\infty} \mathrm{d}\tau \, \frac{H(\tau)}{1 - \mathrm{i}\omega\tau}, \tag{15}$$

where the spectral density $H(\tau)$ is a positive real function of the relaxation time τ, then one can also write

$$\frac{a_0}{a} = 1 - \kappa \int_0^{\infty} \mathrm{d}\tau \, \hat{H}(\tau) \left([1 + b^{-2}(\tau)]^{1/2} - b^{-1}(\tau) \right), \tag{14c}$$

where $b = (2\pi v\tau/a_0)(a_0/a)$ and where

$$\hat{H}(\tau) = \frac{H(\tau)}{\int_0^{\infty} \mathrm{d}\tau' \, H(\tau')}. \tag{16}$$

Note that (14) is an implicit equation for $a(v, T)$, which can be solved, e.g., by iteration, and that $a(v, T)$ only depends on the crack-tip velocity and on the viscoelastic modulus. Numerical results for $a/a_0 = G/G_0$ for a typical case are shown in figure 13. Note that the crack-tip radius may increase by a factor of $E_\infty/E_0 \sim 10^3$, or more, as the crack-tip velocity increases from zero to a high enough value. Equation (14*b*) is most convenient for numerical calculations (where $E(\omega)$ is only known numerically; see appendix B), while (14*c*) may be more useful for some analytical studies. See appendix B for further discussion of the velocity dependence of $G(v, T)$.

Assume that during crack propagation the (average) tensile stress at the crack tip takes the characteristic value $\sigma_c(v, T)$, i.e., $\sigma_c(v, T)$ is the (average) stress necessary to separate the surfaces at the crack tip. One can then write [13]

$$G_0^* = 2\pi a_0 \sigma_c^2(0, T)/E(0), \tag{17}$$

and

$$g(v, T) = \left(\frac{\sigma_c(v, T)}{\sigma_c(0, T)} \right)^2. \tag{18}$$

One may expect that σ_c is similar to the tensile yield (or rupture) stress of a (defect free) block of rubber; see figure 14. The tensile yield stress depends both on the temperature and on the strain rate (which is proportional to the speed with which the rubber block is elongated); see appendix C. Now, if a crack propagates with the velocity v, then the stress in front of the crack tip is $\sigma = K/(2\pi\sqrt{x}) = \sigma_c(a/x)^{1/2}$, since $\sigma = \sigma_c$ at the crack tip $x = a$. Thus, at the crack tip $\mathrm{d}\sigma/\mathrm{d}t = \sigma_c v/2a$. This formula shows that the separation time at the crack tip is of order $t^* = a/v$. We may also define the separation frequency $\omega = 1/t^*$. Thus the $\sigma_c(v, T)$ to be used in the factor $g(v, T)$ in the expression for the crack propagation energy is really the yield

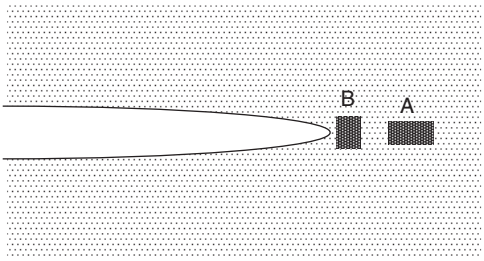

Figure 14. A small volume element (A) in front of the crack tip will elongate (B) as the crack tip propagates toward it, and finally break. The actual deformation process may be very complex, involving cavity formation and other highly nonlinear processes as indicated in figure 11.

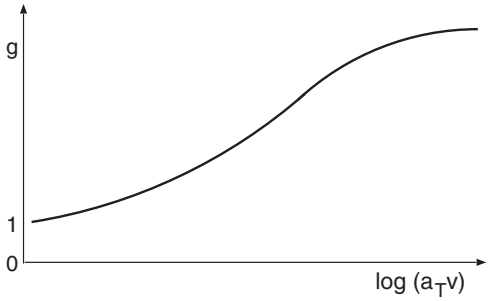

Figure 15. The $g(v, T) \approx g(a_T v)$ as a function of the product $a_T v$ between the crack-tip velocity v and the Williams–Landel–Ferry factor a_T, for a typical rubber (schematic).

stress in a tensile test where the rubber block is elongated with such a speed that the block breaks after the time period t^*. Note also that G_0^* is essentially the product of the crack-tip radius a_0 of a slow crack, and the elastic energy density $U_0 = \sigma_c^2(0, T)/2E(0)$ stored in a rubber block at the point of tensile rupture during slow elongation of the rubber block.

In figure 15 we show $g(v, T) \approx g(a_T v)$ as a function of $a_T v$. Note that g increases continuously with increasing $a_T v$. This is easy to understand physically: at very high crack velocity the surface separation at the crack tip is fast. That is, a small volume element in the rubber immediately in front of the crack tip is experiencing a fast tensile loading and elongation, as indicated in figure 14. During fast loading the polymer chains do not have enough time to rearrange themselves (by thermally activated flipping of polymer segments), and the external tensile force acting on the rubber volume element will distribute itself rather uniformly in the rubber matrix, and a large stress is necessary in order to break the chemical bonds in the block. On the other hand, for a very low crack-tip velocity the tensile loading is very slow, and the polymer chain segments between the cross-links can rearrange themselves in a nearly liquid-like manner so that much of the external load will be distributed on the cross-link bonds. Thus, for a weakly cross-linked rubber, the bond-breaking process (leading to tensile failure) will start much earlier than at high crack velocity. As a result, we expect $\sigma_c(v, T)$, and hence also $g(v, T)$ to increase continuously with crack velocity, and that $g(\infty, T)$ increases with decreasing cross-link density. Note also that this argument predicts that to a good approximation $g(v, T) = g(a_T v)$, since the rearrangement of the polymer chain segments during tensile loading is determined by the same thermally activated process as is the origin of the viscoelastic modulus of rubber-like materials. See appendix C for further discussion of the temperature dependence of G_0.

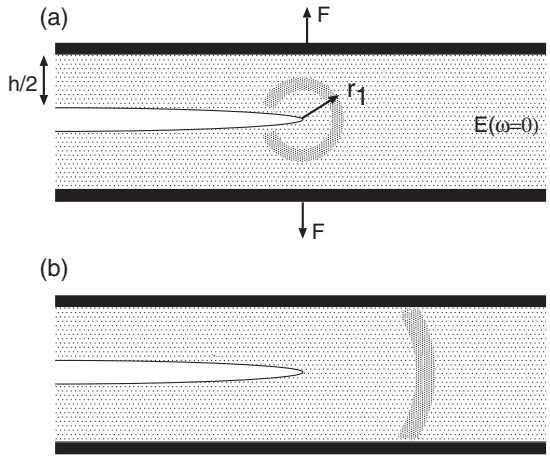

Figure 16. A fast propagating crack in a rubber slab of thickness h. The surfaces $y = \pm h/2$ of the slab are clamped in the perpendicular direction and displaced, thus generating elastic energy in the slab which is the driving force for the crack propagation. The crack propagation theory developed in [7–11, 13, 14] is only valid as long as the viscoelastic dissipative region in front of the tip is in the $r^{-1/2}$ asymptotic stress region (which may be the case in (a) but not in (b)), and as long as the loading is such that far away from the crack tip the stress is related to the strain via the zero-frequency elastic modulus $E(\omega = 0)$. Note that the crack propagation energy G in case (b) may decrease with increasing crack velocity, which may result in unstable crack propagation as already pointed out in [7].

Let us discuss the limitations of the theory presented above and in [7–11, 13, 14]. The theory assumes that the viscoelastic energy dissipation region is completely within the asymptotic region where the stress field exhibits the $r^{-1/2}$ singular behaviour. Thus, for example, if we consider a slab of rubber of thickness h and assume a crack in the middle of the slab (at $y = 0$, where $y = \pm h/2$ denote the boundary surfaces of the slab) then a necessary condition for the validity of the theory is that the radial distance $r = r_1$ of the outer boundary of the dissipative region must be smaller than $h/2$; see figure 16. Secondly, it is assumed that the system has been loaded a long enough time before the crack motion starts, so that the relation between the stress field and the strain field, due to the external loading, is characterized by the zero-frequency viscoelastic modulus $E(\omega = 0)$. In many applications the external stress is oscillating in time, but for this case no rigorous crack propagation theory has been developed so far.

Note that figure 13 describes both fast crack propagation (which may result in catastrophic failure) and slow crack propagation usually involved in fatigue failure. That is, if the stresses acting on the rubber object are so high that the elastic energy stored in the rubber can supply enough energy to drive a crack with the fracture energy $G_0[1 + f(\infty, T)]$, then the crack will propagate with a high velocity, which in some cases may be of the order of the rubber sound velocity (typically $v \sim 20$ m s^{-1}), resulting in sudden catastrophic failure (as in the popping of a balloon). More accurately, the condition for catastrophic failure is $K^2/E \geqslant G_0[1+f(\infty, T)]$. On the other hand, if $G_0 < K^2/E \ll G_0[1 + f(\infty, T)]$ the crack will propagate very slowly. In fact, the crack velocity is given by the condition $K^2/E = G_0[1 + f(v, T)]$, where, in the linear region in the $\log G - \log v$ diagram in figure 13 (see [13]), $f(v, T) \approx (v/v_0)^\alpha$. Here $v_0 = a_0/(2\pi\tau_0)$, where τ_0 is a characteristic rubber relaxation time (which in 'simple' rubber is of order $\omega_2^{-1} E_\infty/E_0$, where ω_2 is the frequency for which the loss tangent $E_2(\omega)/E_1(\omega)$ is maximal; see [13]). In an experiment of Gent [5] for styrene–butadiene rubber at $T = 25\,^\circ$C it was found that $v_0 \approx 10^{-9}$ m s^{-1}. If we assume the low-velocity crack-tip radius $a_0 \approx 1$ nm,

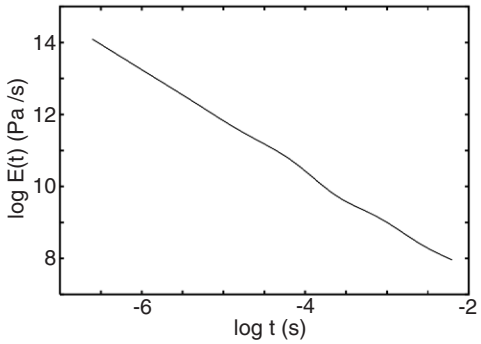

Figure 17. The logarithm of the Fourier transform of the viscoelastic modulus as a function of the logarithm of time. For a styrene–butadiene rubber compound.

then this velocity corresponds to $\tau_0 \approx 1$ s. However, both v_0 and τ_0 depend on the temperature and the type of rubber. In [13] it has been shown that $\alpha \approx 0.3$, but the exact value depends on the rubber compound. Thus, neglecting the v-dependence of G_0, we get when $v \gg v_0$

$$v \approx v_0(K^2/2G_0)^{1/\alpha} \sim \sigma^{2/\alpha}.$$

Most applications involving slowly moving cracks are related to fatigue failure, where the external applied stress is oscillating (frequency ω) in time. In this case one usually speaks about the number of cycles n necessary for crack-induced failure. No rigorous crack propagation theory has been developed for this case.

Let us consider the asymptotic behaviour of $G(v)$ when $v \gg v_0$ (but still not too high velocity). Let us assume an viscoelastic modulus determined by the spectral density $H(\tau) = A\tau^{-s}$ and $0 < s < 1$. For $s = 1/2$ this reduces to the so-called Rouse model. For many rubber compounds a good description of the viscoelastic properties in the transition region, between the rubbery and glassy regions, is obtained if s is slightly larger than 0.5, typically in the range from 0.5 to 0.7. As an example, we show in figure 17 (on a log–log scale) the Fourier transform $E(t)$ of the viscoelastic modulus $E(\omega)$ for a styrene–butadiene rubber compound filled with carbon black. The data are fitted well by a power law, $E(t) \sim t^{-1.4}$, corresponding to $s = 0.6$ (since the exponent is given by $s - 2$). Substituting $H = A\tau^{-s}$ in (16) gives

$$\hat{H} = \frac{(1-s)}{\tau_0}\left(\frac{\tau_0}{\tau}\right)^s.$$

Substituting this in (14*c*) gives for $v \gg v_0$

$$\frac{a}{a_0} = \left(\frac{v}{v_0}\right)^{\alpha}\left(\frac{s}{1-s}\right)^{\beta}, \tag{19}$$

where $\alpha = (1-s)/(2-s)$ and $\beta = 1/(2-s)$. Thus, for example, if $s = 0.6$, $a \sim \gamma_{\text{eff}} \sim v^{2/7}$.

Comments. A lot of work has been published on crack propagation in viscoelastic solids. When classical fracture mechanics is applied to a viscoelastic material, the result is highly unsatisfactory, for the stress singularity at the crack tip implies infinite strain rates when the tip moves, however slowly [27]. Accordingly, the material behaves as an elastic material characterized by the high frequency modulus $E(\infty)$ and there is no speed dependence of the crack propagation energy. This was first realized by Schapery [8] using the Barenblatt concept

of fracture mechanics, which denies the possibility of infinite stresses and regards the stress-intensity factor due to the applied loading simply as a quantity to be opposed by an equal stress-intensity factor produced by surface forces acting across the crack beyond the crack tip. Several papers [9–12, 17, 18, 27] have applied the Schapery general argument to viscoelastic solids and obtained general results for the crack propagation energy $G(v)$.

The energy-loss approach we use [13, 14], and the way we introduce the crack-tip radius a, have several important advantages over the Barenblatt crack-tip model used in most earlier studies: (a) the analysis is much simpler, (b) the analysis can be extended to include the non-uniform temperature distribution at the crack tip (see section 3.6) and (c) the analysis shows that the viscoelastic contribution to the crack-tip propagation energy G does not depend on the detailed processes which occur at the crack tip. This is very important, since these (highly complex) processes cannot be described accurately at present. In addition, (d) by using a simple sum rule for the viscoelastic modulus, we are able to simplify the derivation by avoiding the need to include the (complicated) angular dependence of the crack-tip stress field. Finally, (e) our treatment gives a simple closed formula for $G(v)$, which can be directly applied even when the viscoelastic modulus $E(\omega)$ is only known numerically in a finite frequency region (see appendix B), as will always be the case in practical applications where $E(\omega)$ has been obtained in experiment.

3.3. Numerical results

In this section we present numerical results for the crack propagation energy $G(v)$ for a few important rubber compounds. The results have been obtained from equation (14*b*) (see also appendix B) using the measured viscoelastic modulus $E(\omega)$.

We have calculated the crack propagation energy $G(v)$ for a styrene–butadiene (SB) copolymer rubber, and for poly(2ethylhexyl acrylate) with 2% acrylic acis (PEHA-AA), a rubber used as pressure sensitive adhesive. Figure 18 shows the real part of the elastic modulus, $E_1 = \mathrm{Re}\, E$, and the loss tangent $E_2(\omega)/E_1(\omega)$ as a function of frequency for the unfilled (curve a) and filled (with carbon black) (curve b) SB rubber, and for PEHA-AA (curve c). In figure 19 we show the crack propagation energy for the same three rubber compounds, as obtained using equation (14*b*).

In order to obtain $G(v)$ accurately, the viscoelastic modulus $E(\omega)$ must be known for all frequencies. It is particularly important to know the low-frequency modulus, starting in the rubbery region where $\mathrm{Re}\, E(\omega)$ is (approximately) constant. This is rather well satisfied for the SB rubber compounds, but not for the PEHA-AA tack compound (see figure 18). Note also that the ratio between $G(v)$ for the largest and smallest velocities in figure 19 is equal to the ratio between $\mathrm{Re}\, E(\omega)$ for the highest and lowest frequencies in figure 18, in accordance with the theory of section 3.2.

The crack propagation curves in figure 19 have regions where (on the log–log scale) G is approximately linearly related to the crack-tip velocity. In these regions, the exponent α in the relation $G \sim v^{\alpha}$ is $\alpha \approx 0.32$ and 0.25 for the unfilled and filled SB rubber compounds, and 0.35 for the tack compound. These values are similar to the theoretical values discussed in section 3.2.

3.4. Comparison with experiment

Figure 20 shows the fracture energy G for a styrene–butadiene rubber as a function of the crack-tip velocity [5] (see appendix D for a discussion of how $G(v)$ can be measured). The results have been obtained using the Williams–Landel–Ferry [19] velocity–temperature shifting procedure,

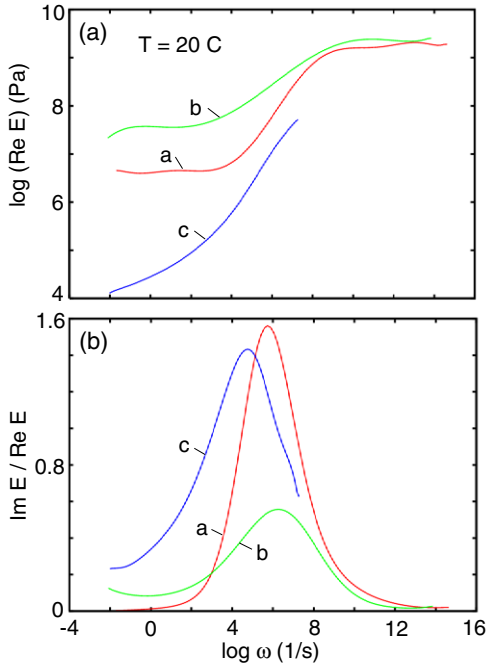

Figure 18. The real part of the elastic modulus (a), and the loss tangent (b), as a function of frequency for the unfilled (curve a) and filled (with carbon black) (curve b) SB rubber, and for PEHA-AA (curve c). For $T = 20\,^{\circ}\mathrm{C}$.

where the original data were obtained for crack velocities below 1 cm s^{-1} in order to reduce the influence of the crack-tip flash temperature. On the log–log scale the experimental data exhibit a straight line corresponding to a velocity dependence $G \sim v^{\alpha}$ with $\alpha \approx 0.27$ in good agreement with the theory presented above (for $s = 0.6$ we have $\alpha = (1-s)/(2-s) \approx 0.28$). Figure 20 also presents a result combining cutting and tearing. In this case rubber is torn apart while a sharp razor blade is pushed into the crack tip. Cutting resistance at low speeds appeared to be rather independent of speed, although at high speeds it increases markedly. In this case the crack tip diameter is presumably given by the blade tip diameter (about 1000 nm), which may explain the approximative independence of the fracture energy on crack velocity for small velocities.

3.5. Comment on closing cracks in viscoelastic solids

The problem of crack growth studied above has many direct applications, e.g., to wear and adhesives. The opposite situation of crack closure in a viscoelastic medium is important during the formation of contact between a viscoelastic solid and another solid, e.g., in the standard adhesion tests where a rubber ball is brought into contact with a hard flat surface. However, in many practical situations irreversible surface processes occur, so that even when crack propagation occurs very slowly the energy (per unit area), $2\gamma_0$, for bond breaking during crack opening is different from the energy gain (per unit area), $2\gamma_0'$, due to bond formation during crack closing, with $\gamma_0 \geqslant \gamma_0'$. However, when only the weak van der Waals interaction occurs between the crack planes, as is usually the case, e.g., when a rubber ball is in contact with a glass surface, one may expect $\gamma_0 \approx \gamma_0'$, and we will assume $\gamma_0 = \gamma_0'$ in what follows.

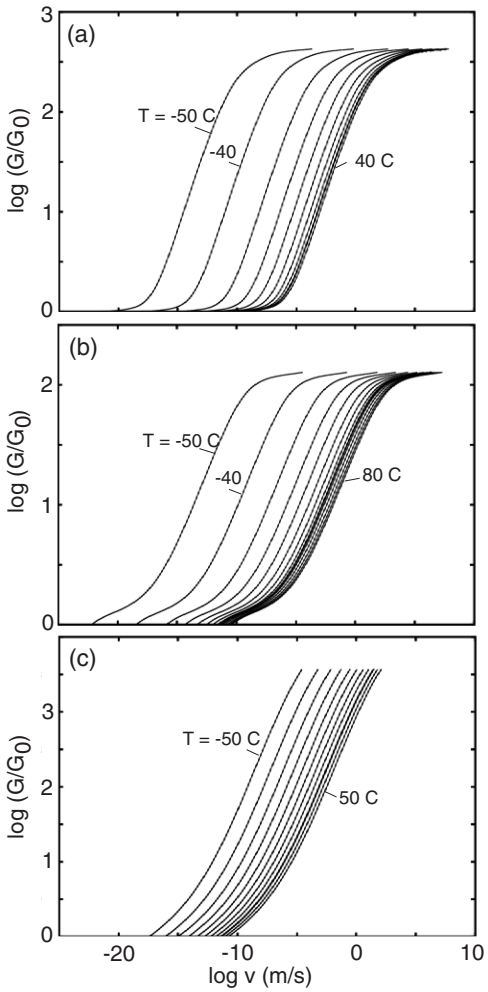

Figure 19. The crack propagation energy $G(v)$ as a function of the crack-tip velocity for styrene–butadiene rubber (a) without and (b) with carbon black filler, and (c) for a pressure sensitive adhesive (PEHA-AA). The different curves show $G(v)$ as the temperature is increased in steps of 10 °C. The $T = 30$ °C curve is denoted by a thicker line.

For a closing crack, the interfacial binding energy (or surface energy) $2\gamma_0$ is partly converted into elastic energy and partly dissipated in the rubber bulk, so that the energy conservation condition now takes the form

$$Gv = G_0 v - P,$$

and it is clear from energy conservation that $\gamma_{\rm eff} \leqslant \gamma_0$. Thus, while during crack growth $\gamma_{\rm eff}$ may increase by a factor of $\sim 10^4$ as the velocity increases, during crack closure $\gamma_{\rm eff} \leqslant \gamma_0$. This large hysteresis in the adhesion energy, $\gamma_{\rm eff}$, during crack growth and closure, has been observed experimentally [44], and may give an important contribution to the friction force during sliding of a rubber block on a smooth asperity, as the sliding process can be considered as resulting from a closing crack at the front edge of the contact region, and a opening crack at the trailing edge [45].

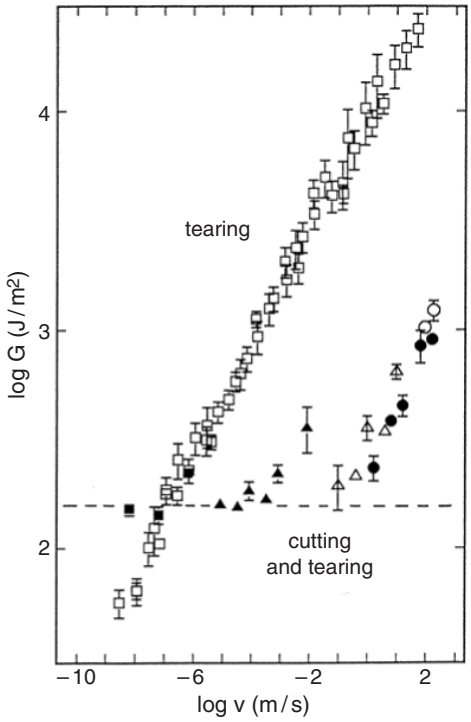

Figure 20. Fracture energy G for styrene–butadiene rubber at various cutting or tearing speed at $T = 25\,^{\circ}\mathrm{C}$. Adapted from [5].

3.6. Flash temperature

When a crack propagates in a viscoelastic solid, heat is produced in the vicinity of the crack tip, which will increase the temperature close to the crack tip. Here we demonstrate the fundamental importance of the non-uniform temperature distribution (flash temperature) at the crack tip.

It is easy to show that the temperature increase at the crack tip may be very high. The crack propagation energy per unit created surface area, for a crack propagating in rubber at the velocity $\sim$10 cm s^{-1}, is typically (see figure 23) $G \approx 10^4$ J m^{-2} ($\approx 10^3$ eV Å^{-2}). Most of the energy dissipation occurs at a typical distance from the crack tip given by $r \sim v/\omega_1$, where v is the crack tip velocity and ω_1 is the frequency for which Im$[1/E(\omega)]$ is maximal (which is related to the frequency ω_2 of the maximum of the loss tangent Im $E(\omega)$/ Re $E(\omega)$ via $\omega_1 \approx (E_0/E_\infty)^{1/2}\omega_2$). For styrene–butadiene rubber at room temperature $\omega_1 \approx 10^4$ s^{-1} and if $v = 10$ cm s^{-1} we get $r \approx 10\,\mu$m. On the timescale $\sim\tau = r/v \approx 10^{-4}$ s and the length scale $\sim r$, heat diffusion is negligible since $D\tau/r^2 \approx 0.1 \ll 1$, where the heat diffusivity $D = \lambda/\rho C_V \approx 10^{-7}$ m^2 s^{-1} ($\rho \approx 1200$ kg m^{-3} is the mass density, $\lambda \approx 0.15$ W mK^{-1} the heat conductivity and $C_V \approx 1400$ J kg^{-1} K^{-1} the heat capacity). Thus the temperature increase at the crack tip can be estimated using $\rho C_V \Delta T \approx G/r$ or $\Delta T \approx G/(\rho C_V r) \approx 10^3$ K. Note also that for $v \ll v_c$ the temperature increase will be negligible, where v_c is determined by the condition $D\tau/r^2 \approx 1$. Using that $\tau = 1/\omega_1$ and $r = v_c\tau$ gives $D\omega_1/v_c^2 = 1$ so that $v_c = (D\omega_1)^{1/2} \approx 3$ cm s^{-1}.

In [14] a theory has been developed which takes into account the crack-tip flash temperature in an approximate way. The crack propagation energy was found to have the qualitative

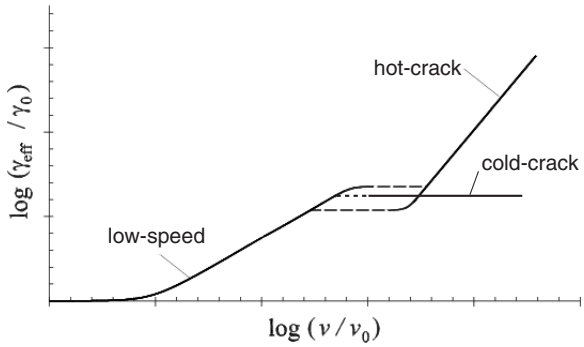

Figure 21. The crack propagation energy as a function of the crack speed. The characteristic stick–slip region, where the crack-tip velocity is oscillating in time, is shown as dashed lines (schematic). Adapted from [14].

form shown in figure 21, with a *low-speed* crack propagation branch described by the theory presented in section 3.2, and a *hot*-crack branch and a *cold*-crack branch at 'high' crack-tip velocities. For the *hot*-crack branch the temperature increase at the crack tip is important.

The reason the crack propagation energy increases (for large crack-tip velocities on the hot-crack branch) when the crack-tip flash temperature effect is taken into account can be understood as follows. Consider a fast-propagating crack and let us first neglect the flash temperature effect, i.e., we assume that the temperature everywhere equals the background temperature T_0 (figure 22(a)). At high crack-tip velocity v, the region close to the crack tip is effectively in the glassy state, and contributes very little to the total viscoelastic energy dissipation. Similarly, the region very far away from the crack tip is effectively in the rubbery region of the viscoelastic spectra, and also contributes very little to the total energy dissipation. Most of the viscoelastic energy dissipation occurs in the transition region between the rubbery and glassy regions (dark grey area in figure 22). Now, let us include the flash-temperature effect. Because the crack tip moves toward the region where the viscoelastic energy dissipation occur, the temperature increase is highest close to the crack tip. Thus, part of what was the glassy region when the temperature effect was neglected will now correspond to the transition region and will contribute strongly to the total viscoelastic energy dissipation. On the other hand, what was the outer rim of the transition region when the flash-temperature effect was neglected will now be converted into the rubbery region, and will contribute very little to the total energy dissipation. However, since the temperature decreases monotonically with the distance from the crack tip, the reduction in the energy dissipation in the outer region is overcompensated by the increases in the energy dissipation in the inner region closer to the crack tip. The net effect is that the total energy dissipation *increases* when the flash-temperature effect is taken into account. By increasing the crack speed the dark grey region will become larger and larger until it reaches the crack tip: when this happens the crack is in the asymptotic *hot-crack* regime. Note, however, that because of heat diffusion, for very low crack-tip velocities the temperature increase in the vicinity of the crack tip is negligible, resulting in a negligible (temperature-induced) increase in the crack propagation energy for small crack-tip velocities.

Comparison with experiment. The theory described above (see also [14]) explains why unstable crack propagation is observed in some cases, e.g. for tyre rubber [47–49]. The most detailed experimental study of stick–slip crack propagation in rubber was presented in [49]. In figure 23 we show the logarithm of the crack propagation energy $G = 2\gamma_{\rm eff}$ as a function

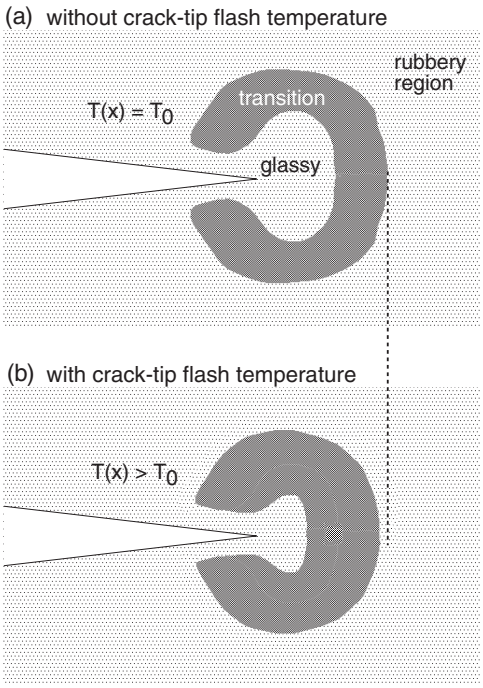

Figure 22. A qualitative picture of what happens when the flash-temperature effect is included in the theory. (a) For isothermal conditions most of the viscoelastic energy dissipation occurs in the transition region between the rubbery and glassy regions of the rubber viscoelastic spectra (dark area). (b) When the flash-temperature effect is included, because the temperature increase is very large close to the crack tip, the transition region (dark area) extends closer to the crack tip than in (a). On the other hand, the outer rim of the transition region in (a) is converted into the rubbery region. However, since the temperature decreases monotonically with the distance from the crack tip the total energy dissipation increases. Adapted from [14].

of the logarithm of the crack-tip velocity for a styrene–butadiene rubber with carbon black filler. When the (average) crack-tip velocity is in the range ∼0.1–10 cm s^{-1}, unstable crack propagation occurs. In this velocity region cracks grow at a slow or fast rate corresponding to the data symbols on the left (low-velocity) and right (high-velocity) branches of the $G(v)$-curve in figure 21. Note also that the slope of the $\log G - \log v$ curve is much higher for the high-velocity branch. Both these facts are in good qualitative agreement with the analytical results (see [14]). In [49] it was also found that the crack surfaces during slow crack propagation (left branch in figure 21) were very rough, while very smooth crack surfaces resulted when the crack propagated fast (right branch in figure 21). However, this change in surface morphology is not the primary reason for the two $G(v)$ crack-propagation branches, but rather a consequence of it. The fundamental reason is instead the flash temperature, and its influence on the viscoelastic energy dissipation in front of the crack tip. We believe that at high crack-tip velocities the high temperature at the crack tip will result in a 'liquid-like' region at the crack tip. This in turn will result in the formation of thin uniform layers of modified (degraded) rubber on the crack surfaces. It is clear that information about the peak temperature development during fracture of rubber-like materials can be gained by observing the amount of decomposition products formed by the propagation of the crack [59]. Finally, we note that it should be possible to study the temperature rise in the vicinity of the crack tip using an infrared camera with high spatial and temporal resolution.

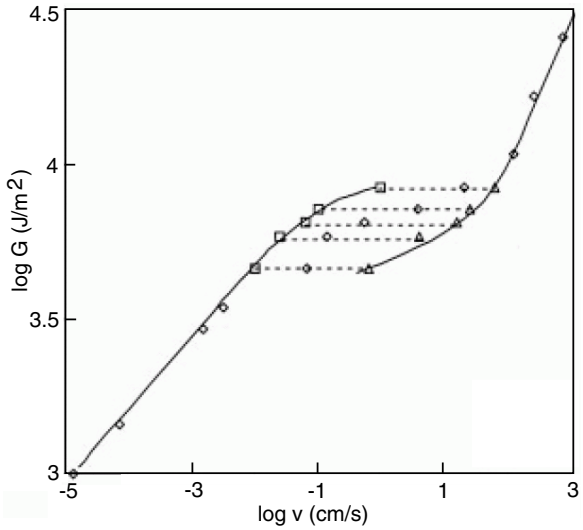

Figure 23. The crack propagation energy as a function of the crack speed for styrene–butadiene copolymer rubber with carbon-black filler. The characteristic stick–slip region, where the crack tip velocity is oscillating in time, is shown as dotted lines (adapted from [49]).

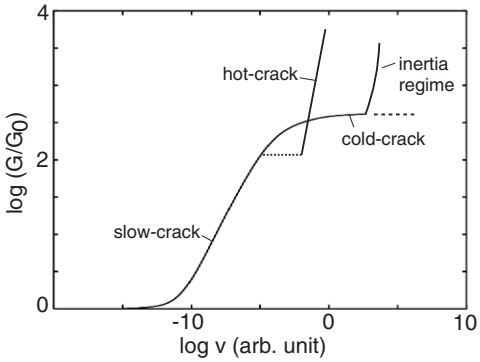

Figure 24. The relation between the crack propagation energy G and the crack-tip velocity v when inertia effects are included (qualitative picture). If the crack-tip velocity is increased very slowly, the crack will follow the hot-crack branch. However, if the crack tip is initially accelerating very fast, there is not enough time for the full temperature distribution to develop, and the system may follow the cold-branch. In the latter case, when the crack velocity becomes of the order of the sound velocity c, the crack propagation energy will rapidly increase (inertia regime).

3.7. Fast cracks in rubber—role of inertia

Recent experiments [28] have detected fast crack propagation in rubber, where the crack-tip velocity $\sim$60 m s^{-1} is of the order of the rubber sound velocity. We believe that this motion is on the continuation of the cold-crack branch to higher velocities than considered in [14]. When the crack velocity becomes of the order of the (transverse) sound velocity, inertia effects can no longer be neglected, and the analysis presented in [14] is no longer valid. Nevertheless, from theory (see section 2) [29], one expects the crack propagation energy to rapidly increase as the crack-tip velocity approaches the sound velocity c, and we therefore expect the complete relation between the crack propagation energy and the crack-tip velocity to take the schematic form indicated in figure 24.

Slowly moving cracks in rubber have the typical shape shown in figure C.1 (see also figure 9 in [12]). However, cracks which travel faster than the shear wave speed have wedge-like shape resembling a shock, and recently Marder [30] has developed a shock-wave theory for rapid crack propagation in rubber. The analysis of Marder was based on the elastic free energy density due to Mooney and Rivin. This model accounts for the non-linear properties of rubber but does not take into account correctly the viscoelastic nature of real rubber-like materials. Thus, the model study of Marder does not account for the increase of the elastic modulus by perhaps a factor of $\sim$1000 which will occur close to the crack tip during the fast crack propagation, and it is not clear to us how well the study of Marder is able to describe the fast crack propagation in real rubber.

An important problem is to determine under what circumstances crack propagation will follow the hot-crack branch and the cold-crack branch. If the crack-tip velocity is increased very slowly so that the temperature field around the crack tip can be fully developed, the calculations in [14] show that for all physically reasonable rubber parameters the crack will always follow the hot-crack branch. However, if the crack tip is initially accelerating very fast, there is not enough time for the full temperature distribution to develop, and in this case the system may follow the cold-crack branch. Thus, we believe that the path the system takes depends on how the crack is generated initially. For example, if a balloon is picked, the resulting crack will accelerate, and in an extremely short time reach a velocity of the order of the sound velocity, and the system will follow the cold-crack branch. On the other hand, if in a trouser test the legs are pulled with a slowly increasing velocity, the temperature field will at any moment in time be fully developed, and the system will follow the hot-crack branch of the $G(v)$ relation. We believe that this is the explanation why in [28] very fast crack propagation was observed when a stretched rubber sheet was picked, while the hot-crack branch was observed in the trouser tests presented in [49].

The scenario described above is very similar to the ductile–brittle transition often observed for metals. In some specific temperature regime, if a metal block with a crack is elongated slowly, the metal in the vicinity of the crack edges will undergo very large plastic deformation resulting in a large crack-tip radius (blunted tip), and very slow crack growth; in this case the crack propagation energy will be very high because of the large energy involved in the plastic deformation. This crack propagation mode is similar to our hot-crack mode, where a lot of energy is dissipated in front of the crack tip, but now because of viscoelastic deformations rather than plastic deformations. On the other hand, if the elongation is very fast (fast loading) the crack may propagate very fast in a brittle-like manner, involving very small plastic deformation and a much lower crack propagation energy $G(v)$. This is similar to our cold-crack branch.

To summarize, the theory presented in [14] assumes that the crack-tip velocity is much smaller than the sound velocities c in the rubber. Since typically $c > 10$ m s^{-1} this is a good approximation as long as the crack-tip velocity is not higher than a few metres per second. At higher crack-tip velocities inertia effects becomes important, and the full $G(v)$-relation is expected to take the qualitative form discussed above.

3.8. Influence of strain crystallization on crack propagation

Some types of rubber, e.g., natural rubber, exhibit strain crystallization; see figure 25. Since the strain at the crack tip during fracture of rubber-like materials is very high, a region of crystallized rubber may form close to the crack tip. Strain crystallization only occurs when the strain is larger than $\sim$3 so that the strain crystallized region will be part of the crack-tip process zone. Experiment has shown that no (detectable) crack propagation occurs in rubber undergoing strain crystallization until the stress is so high as to generate abrupt (catastrophic)

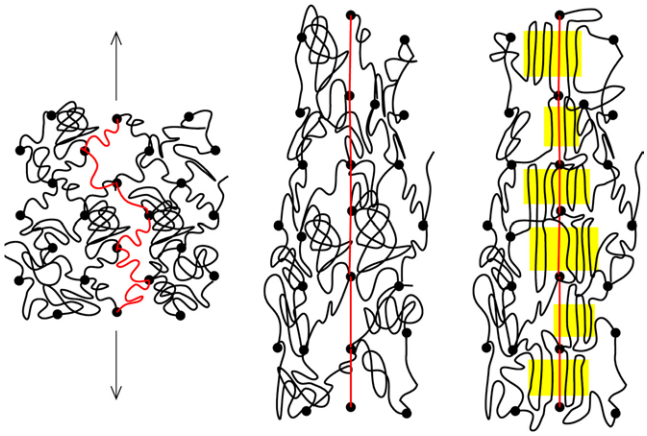

Figure 25. Model of nucleation and crystallization in vulcanized natural rubber[5]. Relatively short chains are drawn as red lines. Filled circles represent cross-links. (a) Before deformation: cross-links are distributed uniformly. (b) After deformation: short chains are fully stretched. (c) The fully stretched chains act as a nucleus of crystallites (yellow part). The first crystallites occur at a strain ~ 3. Adapted from [51].

fracture; see figure 26. Styrene–butadiene (SB) rubber does not exhibit strain crystallization, and has therefore worse wear resistance as compared to natural rubber. In fact, the lack of strain crystallization in synthetic SB rubber presented a critical engineering challenge during World War II when the supply of natural rubber was severely reduced. Because of its high wear resistance, natural rubber is used in truck tyres (see below).

Since the region where strain crystallization occurs is part of the crack-tip process zone, the theory described earlier should also be valid for rubber undergoing strain crystallization. However, since no (slow) steady crack propagation is observed for strain crystallizing rubbers, the prefactor $G_0(v)$ in the expression for the crack propagation energy must decrease with increasing velocity v, in such a way that the product $G_0(v)[1 + f(v)]$ is a decreasing function of v; see figure 27. This can be explained if one notes that some characteristic (relaxation) time $\tau \approx 0.1$ s is necessary for the strain crystallization to occur [52]. Thus, as v increases the amount of strain crystallization at the crack tip will decrease. In particular, if the characteristic time $t^* = a/v$ (where a is the crack-tip radius) for stretching a polymer chain at the crack tip is shorter than τ no strain crystallization can occur. For a slowly moving crack a may be 100 nm (or less). Thus, stain crystallization may be totally removed already for crack-tip velocities $v \approx a/\tau \approx 1\ \mu\text{m s}^{-1}$.

One important class of rubber crack propagation problems involves interfacial cracks, e.g., when a rubber ball is separated from a hard inert substrate (see section 6). Here the crack propagation involves breaking very weak adhesive bonds (e.g., van der Waals bonds) at the interface between the solids. In this case the strain at the crack tip will be so small that no strain crystallization occurs even for natural rubber, and the theory presented in section 3.2 should

[5] Strain crystallization in natural rubber is more complex than indicated by figure 25, since it requires certain non-rubber constituents, mainly fatty acids [50]. Thus synthetic *cis*-1,4-polyisoprene has a similar structure to that of natural rubber, but the rate of crystallization is significantly smaller than for natural rubber. In spite of intense research, it has not been possible to produce synthetic rubber with similar high tear strength to natural rubber. Kautschuk is used by the rubber tree (*Hevae brasiliensis*) as a tough elastic coating on damaged surface area (similarly as a blood clot is used on damaged areas on the human skin). It is interesting to speculate whether the outstanding tear strength and tensile strength of natural rubber is of biological importance, as the result of optimization by millions of years of natural selection.

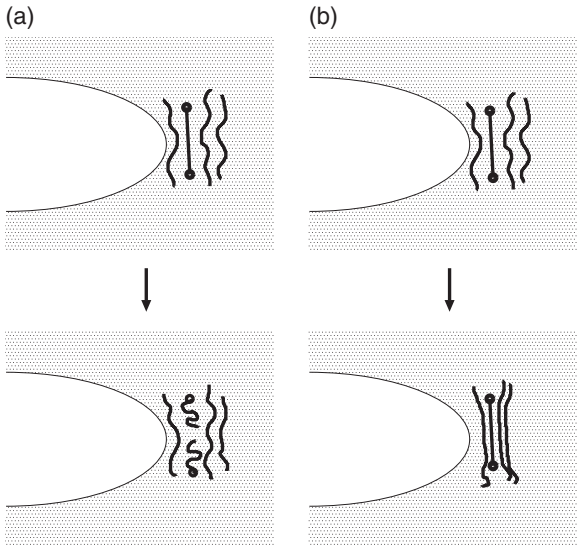

Figure 26. The bond-breaking process at a crack tip in a rubber undergoing strain crystallization (b), and in a rubber where no strain crystallization can occur (a). Because of the inhomogeneous nature of rubber-like materials, the different polymer chains at the crack tip will be stretched to the break-limit at different times. For rubber which undergoes strain crystallization (b), the chains in the vicinity of a fully stretched chain will adhere in a commensurate way to the stretched chain, thus strengthening the weakest link. This will result in a strong enhancement in the (average) stress at the crack tip necessary for the onset of crack propagation.

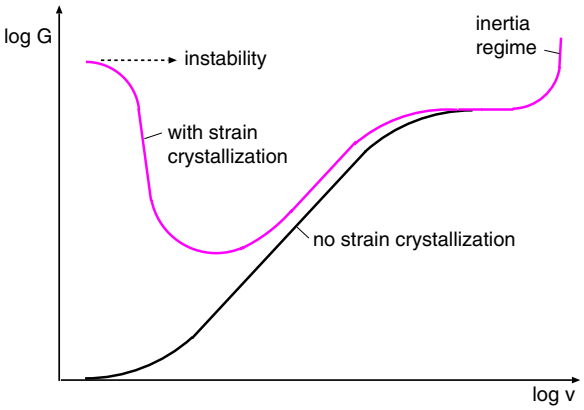

Figure 27. The crack propagation energy G as a function of the crack-tip velocity v for a rubber which undergoes no strain crystallization, and for a rubber which strain crystallizes (schematic).

hold for this type of crack propagation. In fact, the effective interfacial energy γ_{eff} deduced from rolling resistance data involving natural rubber is in good agreement with theory (see section 6.3).

In addition to natural rubber, isoprene rubber and polychloroprene exhibit strain crystallization. Polymers exhibiting little or no crystallization include styrene–butadiene rubber, polybutadiene, butyl rubber, acrylonitrile–butadiene rubber and ethylene–propylene rubber [53].

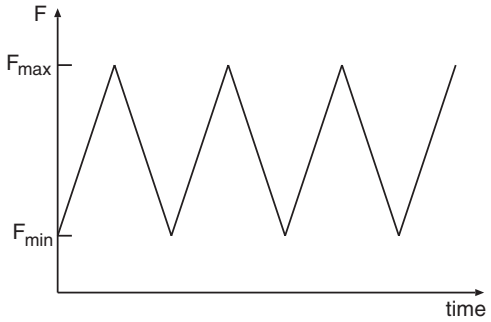

Figure 28. When a rubber block with a crack is exposed to an oscillatory force (load) $F(t)$, slow *fatigue* crack propagation may occur. The crack propagation speed depends not only on the maximum F_{max} and the minimum F_{min} of $F(t)$ but also on the curve form. For rubber which undergoes strain crystallization, the crack speed depends sensitively on the ratio $R = F_{min}/F_{max}$.

3.9. Pulsating external stresses and fatigue wear

The mechanical strength of solids is often much lower when exposed to a fluctuating (in time) stress (or load) (see figure 28), as compared to a constant stress of similar magnitude. For crystalline materials such as metals this is caused by strong irreversible flow-processes which occur close to the crack tip. Thus, after each stress oscillation the physical state of the material at the crack tip is different as a result of irreversible motion of dislocations or point defects. The accumulation of defects will result in a hardening of the material at the crack tip, which finally fractures.

Strain crystallization. As pointed out above, some types of rubber, e.g., natural rubber, undergo crystallization when exposed to large strain. Since the strain at the crack tip during fracture of rubber-like materials is very high, a region of strain crystallized rubber may form close to the crack tip.

For rubber compounds undergoing strain crystallization, the crack propagation speed depends sensitively on the ratio $R = F_{min}/F_{max}$ between the minimum and maximum loading force (figure 28). This is illustrated in figure 29, which shows the crack propagation energy (or tear energy) $G = G_{max}$ for natural rubber, as a function of the crack propagation velocity for several values of the ratio R. Here G_{max} is the maximum tearing energy calculated from the strain energy U_{el} at maximal strain (the strain energy varies periodically with time because of the oscillating external load). Note that G_{max} decreases when R decreases (i.e., F_{min} decreases, since F_{max} is constant). It has been suggested that this is caused by increased melting of crystallites as the (minimum) loading force F_{min} decreases, but there is at present no theory which can describe the observed effect (or the influence of strain crystallization on the crack propagation in general).

The curve for $R = 0$ in figure 29 has a similar form as predicted by the theory in sections 3.2 and 3.3, but the slope of the linear part (on the log–log scale) is ≈ 0.5 instead of ≈ 0.25 as expected from the theory. We believe that this is due to the strain crystallization which will also occur when $R = 0$. In fact, the $\gamma_{eff}(v)$ function obtained from rolling resistance data involving natural rubber (where the strain at the opening crack tip is so small that no crystallization can occur) exhibits an (average) slope ~ 0.25 (see section 6.3).

Figure 29 shows that when G is below some critical value $G = G_c$ crack propagation occurs at a constant speed (independent of G). This is due to chemical reaction between ozone

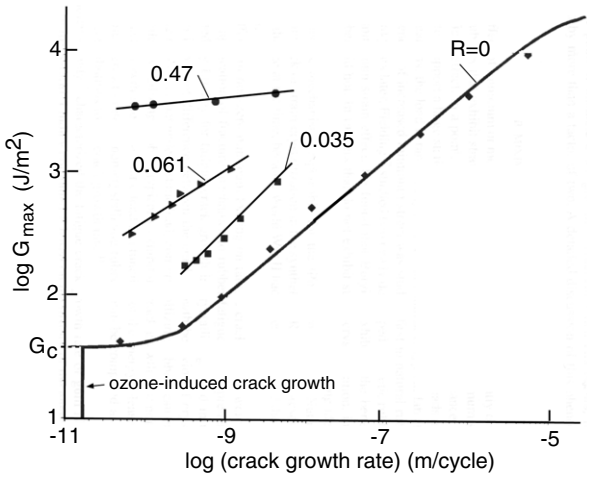

Figure 29. Fatigue crack growth for unfilled natural rubber. The (maximal) crack propagation energy $G_{\max}$ is shown as a function of the crack velocity. Results are for different ratios $R = F_{\min}/F_{\max}$ between the minimal and maximal loading force. Adapted from [54].

(and other molecules in the normal atmosphere) and the rubber molecules at the crack tip. Thus, experiments performed in vacuum detect no crack motion when $G < G_c$.

Let c denote the crack length. The crack growth rate per cycle is denoted by $\mathrm{d}c/\mathrm{d}N$ (where N is the number of cycles). The curve in figure 29 is accurately described by the following equations:

$$\frac{\mathrm{d}c}{\mathrm{d}N} = \text{constant} = r \qquad \text{for } G < G_c \tag{20}$$

where r is proportional to the ozone concentration in the surrounding air. At tearing energies immediately above the threshold

$$\frac{\mathrm{d}c}{\mathrm{d}N} = A(G - G_c) + r \qquad \text{for } G_c < G < G_1 \tag{21}$$

where A is a constant. At intermediate and high tearing energies

$$\frac{\mathrm{d}c}{\mathrm{d}N} = BG^{\mu} \qquad \text{for } G_1 < G < G_2 \tag{22}$$

where B and μ depend on the type of rubber used. For unfilled natural rubber $\mu \approx 2$ while for styrene–butadiene rubber $\mu \approx 4$. Finally, for $G > G_2$ catastrophic tearing occurs,

$$\frac{\mathrm{d}c}{\mathrm{d}N} = \infty \qquad \text{for } G_2 < G. \tag{23}$$

These (approximate) relations between G and $\mathrm{d}c/\mathrm{d}N$ are useful for estimating the fatigue lifetime of rubber components; see section 6.5. Equations (20)–(23) hold (approximately) for all types of rubber. For rubber which does not undergoes strain crystallization, for low frequency of the pulsating forces, it is possible to derive the relation between $\mathrm{d}c/\mathrm{d}N$ and G from the dependence of $G(v)$ on the crack tip velocity for steady motion (constant driving force). Thus, for example, when v is large enough $G(v) = G_0(v/v_0)^{\alpha}$ (see sections 3.2–3.4), which gives

$$\frac{\mathrm{d}c}{\mathrm{d}t} = v_0(G/G_0)^{1/\alpha}.$$

Since[6]

$$\frac{\mathrm{d}c}{\mathrm{d}t} \approx \frac{\mathrm{d}c}{\mathrm{d}N}\frac{1}{\zeta T},$$

where T is the period of the oscillating force and ζ a number of order unity (see footnote 6), we get

$$\frac{\mathrm{d}c}{\mathrm{d}N} \approx (v_0 T)\zeta (G_{\max}/G_0)^{1/\alpha} \tag{24}$$

which is of the form (22) with $B \approx v_0 T \zeta G_0^{-1/\alpha}$ and $\mu = 1/\alpha$. Since for styrene–butadiene rubber $\alpha \approx 0.25$ we get $\mu \approx 4$, in good agreement with experiment (see section 6.5).

Temperature effect. During crack propagation, energy is dissipated close to the crack tip. For a slowly moving crack this will give rise to negligible temperature rise at the crack tip because there is enough time for the heat to diffuse away from the crack-tip region. However, if instead of a static applied driving stress the external stress is pulsating in time, the situation is very different. In this case, if the oscillation frequency and amplitude are high enough, a lot of energy will be dissipated in the vicinity of the crack tip even if the crack propagates very slowly (and, in fact, even if the crack does not propagate at all). This may result in a strong increase in the temperature close to the crack tip which will shift the viscoelastic loss peak to higher frequencies. This will make the rubber more 'elastic' and, as shown above, this will reduce the viscoelastic energy dissipation in front of the crack tip and hence reduce the crack propagation energy.

The magnitude of the temperature increase will depend on the rubber used, and on the nature of the fluctuating stress. Thus, butadiene rubber has the viscoelastic peak centred at relatively high frequency, while for styrene–butadiene rubber the viscoelastic peak is centred at much lower frequency. Hence, assuming identical loading conditions, the temperature increase in the vicinity of the crack tip should be largest for styrene–butadiene rubber.

The temperature increase resulting from a pulsating external stress (which will occur even in the absence of a crack) will also influence the rate of nucleation of cracks (and other defects). In fact, in the context of tyre tread block wear, the wear rate may be mainly determined by the rate of *nucleation* of crack-like defects (see section 6.6). Thus, the higher temperature and stress which occur in the contact area between the road asperities and a rubber tread block for styrene–butadiene rubber, as compared to butadiene rubber, may in part explain why the latter rubber (in combination with natural rubber) has better tyre tread wear resistance, at least in truck tyre applications where the tread blocks are very thick and heating effects therefore particularly severe. Nevertheless, in extreme situations 'thermal runaway' may occur, where the temperature becomes so high that severe degradation of the rubber occurs in a very short time [56]. The temperature increase at the crack tip will also reduce the stress σ_c at the crack tip, which is necessary for crack propagation (see appendix C).

Finally, we note that in non-crystallizing rubbers, and when the temperature effects discussed above can be neglected, the crack growth rate under cyclic load can be computed (or estimated) directly from the $G(v)$ relation for steady crack growth (see equation (24)), i.e., no new physics enters in this case [57].

[6] The exact relation between $\mathrm{d}c/\mathrm{d}t$ and $\mathrm{d}c/\mathrm{d}N$ depends on the nature of the fluctuating force. For example, if the external force $F(t)$ fluctuates harmonically between F_0 and F_1, $F = F_0 + (1/2)(F_1 - F_0)[1 + \cos(\omega t)]$, then since $G \sim K^2 \sim F^2$ we get $G(t) = G_{\max}(R + (1/2)(1-R)[1+\cos(\omega t)])^2$, where $R = F_0/F_1$. Substituting this result in $\mathrm{d}c/\mathrm{d}t = v_0(G/G_0)^{1/\alpha}$ and integrating from $t = 0$ to $t = T = 2\pi/\omega$ gives $\mathrm{d}c/\mathrm{d}N = \zeta(v_0 T)(G_{\max}/G_0)^{1/\alpha}$, where $\zeta = (1/2\pi)\int_0^{2\pi} \mathrm{d}\theta\,[(1/2)(1+R) + (1/2)(1-R)\cos\theta]^{2/\alpha}$. For $R = 1$ we get $\zeta = 1$ and for $R = 0$ and $\alpha = 0.25$ we get $\zeta \approx 0.196$.

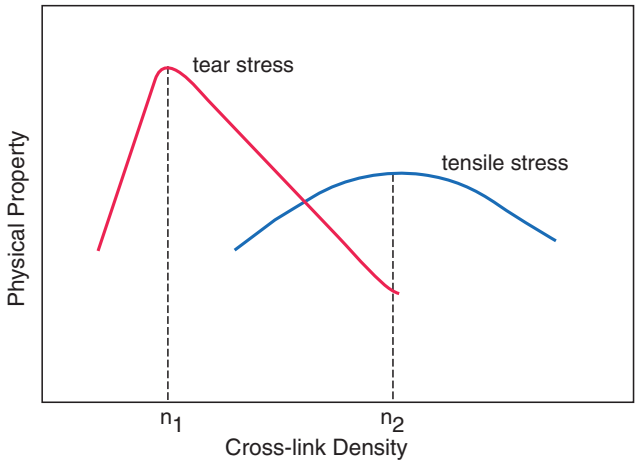

Figure 30. The dependence of the tear strength and the tensile stress on the cross-link density.

The topic of fatigue crack propagation in rubber is very wide and complex, and we refer the readers to two recent reviews for further details. The article by Selden [55] presents an overview of fracture mechanics analysis of fatigue of rubber, while Mars and Fatemi [58] study the factors which affect the fatigue life of rubber.

4. Relation between the tear strength, tensile strength and the internal friction of rubber-like materials

The tensile strength is determined by the stress σ_c needed to 'break' a (defect free) rubber block exposed to uniaxial stress. The tear strength is determined by the energy per unit area, G, to propagate a crack in a rubber block, and the internal friction, at a given frequency ω, is determined by the loss tangent $E_2(\omega)/E_1(\omega)$. The dependence of the tear strength and the tensile strength on the cross-link density typically take the form shown in figure 30. The tensile yield stress σ_c increases from zero, at zero cross-link density, and takes a maximum at a relatively high cross-link density. The tear strength has a similar dependence on the cross-link density. The loss tangent as a function of frequency ω is usually a broad Lorentzian-like peak (see figure 5), which shifts to lower frequencies with increasing cross-link density. These results can be understood as follows.

Rubber without cross-links is a (high viscosity) fluid, which flows when exposed to arbitrary low external stress, so the tensile yield stress (at low elongation speed) vanishes at zero cross-link density. For a cross-linked material, the applied stress will distribute itself on the cross-links. Thus, the average tensile force acting on a cross-link will decrease as the cross-link density increases. Since a (cross-link) bond will not break until the tensile force has reached some critical value, the tensile yield stress, σ_c, will increase with increasing cross-link density. However, at very high cross-link density the tensile yield stress will decrease for the following reason. Because of the inhomogeneous nature of rubber-like materials, there will be a wide distribution of tensile forces acting on the cross-links during tensile loading. Thus, some cross-links will break when the applied stress is well below the critical stress for tensile failure. When the cross-link density is not too high, the rubber in the vicinity of the broken cross-link can rearrange itself in a fluid-like manner and remove (or reduce) the stress concentration which otherwise would occur in the vicinity of the broken bond. However, this

will not be the case at very high cross-link density where the material will be brittle-like, and where strong stress concentration will occur in the vicinity of the broken bond leading to further bond breaking—and even higher stress concentration—and finally to a crack-like defect propagating rapidly across the cross section of the rubber block. The discussion above assumes that the rubber block has no (large) crack-like defects to start with. If such large cracks occur the tensile strength of the rubber block would be much smaller, and determined by the tear strength of the material.

The internal friction of rubber-like materials originates from stress-biased thermally activated transitions, where segments of the polymer chains flip between different configurations. At low cross-link density small energy barriers separate the different configurational states, and the polymer segments can (at high enough temperature) rapidly switch from one state to another. This results in short rubber relaxation times, and consequently the maximum of the loss tangent $E_2(\omega)/E_1(\omega)$ will be centred at a 'high' frequency $\omega = 1/\tau$. However, at high cross-link density the movement of the polymer segments is highly restricted (i.e., the barriers for configurational changes have increased), resulting in longer rubber relaxation times (i.e., τ increases), and the maximum of the loss tangent is shifted to lower frequencies. At very high cross-link density the 'height' of the viscoelastic loss peak is also reduced. At extremely high cross-link density, rubber behaves as any normal 'hard' solid with a low internal friction.

Let us now discuss the tear strength of rubber for relatively low crack-tip velocities. The tear strength is related to the energy $G(v, T)$ necessary to propagate a crack one unit surface area. Note that G depends in general on the temperature T and the crack-tip velocity v, and can be written according to (1):

$$G = G_0 [1 + f(v, T)]$$

where G_0 is the energy per unit area necessary to break the bonds at the crack tip, while $f(v, T)$ arises from the viscoelastic energy dissipation in front of the tip (see section 3 and figure 6). The function $f(v, T)$ is usually much larger than unity, and we can therefore approximate $1 + f \approx f$ so that the crack propagation energy G is simply the product of G_0 and f. Now let us focus on the case where the crack propagates with a low velocity but still $v \gg v_0$. In this case $f(v, T) \approx (v/v_0)^\alpha$ where $\alpha \approx 0.3$. Thus

$$G \approx G_0 (v/v_0)^\alpha \sim \sigma_c^2(v, T)\tau_0^\alpha / E(0). \tag{25}$$

Now, $1/E(0)$ (the inverse of the low-frequency elastic modulus) will decrease with increasing cross-link density. However, the rubber relaxation time τ_0 will increase with increasing cross-link density. The product in (25) will be maximal at some cross-link density between zero and one, and take the general form shown in figure 30.

5. Dependence of crack propagation on rubber properties

Many types of rubber are used in practical applications and they are (almost) always cross-linked and usually contain filler particles. Cross-linking and filler particles have great influence on rubber friction and on the tear strength of rubber. In this section we will briefly describe how these properties depend on the rubber micro-structure, the cross-link density and the concentration of filler particles.

5.1. Dependence on rubber molecular structure

A broad range of molecular mobilities and therefore viscoelastic spectra is obtained by using polymers with different side groups. Large side groups increase the barrier for local

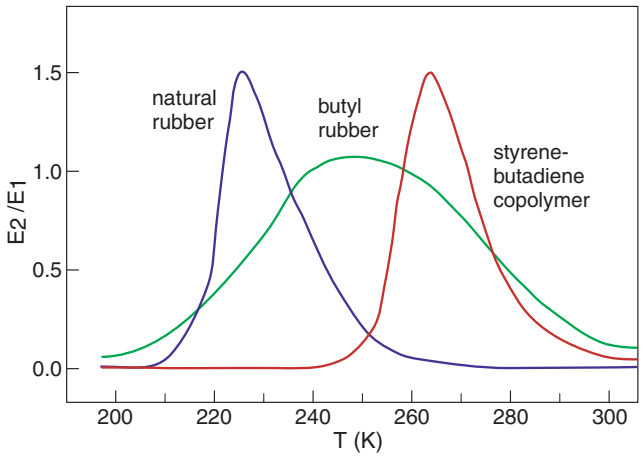

Figure 31. The loss tangent E_2/E_1 as a function of temperature for the deformation frequency 10 Hz. Results are shown for three standard rubber materials.

configurational changes and hence increase the rubber relaxation times and (at a fixed temperature) shift the viscoelastic peak to lower frequencies or, equivalently (at a fixed frequency), to higher temperatures. Here we focus on the loss tangent E_2/E_1 (at 10 Hz deformation frequency), as this quantity is directly relevant for the rubber friction and wear. Figure 31 shows the loss tangent E_2/E_1 as a function of temperature for natural rubber, butyl rubber and a styrene–butadiene rubber, all weakly cross-linked and with low (carbon black) filler concentration [34]. Note that in the temperature range $T > 280$ K the butyl rubber has the highest loss tangent followed by styrene–butadiene rubber and then natural rubber. This is also the ranking of the rubbers with respect to friction at typical sliding velocities involved in tyre applications [35]. One expects the tear strength at relatively low crack-tip velocities to have a similar ranking as the friction, since it too depends mainly on the viscoelastic modulus for relatively low frequencies (or high temperatures). This is confirmed by tear measurements by Ahagon *et al* [36] for butadiene rubber and styrene–butadiene rubber (for natural rubber the situation is more complex because of strain crystallization). The experiments were performed at room temperature and at low crack-tip velocities (of order $\sim 10^{-5}$ m s^{-1}). The viscoelastic peak in butadiene rubber is centred at very high frequency (higher than for natural rubber) and consequently one expects a much smaller crack propagation energy for butadiene rubber compared to styrene–butadiene rubber. This is in accordance with the experiments, where for butadiene rubber (without filler) $G \approx 86$ J m^{-2} (at $T = 120\,^{\circ}$C, $G \approx 59$ J m^{-2}), while for styrene–butadiene rubber (without filler) $G \approx 2100$ J m^{-2}. For styrene–butadiene copolymer rubber with 54% carbon black the crack propagation energy was even higher, $G \approx 30\,000$ J m^{-2}, which indeed is expected (see section 5.3).

5.2. Dependence on cross-link density

Figure 32 shows the loss tangent (at 10 Hz deformation frequency) for an unfilled styrene–butadiene rubber as a function of the sulfur concentration [37]. In this case the cross-links are formed by sulfur bridges and the concentration of cross-links is expected to increase continuously with the sulfur concentration. Note that the loss tangent shifts to higher temperatures as the sulfur concentration increases. This means that the activation barriers for motion of polymer segments increase with increasing cross-link density. This is, of course,

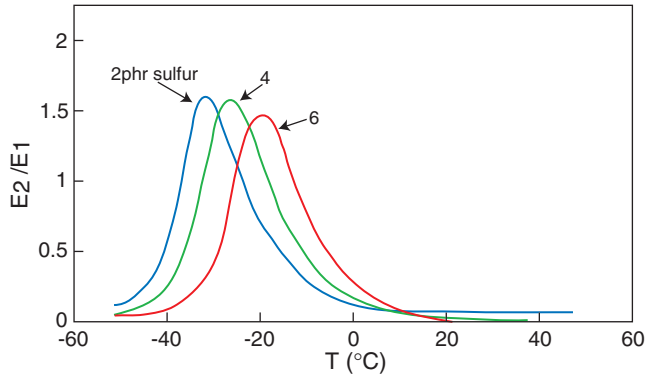

Figure 32. The loss tangent E_2/E_1 as a function of temperature for the deformation frequency 10 Hz. Results are shown for several sulfur concentrations.

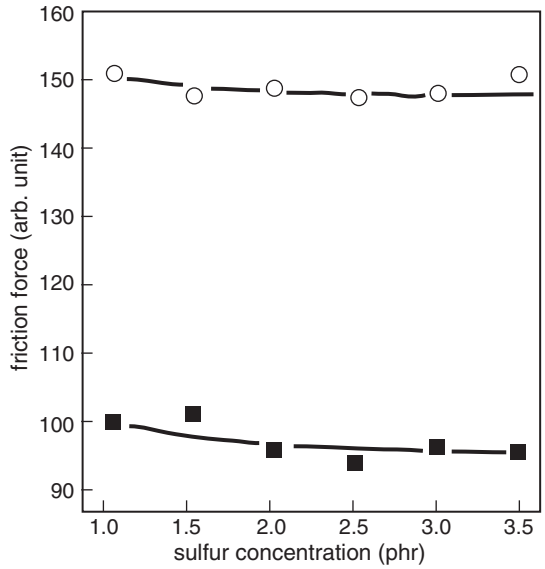

Figure 33. Friction force measured as a function of sulfur concentration for two different rubber compounds.

the expected result as the cross-links severely limit the motion of polymer segments close to the cross-links. The shift of the loss tangent, as a function of temperature, to higher temperatures is equivalent of a shift of the loss tangent, as a function of frequency, to lower frequencies. This will increase both the rubber friction and the tear strength. However, increasing cross-link density also increases the real part of the elastic modulus (the rubber gets stiffer), which will reduce the rubber–substrate contact area, which will reduce the friction. As a result of both effects there is usually only a relatively small change in the rubber sliding friction; see figure 33 for one example [38]. The dependence of $G(v)$ on the cross-link density was discussed in section 4.

Although the influence of the cross-link density on the viscoelastic modulus is similar to the way the steric hindrance of side groups of the polymer affects the viscoelastic modulus, a more

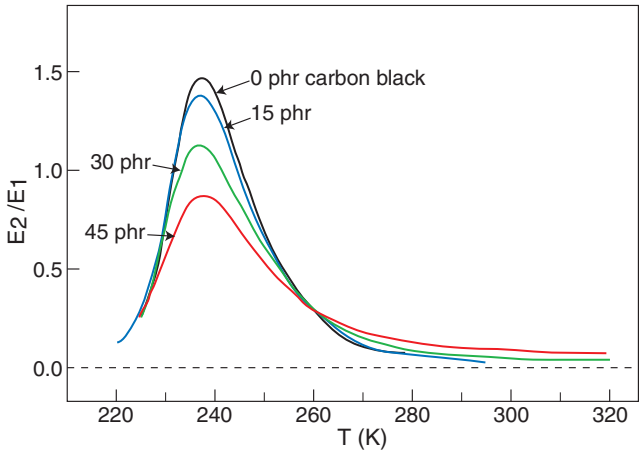

Figure 34. The loss tangent E_2/E_1 as a function of temperature for the deformation frequency 10 Hz. Results are shown for several concentrations of carbon-black filler particles.

detailed study shows that the mobility of the polymer chain segments is affected differently by cross-linking and polymer side groups; see [39].

5.3. Dependence on filler concentration

Figure 34 shows the dependence of the loss tangent (of a weakly cross-linked styrene–butadiene rubber) on the (carbon black) filler concentration [34]. As the filler concentration increases from zero to 45% volume fraction, the maximum value of loss tangent decreases by roughly 60% and the tail of the loss tangent towards increasing temperatures increases. This can be understood as the result of the decreased mobility of one or a few layers of hydrocarbon chains bound (physisorbed in the case of carbon black and chemisorbed for more active fillers such as silica) to the surfaces of the filler particles. At the same time the rubber elastic modulus (at low frequencies) increases. Both effects will reduce the maximal friction coefficient, as indeed observed experimentally by Grosch [40]. However, the friction at low sliding velocities will increase because of the increased high-temperature tail of the loss tangent. This is again in agreement with experimental data [40]. Similarly, the tear strength will increase because of the increase of the high-temperature tail of the loss tangent.

6. Applications

Here we present a few applications involving the propagation of cracks in rubber. We consider first the propagations of cracks at the interface between a smooth rubber surface and a smooth substrate surface, e.g., a steel or glass surface. Such interfacial cracks may have a large influence on the adhesion and sliding friction between the bodies. We also consider rubber wear, e.g., as a tyre slides on a road surface.

6.1. Adhesion between smooth surfaces

Many aspects of adhesion involve crack propagation. Here we consider the perhaps most fundamental and well defined adhesion problem, namely a spherical (or cylindrical) object in adhesive contact with a flat substrate; see figure 35. Both surfaces are assumed to be perfectly smooth and clean and at least one of the solids elastically soft.

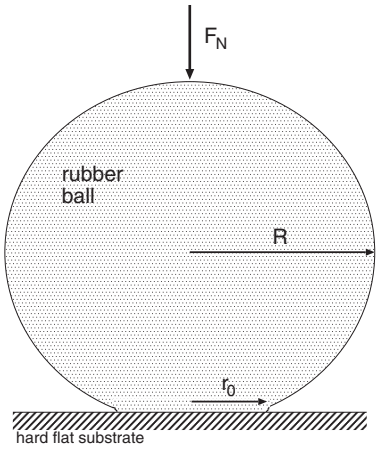

Figure 35. A rubber ball in contact with a hard flat substrate. The contact region is circular with the radius r_0. The radius of the ball $R \gg r_0$. The applied force F_N can be either positive (squeezing) or negative (pull-off).

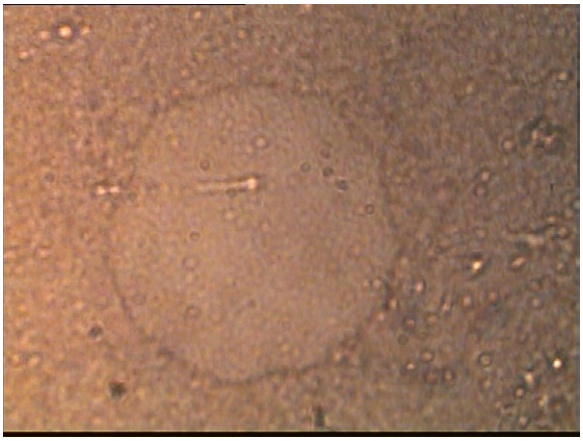

Figure 36. Snap shot picture of the contact area between a silicon rubber ball and a clean epoxy substrate. The contact area is nearly circular. From [67].

Figure 36 shows a snapshot picture of the contact area between a soft silicon ball and a clean flat epoxy substrate. The contact area is nearly circular. Figure 37 shows a snap shot picture of the contact area between another silicon rubber ball and a contaminated epoxy surface. The boundary line is very rough as a result of pinning effects induced by the contamination. In the experiments reported on in section 6.1.2 great care was taken to make sure that the surfaces studied were clean.

The analytical theory of the adhesive contact between an elastic ball and a flat was developed by Johnson, Kendall and Robers (JKR) [41]. The radius r_0 of the circular contact area and the elastic deformation fields in the solids can be determined by minimizing the total energy $U = U_{el} + U_{ad}$, where U_{el} is the elastic energy stored in the solids and $U_{ad} = -\pi r_0^2 \Delta\gamma$ is the change in the surface energy upon bringing the solids into contact, i.e., $\Delta\gamma = \gamma_1 + \gamma_2 - \gamma_{12}$ is the change in the surface free energy per unit area when flat surfaces of the two materials is brought into contact. The most important result of the study is the pull-off force

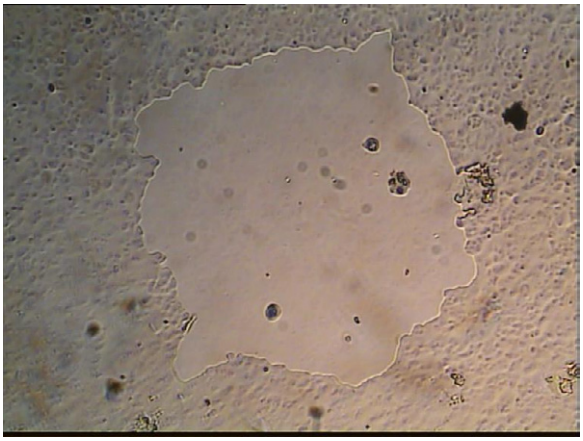

Figure 37. Snap shot picture of the contact area between a hard silicon rubber ball and a contaminated epoxy surface. The boundary line is very rough as a results of pinning effects induced by the contamination. From [67].

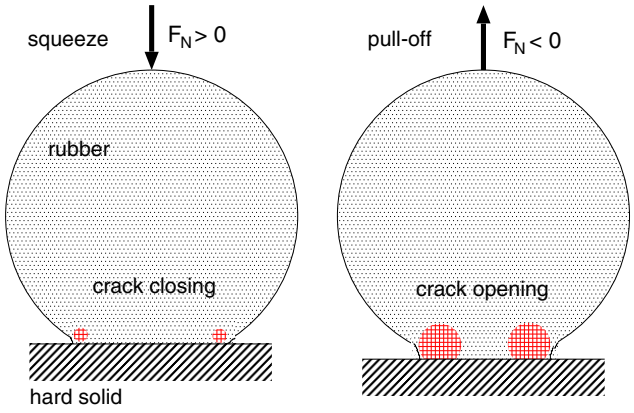

Figure 38. Contact between a viscoelastic sphere and a flat rigid surface. During squeezing, the contact area increases via the propagation of an interfacial closing crack. During pull-off, the contact area decreases via the propagation of an interfacial opening crack. In general, the bulk viscoelastic energy dissipation close to the crack tips (red dashed area) is much higher for the opening crack than for the closing crack.

determined by

$$F_{\text{pull-off}} = 3\pi R\Delta\gamma/2. \tag{26}$$

The discussion above is only valid for purely elastic solids. For viscoelastic solids, which interest us here, it is not useful to discuss the energy, but one must consider the stress distribution directly. Thus, consider a viscoelastic sphere squeezed against (or pulled away from) a hard flat substrate. By symmetry, the contact area between the ball and the substrate will be circular with a time dependent radius $r_0(t)$, and we can define the velocity $v = -\dot{r}_0(t)$, which is positive for crack opening. We can consider the circular boundary line of the contact region as a *crack* which propagates with the (radial) velocity v. This novel and fundamental idea was first proposed by Westergaard in 1939 [42]. When $v < 0$ we have a closing crack while when $v > 0$ we have an opening crack; see figure 38. We now make the basic assumption that the

perturbing frequencies in the rubber are so small that the ball behaves purely elastically with the elastic modulus $E(\omega = 0) = E_0$ everywhere, except in the vicinity of the crack edge. Thus, the stress distribution in the ball will be the same as for a purely elastic solid, except very close to the crack edges. When an elastic ball is squeezed against a flat substrate the pressure distribution acting in the contact area is given by [43]

$$P(r) = \frac{2E^*}{\pi R}\left(r_0^2 - r^2\right)^{1/2} - C\left(r_0^2 - r^2\right)^{-1/2} \tag{27}$$

where C is a so far unknown constant. In (27) the effective elastic modulus E^* is defined by

$$1/E^* = (1 - \nu_1^2)/E_1 + (1 - \nu_2^2)/E_2$$

where ν_1 and E_1 are the Poisson ratio and the elastic modulus of solid 1, and similarly for solid 2. Equation (27) is valid everywhere in the contact area except very close to the crack edge. Close to the crack edge $r = r_0$ the last term in (27) has the expected stress singularity $\sim x^{-1/2}$ (where $x = r_0 - r$):

$$P(r) \approx -C(2r_0)^{-1/2}x^{-1/2}.$$

Thus, the stress intensity factor $K = (\pi/r_0)^{1/2}C$. However (see appendix A), $K = (GE^*)^{1/2}$, where $G(v) = 2\gamma_{\rm eff}$ is the crack propagation energy. Thus, $C = (r_0 GE^*/\pi)^{1/2}$, and substituting this in (27) gives the pressure distribution everywhere in the contact region except very close to the boundary line $r = r_0(t)$. The total load $F_{\rm N}$ is obtained by integrating the pressure distribution (27) over the contact area $r < r_0$, which gives

$$F_{\rm N} = \frac{4E^* r_0^3}{3R} - 2r_0^{3/2}(2\pi E^* \gamma_{\rm eff})^{1/2}. \tag{28}$$

In the case where $\gamma_{\rm eff}$ is independent of the velocity v (which may not be strictly true even if the solids are purely elastic, because the bond-breaking processes at the interface will in general depend on the separation velocity, which is proportional to v) the pull-off force can be determined by minimizing (28) with respect to r_0, which gives the JKR result (26). In general, when $\gamma_{\rm eff}(v)$ depends on the crack-tip velocity $v(t) = -\dot{r}_0(t)$, equation (28) becomes a differential equation for $r_0(t)$. In some experiments the time dependence of the displacement of the centre of mass of the ball is prescribed, rather than $F_{\rm N}(t)$. However, under the assumption above, that the bulk of the ball behaves purely elastically, the displacement of the centre of mass is related to $F_{\rm N}(t)$ via the Hertz contact theory.

The theory above is based on a crucial assumption: the deformation rate in the ball must be so small that the ball behaves purely elastically everywhere except in small region close to the crack edge. This implies that the contact mechanics theory is only valid if the radius R of the rubber ball and the radius r_0 of the contact area are large enough. Here the statement 'large enough' in fact depends on the squeeze or the pull-off speed since the size of the dissipative region close to the crack edge increases with the speed of the crack edge. Thus, for a crack which propagates with the speed 10 cm s^{-1} the dissipative region may extend more that 10 μm away from the crack tip edge (see section 3.6) and this distance must be *much* smaller than the radius r_0 in order for the theory to be valid. Thus, for fast separation, the theory may be limited to macroscopic bodies and relatively soft viscoelastic solids so that r_0 is large enough.

6.1.1. Three applications. We now present three applications of the results presented above.

Contact between a rubber ball and a flat smooth glass surface. Contact adhesion experiments have been performed by placing thin microscope coverslips of glass on different compounded rubber balls (see figure 39) with optically smooth surfaces [44]. Since the coverslip weight

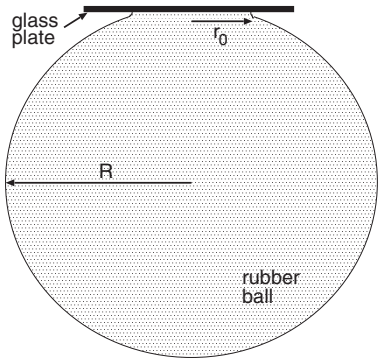

Figure 39. A glass plate adhering to a rubber ball.

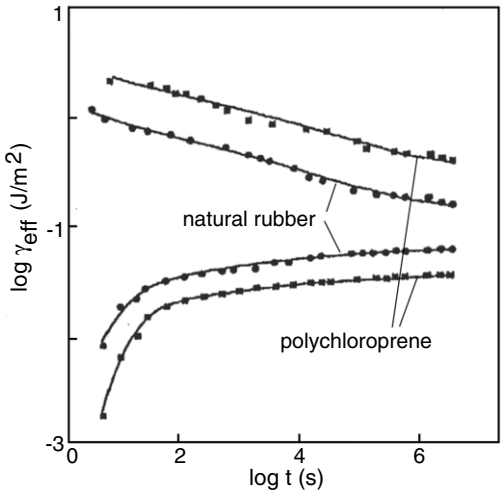

Figure 40. The logarithm (with 10 as basis) of the effective surface energy γ_{eff} as a function of the logarithm of the contact time deduced from the time dependence of the contact area between rubber balls and glass surfaces. Results are shown for natural rubber and for polychloroprene rubber. Values of γ_{eff} were calculated from (29). The upper two curves are for 'overloading' and the lower two for 'underloading'. Adapted from [44].

was less than 0.1 g, it could be neglected compared to the apparent joining load due to the surface attractive forces. For zero load, equation (28) takes the form

$$r_0^3 = \frac{27\pi R^2 \gamma_{\text{eff}}}{8E_0} \tag{29}$$

where we have assumed the Poisson ratio $\nu = 1/2$ as is typical for rubber. The initial radius $r_0(0)$ will be either smaller or larger than the equilibrium radius r_{eq} depending on how the glass surface was brought into contact with the rubber ball. In figure 40 we show the time evolution of γ_{eff} (obtained from (29)) for both *underload* ($r_0(0) < r_{\text{eq}}$), where the coverslips were brought very gently into contact with the rubber balls, and for *overload* ($r_0(0) > r_{\text{eq}}$), where the coverslips were pressed firmly onto the rubber balls. In the former case the contact area grows with increasing time due to crack closing, while in the latter case the contact area decreases due to crack opening. Figure 40 shows results for natural rubber and for polychloroprene, with

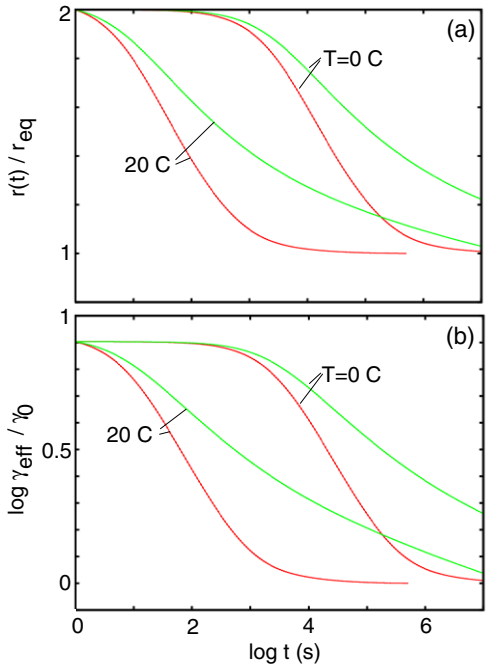

Figure 41. The radius of the contact area (a) and the effective interfacial energy (b), as a function of the logarithm (with 10 as basis) of the contact time. Results are for a styrene butadiene copolymer without (red curves) and with (green curves) filler and for the temperatures $T = 0$ and 20 °C.

the low-frequency modulus $E_0 \approx 1.7$ and 2.0 MPa, respectively. Note that even after more than 1 month of contact the contact area has not reached its equilibrium value, but continues to decrease for the overload situation and continues to increase for the underload situation. The interfacial surface energy can be estimated by extrapolation to infinitely long contact time, which gives about $\Delta\gamma \approx 0.1\,\mathrm{J\,m^{-2}}$ or 6 meV $\mathrm{Å}^{-2}$ for the rubber–glass interface. However, the effective interfacial energy for short contact time during overloading is much higher because of the large enhancement in γ_{eff} when the (opening) crack propagates 'fast'. This reflect sthe wide distribution of relaxation times in rubber materials.

The interfacial energy γ_{eff} occurring in (29) is a function of the crack-tip velocity and (29) is therefore a differential equation for $r_0(t)$ which can be solved to obtain the time evolution of the radius of the contact area. Thus, if we write $\gamma_{\mathrm{eff}} = \gamma_0 F(v)$ and if we denote

$$b = \left(\frac{27\pi R^2 \gamma_0}{8E_0}\right)^{1/3} \tag{30}$$

and $r_0(t) = by(t)$, then (29) takes the form

$$y^3 = F(b\dot{y})$$

where $\dot{y} = \mathrm{d}y/\mathrm{d}t$. It is also convenient to introduce $x = \log(t/t_0)$, where t_0 is a reference time. Thus $\dot{y}(t) = y'(x)\mathrm{e}^{-x}/t_0$ where $y'(x) = \mathrm{d}y/\mathrm{d}x$, and we get

$$y^3 = F(v_1 y' \mathrm{e}^{-x}) \tag{31}$$

where $v_1 = b/t_0$ is a reference velocity. If we measure time in seconds (i.e., $t_0 = 1$ s) then typically $v_1 \approx 5 \times 10^{-4}\,\mathrm{m\,s^{-1}}$.

In figure 41 we show the calculated radius of the contact area (a) and the effective interfacial energy (b), as a function of the logarithm (with 10 as basis) of the contact time. Results are for a

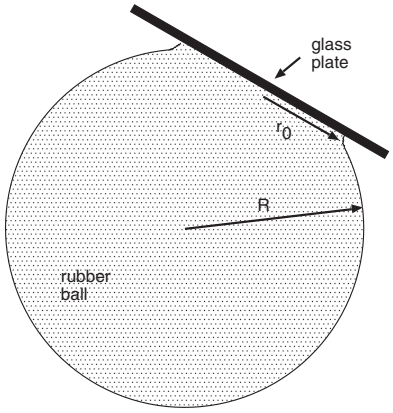

Figure 42. The glass plate on the clean rubber ball does not roll with any measurable velocity. However, if the rubber surface is powdered with French chalk, once displaced the glass plate will oscillate for some time before coming to rest.

styrene butadiene copolymer without (red curves) and with (green curves) filler (60% carbon), and for the temperatures $T = 0$ and 20 °C. We have assumed overload, where the initial radius $r(0) = 2r_{\rm eq}$. Note the much slower approach to equilibrium for the filled compound, which reflects the much wider distribution of relaxation times in filled rubbers. For the unfilled SB rubber, the approach to thermal equilibrium is much faster than observed for natural rubber and polychloroprene (see figure 40).

Roberts and Thomas also observed that coverslips adhering to rubber balls could not be rolled over them; see figure 42. For a perfectly elastic sphere the coverslip rolls easily because the energy 'lost' over the rear half of the circle of contact as surface is created will be fully compensated for by the energy 'gained' over the front half of the contact circle. This does happen if the rubber sphere is rough or powdered with chalk. However, for smooth surfaces a very considerable force F must be applied to make the coverslip roll; that is, the energy required to create surface by peeling apart the coverslip and the rubber over the trailing edge of the contact circle is far greater than that gained as surfaces come together over the leading edge. This just reflects the much larger energy necessary to propagate an opening crack as compared to the gain in energy during crack closing, which results from the bulk viscoelastic deformations in the vicinity of the crack tip.

Release of steel ball from a flat smooth rubber surface under gravity. If a clean plane rubber surface is brought firmly into contact with a steel ball and then raised, the ball will, in general, detach itself in time under the action of gravity. This phenomenon is recognized as 'tackiness'.

The situation is shown in figure 43. In the present case the force in (28) is the gravity force $F_{\rm N} = 4\pi R^3 \rho g/3$, where ρ is the mass density of the ball, so that

$$\gamma_{\rm eff} = \frac{1}{6\pi E_0 r_0^3}\left(\frac{4E_0 r_0^3}{3R} + \pi R^3 \rho g\right)^2. \tag{32}$$

We assume that the crack propagation energy depends on the crack tip velocity $v = -{\rm d}r_0/{\rm d}t$ according to equation (19)

$$\gamma_{\rm eff} \approx \gamma_0 (v/v_0)^{\alpha}.$$

Substituting this in (32) gives a differential equation for $r_0(t)$, which can be integrated to give the detachment time t_1 defined by $r_0(t_1) = 0$. In [44] the calculated detachment time

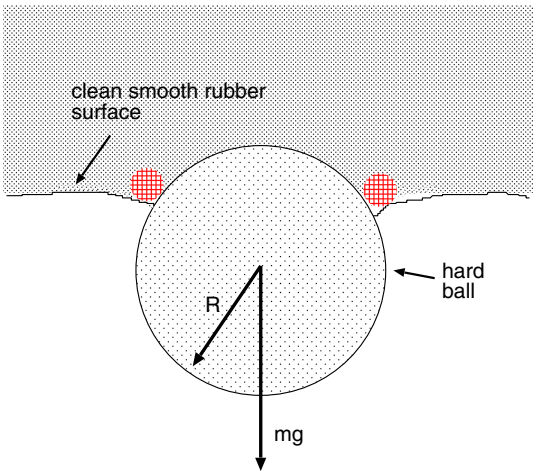

Figure 43. A hard ball in contact with a rubber ceiling. The ball detaches from the ceiling after a contact time t_1.

was compared to the measured time for steel balls of different sizes, in contact with both natural rubber and polychloroprene rubber surfaces. In the calculations, the parameter $\gamma_0 v_0^{-\alpha}$ and the exponent α was determined from independent experiments involving interfacial crack propagation. In all cases the agreement between the theory and experiment was very good, indicating that the basic assumption that the detachment time is determined mainly by the propagation of a circular crack is correct.

The crack propagation energy for the crack velocities involved in the ball detachment is higher for polychloroprene rubber than for natural rubber (because it has a higher glass transition temperature). This explains why the ball detachment times for the polychloroprene surface (170, 21 and 7 s, for steel balls with the radius $R = 0.24, 0.39$ and 0.55 cm, respectively) were found to be longer for the natural rubber surface (4, 0.5 s and less than 0.25 s, respectively). The detachment time was also very sensitive to the temperature, and a 4 °C change in the temperature altered the detachment time by a factor of two. This is again expected because of the strong temperature dependence of the viscoelastic modulus $E(\omega)$ of rubber.

For softer rubber compounds, and for other geometries, e.g., the contact between flat surfaces, more complex processes, such as the formation of interfacial cavities, may occur. This is often the case in practical studies of tackiness, e.g., involving pressure sensitive adhesives, and we will briefly discuss this point in section 6.2.

Steel balls bounced off a flat smooth rubber surface. It has often been observed that small steel balls do not rebound very much, or sometimes not at all, from the surface of clean rubber when dropped onto it (see figure 44). Dusting the surface increases the rebound. This phenomenon is due to the adhesion and crack propagation at the interface between the ball and the rubber, and is of the same character as that phenomenon studied above.

As the ball collides with the rubber it indents it as illustrated in figure 44. The amount of indentation and the maximum radius of the circle of contact is often well described by the Hertz contact theory even for the large strain experienced in the rubber [46]. For a perfectly elastic solid the elastic energy stored in the solid during indentation is fully recovered by the ball during movement of the ball out of contact, and in this case (neglecting the air resistance) the ball will bounce back to the same height from which it was dropped on the substrate, which

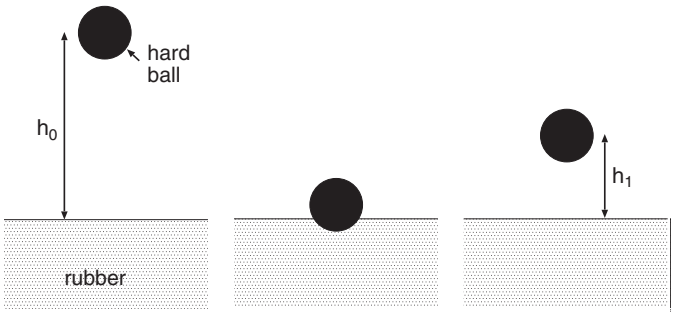

Figure 44. A hard ball dropped on a clean smooth rubber surface. The rebound height h_1 is smaller than the drop-off height h_0 because of energy 'dissipation' in the rubber.

is often the case for dusted rubber. However, for a clean rubber surface during the movement of the ball out of contact with the rubber work has to be done to peel the rubber off the rigid surface, and this energy will be the amount by which the surface adhesion effect reduces the resilience.

As in the release of a ball under gravity, the crack-tip velocity during peeling is given by $v = -\mathrm{d}r_0/\mathrm{d}t$. Using (23) it is possible to obtain a differential equation relating the dynamics of the movement of the ball to the parameters of the system. Such a study was presented by Roberts and Thomas in [44], and the theory was found to be in excellent agreement with experiments performed by the same authors. In particular, small steel balls were always observed to stick on polychloroprene rubber, while on natural rubber they either stick or bounce back, depending on the height above the rubber surface from which they were dropped.

6.1.2. Adhesion and overload experiments involving silicon rubber. Silicon rubber is usually considered as a nearly ideal elastic solid, at least with respect to 'slow' experiments at room temperature. However, adhesion experiments have recently been performed [67] where silicon rubber balls were pulled off slowly (speed $\sim$0.1–1 μm s^{-1}) from epoxy substrates. From the pull-off force the effective interfacial energy was calculated using the JKR theory. The measured $\gamma_{\mathrm{eff}} \approx 0.13$ J m^{-2} is a factor of $\sim$2–3 times larger than expected for the thermal equilibrium PDMS–epoxy interfacial binding energy (for PDMS in contact with PDMS [68], and for PDMS in contact with acrylic resin [69] we have $\Delta\gamma \approx 0.05$ J m^{-2}, and we expect a similar value for PDMS in contact with epoxy resin). This enhancement is caused by viscoelastic energy dissipation at the opening crack during pull-off. To prove this, in figure 45 we show the variation of the crack propagation energy with the crack tip velocity calculated from equation (14*b*) using the measured viscoelastic modulus $E(\omega)$. Here $G_0 = \Delta\gamma$ is the thermodynamic (infinitesimally slowly propagating crack) value for the interfacial binding energy. The dotted region indicates the typical crack-tip velocities during pull-off (which are higher than the pull-off velocity by roughly a factor of 10). Note that G is typically a factor of two to three larger than G_0 in the relevant velocity range, in good agreement with the experimental observations [67].

Let us present results of overload experiments [67] which show that silicon rubber exhibits viscoelasticity even for very 'slow' experiments. In figure 46 we show the radius of the time-dependent contact area between a silicon rubber ball and a thin plate after 'overloading', where the two solids are first squeezed into contact resulting in a larger contact area than the equilibrium area. The equilibrium state is only reached after $\sim$8 h of contact.

In figure 47 we show the crack propagation energy $G/G_0 = a(v)/a_0$ as a function of the crack-tip velocity as obtained using equation (14*b*). In the calculation we have used the

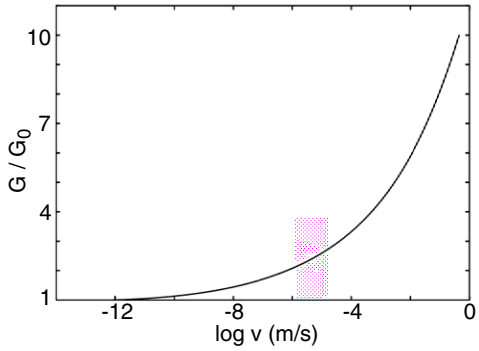

Figure 45. The calculated crack propagation energy G/G_0 as a function of the crack tip velocity v for $T = 28\,^{\circ}\mathrm{C}$. In the calculation we used the measured viscoelastic modulus $E(\omega)$ for a silicon rubber with the low-frequency modulus $E = 2.3$ MPa and for $a_0 = 1$ nm.

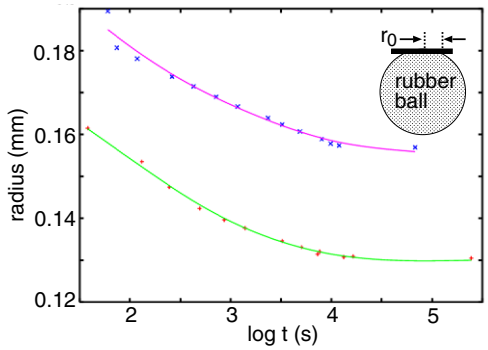

Figure 46. The radius $r_0(t)$ of the time-dependent contact area between a rubber ball and a surface after 'overloading', where the two solids are first squeezed into contact, resulting in a larger contact area than the equilibrium area. The equilibrium state is reached after ~8 h of contact. For a PDMS silicon rubber ball at $T = 25\,^{\circ}\mathrm{C}$, in contact with two epoxy surfaces with slightly different surface roughnesses. From [67].

measured viscoelastic modulus for the PDMS silicon rubber used in figure 46, with the low-frequency elastic modulus $E \approx 0.6$ MPa.

In figure 48 we compare the calculated radius of the time-dependent contact area between a rubber ball and a surface after 'overloading', with the measured data from figure 46. The theoretical results were obtained from equation (31) with $r_0(0) = 2.0\, r_{\mathrm{eq}}$, and using the crack propagation energy $G(v)/G_0$ from figure 47 for $T = 25\,^{\circ}\mathrm{C}$. We note that in the time interval shown in figure 48, $r_0(t)$, is *independent* of $r_0(0)$ as long as $r_0(0) > 1.5\, r_{\mathrm{eq}}$. In the calculation we have also used $v_1 = 1.25 \times 10^{-4}$ m s^{-1} as obtained from equation (30). Note the remarkably good agreement between theory and experiment both with respect to the curve-form and the decay rate: in both theory and experiment it takes about 8 h to reach the equilibrium state. This constitutes the first detailed experimental test of the rubber crack propagation theory for very small crack propagation velocities where $\log G$ depends non-linearly on $\log v$ (see figure 47).

For an elastically harder rubber than above (with the low-frequency modulus 2.3 MPa instead of 0.6 MPa) we obtain a decay constant which is slightly larger than that for the softer rubber; see figure 49(b). Since an increase in the cross-link density will decrease the mobility of the polymer segments, and hence increase the rubber relaxation times, one indeed expects

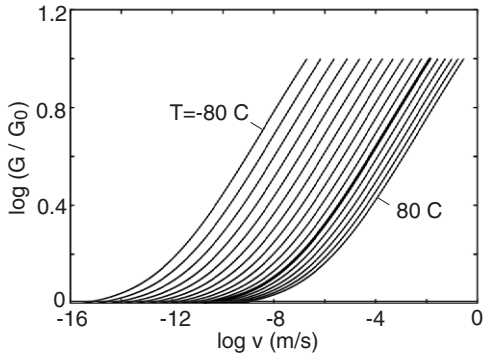

Figure 47. The crack propagation energy G/G_0 as a function of the crack-tip velocity v for several different temperatures. The results have been calculated from (14*b*) using the measured viscoelastic modulus for the soft PDMS. The thicker line is for $T = 30\,^{\circ}\mathrm{C}$. In the calculation we used $a_0 = 1$ nm.

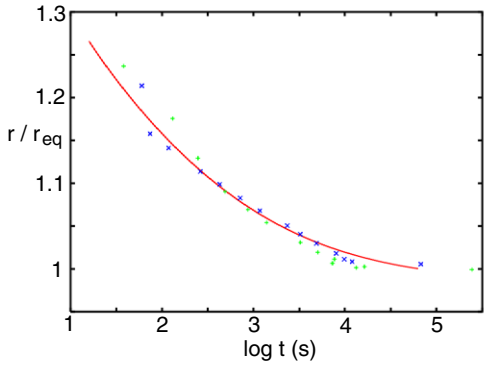

Figure 48. The calculated (using equation (31)) radius of the time-dependent contact area between a rubber ball and a surface after 'overloading', where the two solids are first squeezed into contact, resulting in a larger contact area than the equilibrium area, $r_0(0) = 2.0\, r_{\mathrm{eq}}$. The $\times$ and + symbols are the experimental data from figure 46.

a slower time variation of $r_0(t)$ for the higher cross-linked rubber, in qualitative agreement with the theoretical results. Figure 49(a) shows the effective interfacial binding energy $\gamma_{\mathrm{eff}}(t)$. Note that $\gamma_{\mathrm{eff}}(t)/\Delta\gamma$ is below 1.8 in the studied time interval, which implies that the results only depend on the crack propagation curve for $\log(G/G_0) < 0.25$.

To summarize, overload experiments show that even silicon rubber, which has the lowest glass transition temperature of all known rubbers, is not perfectly elastic even with respect to apparently very 'slow' experiments. The reason for this is that the breaking of the bonds between the rubber ball and the substrate occurs via the propagation of a (circular) interfacial crack, from the periphery of the contact area towards the centre. At the crack edge the strain rate may be very high. Thus we may define a deformation frequency $\omega = \omega_1 = v/a$, where v is the crack-tip velocity and where a is a cut-off distance, which can be interpreted as the crack-tip radius. For a slowly moving crack $a \approx 1$ nm and if $v \approx 1\ \mu\mathrm{m\ s}^{-1}$ we get $\omega_1 \approx 10^3\ \mathrm{s}^{-1}$. For the soft silicon rubber at room temperature $\mathrm{Im}\, E(\omega_1)/\mathrm{Re}\, E(\omega_1) \approx 0.15$; thus considerable viscoelastic energy dissipation may be expected close to the crack edge, and the rubber cannot be considered as perfectly elastic.

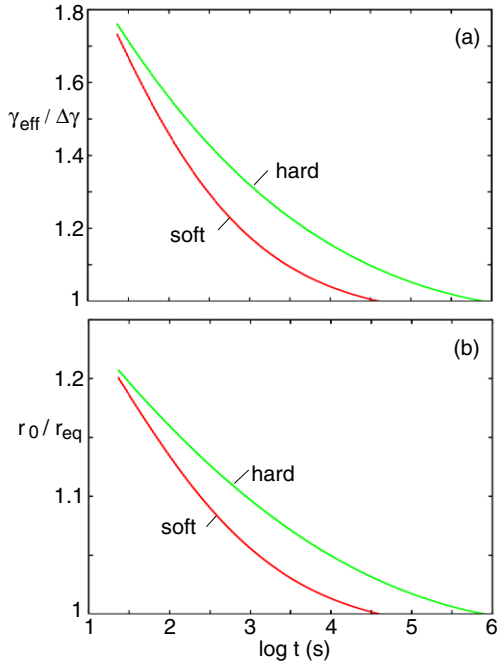

Figure 49. The calculated (using equation (31)) (a) effective interfacial energy $\gamma_{\rm eff}(t)/\Delta\gamma$, and (b) radius of the time-dependent contact area between a rubber ball and a surface after 'overloading', where the two solids are first squeezed into contact, resulting in a larger contact area than the equilibrium area, $r_0(0) = 1.3r_{\rm eq}$. In the calculation we have used the measured viscoelastic modulus for 'soft' and 'hard' PDMS silicon rubber with the low-frequency elastic modulus $E \approx 0.6$ MPa and ≈2.3 MPa, respectively, in contact with a flat substrate.

6.2. Tack

Pressure sensitive adhesives are used in many important applications, e.g., Scotch tape, post-it pads and self-adhesive labels and envelopes. The adhesives consist of very thin layers (usually of order ∼20–100 μm) of very soft (weakly cross-linked) rubber compounds. The low frequency elastic modulus is typically of the order of 10^5 Pa or less. As a result of the low elastic modulus, nearly complete contact will occur in the apparent contact area even for relatively rough surfaces and low squeezing pressures [66]. The theoretical description of the contact formation during squeezing is quite well understood [66]. However, the description of the dynamical processes occurring in the rubber compound during pull-off is much more complex and not fully understood [65]. Here we briefly discuss some aspects of pull-off involving interfacial crack propagation.

A typical tack experiment consist of squeezing a cylindric steel bar with a flat surface against a hard substrate with a thin layer of the rubber compound. After a given contact time (which may be of the order of ∼1 s) the steel bar is removed from the substrate with a constant pull-off velocity v_0; see figure 50. The inset in figure 50 shows a typical case where cavities and interfacial cracks appear in the rubber adhesive during pull-off. Figure 51 shows an example where the pull-off stress $\sigma = F/A$ (where A is the contact area) is plotted as a function of the strain $\epsilon = z/d$, where $z = v_0 t$ is the pull distance. The figure also shows three snapshot pictures of the rubber–substrate interface at three different strains indicated in the figure. For this particular system only interfacial cracks occur during pull-off.

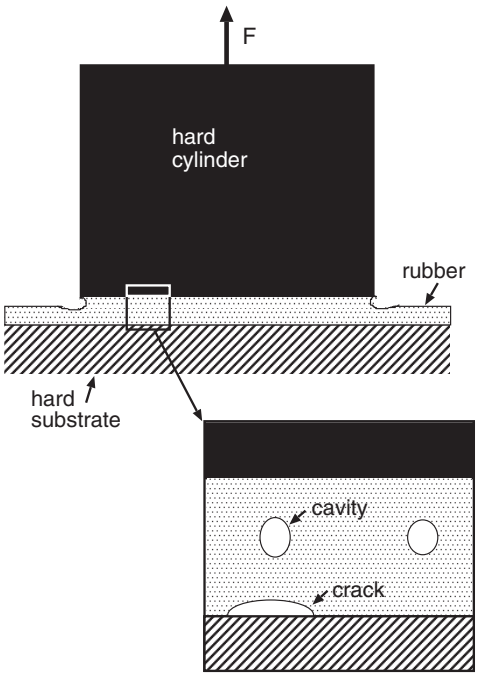

Figure 50. A typical configuration used for studying tackiness. During pull-off, cavities and interfacial cracks may appear in the rubber film.

Let us consider the following highly idealized model of the separation process during a tack test. Consider a $d \approx 100\ \mu$m thick rubber layer between two perfectly hard surfaces. We 'divide' the polymer film into cubic blocks $d \times d \times d$; see figure 52. Assume that at the rubber–substrate interface there occur small detached areas as a result of, e.g., surface roughness. The size of the detached areas will follow some (unknown) probability distribution but here we only focus on the largest detached area in each block. For simplicity, assume that the largest detached areas have the same linear size R_0 in each block.

Assume that the rubber can be treated as incompressible. Thus, as the upper hard surface is displaced by $z = v_0 t$ from the bottom surface (where v_0 is the separation speed and t the time of separation) the volume change $\Delta V = v_0 t d^2$ must be equal to the increase in the volume of the detached region which is given by $\sim R^2 h$ where the height of the detached area $h \approx (\sigma/E)R$ (where the elastic modulus E is defined below). Here $R = R(t)$ is the linear size of the detached area at time t with $R(0) = R_0$. Thus we get

$$v_0 t = \frac{\sigma}{E}\frac{R^3}{d^2}. \tag{33}$$

If $v = \dot{R}$ is the crack-tip velocity, then the energy per unit time to propagate the crack $\sim G(v)Rv$ must be equal to the local change in the elastic energy, which equals $\sim R^2 v(\sigma^2/E)$. Thus we get

$$G(\dot{R}) = R\sigma^2/E. \tag{34}$$

Combining (33) and (34) gives

$$G(\dot{R}) = (v_0 t)^2 d^4 E/R^5. \tag{35}$$

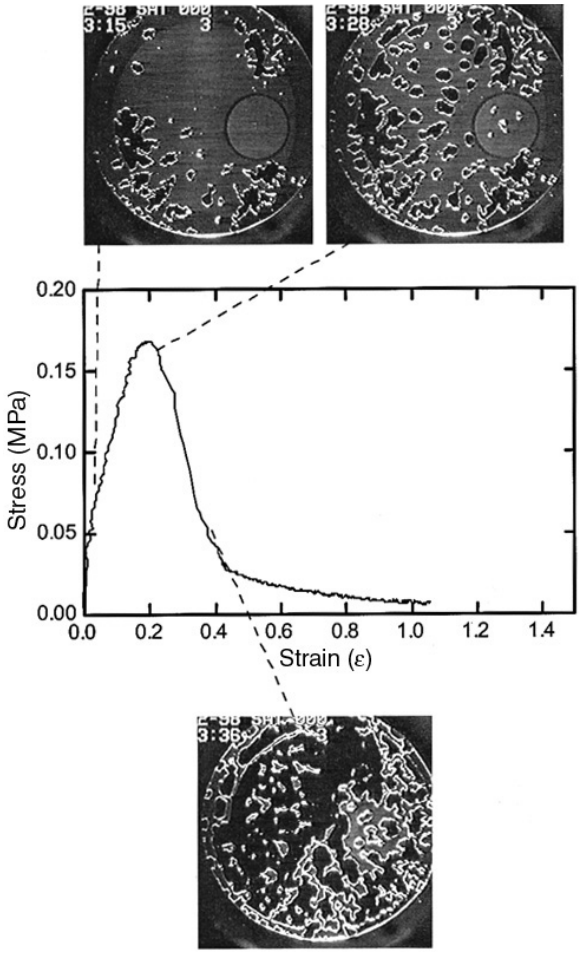

Figure 51. Bonding of a flat glass surface to a flat substrate by a thin film (∼100 μm) of a rubber tack compound. The steel surface is 'passivated' by a grafted monolayer of poly(dimethylsiloxane) (PDMS). Representative tack curve and corresponding contact area images for SIS adhesive adhering to a PDMS-coated probe. Probe velocity 1 μm s^{-1}. The three snap-shot pictures show the formation and propagation of interfacial cracks at the PDMS–rubber interface during (vertical) separation of the surfaces. Adapted from [61].

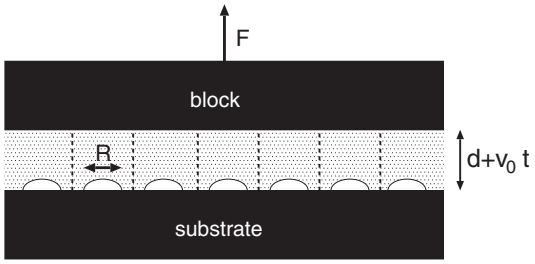

Figure 52. Interfacial cavity growth during the pull-off.

Let us write $y = R/R_0$ and $x = t/t_0$, where $t_0 = R_0/v_0$. We also write $G(v) = \gamma_0 F(v)$. Thus, (35) takes the form

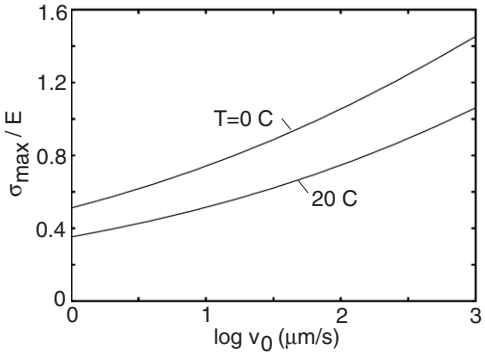

Figure 53. The calculated maximal stress during pull-off as a function of the logarithm (with 10 as basis) of the pull-off velocity v_0. In the calculation we have used the viscoelastic modulus for the tack compound shown in figure 18, for which the crack propagation energy has the form shown in figure 19. For $Q_0 = 10^9$ and $Q_1 = 10^3$.

$$F(v_0 y') = Q_0 \frac{x^2}{y^5}$$

and the stress

$$\frac{\sigma}{E} = Q_1 \frac{x}{y^3}$$

where

$$Q_0 = \frac{E d^4}{\gamma_0 R_0^3}, \qquad Q_1 = \left(\frac{d}{R_0}\right)^2.$$

The theory presented above predicts a maximum in the pull-off stress at lower strain than what is observed experimentally. We believe that this may be due to the distribution of size of the initial detached regions at the interface: a small detached region needs a higher applied stress to start to grow than a larger detached region, and the interfacial cracks will start to grow at different stages during pull-off, leading to a broader peak in the stress as a function of strain, with the maximum centred at higher strain. In figure 53 we show the (calculated) dependence of the maximal pull-off stress in units of the low-frequency elastic modulus, $\sigma_{\max}/E$, as a function of the logarithm (with 10 as basis) of the pull-off speed v_0 for $T = 0$ and 20 °C for the tack compound shown in figure 18. Note that the maximal pull-off stress increases as the temperature is lowered or the pull-off speed increased. This is in good qualitative agreement with the experimental data in figure 54.

Interfacial crack propagation will be the dominant detachment process if the maximum stress is smaller than the relevant elastic modulus E of the adhesive, which we may take as the real part (or the absolute value) of the viscoelastic modulus $E(\omega)$ calculated at the typical separation frequency $\omega \sim v_0/d$. However, if the stress during detachments becomes higher than E, cavitation may occur in the rubber [64]. When cavitation occurs, long rubber filaments typically form during pull-off, resulting in a very large energy to separate the surfaces. This is the ideal case, and rubber adhesives used for practical applications are designed to undergo bulk cavitation and stringing during pull-off.

Figure 54 shows the maximum stress observed during pull-off for four different systems, namely for two types of rubber which we denote as 'hard' (square symbols) and 'soft' (circles), and for two different substrates which we denote as 'inert' (filled symbols) and 'reactive' (open symbols). The hard rubber compound (a compound based on a styrene block copolymer) has a

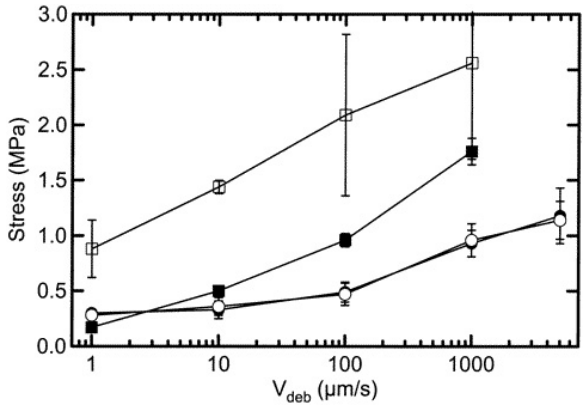

Figure 54. The maximum stress at $T = 20\,^{\circ}\mathrm{C}$ for four adhesion systems. Adapted from [61].

much higher low-frequency elastic modulus than the soft compound (an acrylic adhesive). The reactive substrate is a polished steel surface, while the inert substrate is a surface covered by an inert grafted monolayer film (poly(dimethylsiloxane)). For the soft compound no interfacial crack propagation occurs for either of the two substrates, but the detachment occurs via the nucleation and expansion of cavities in the rubber compound. This explains why the maximum stress as a function of the pull-off stress is identical for these two substrates. For the hard compound on the inert surface, the stress in the rubber film is always below the (low-frequency) elastic modulus, and the detachment occurs by interfacial crack propagation as indicated by the snapshot pictures in figure 51. However, on the reactive surface $\Delta\gamma$ is much higher, resulting in a much larger crack propagation energy, and for this substrate bulk cavity formation occurs before the onset of interfacial crack propagation. This explains why for the hard compound the two $\sigma_{\max}(v_0)$ curves differ greatly.

6.3. Rolling resistance for smooth surfaces

Crack propagation is also involved in rolling of a sphere or a cylinder with smooth surfaces on a smooth substrate. Since the rolling process consist of two bodies continuously adhering at the leading edge of contact (closing crack) and being separated at the trailing edge (opening crack), this means that for viscoelastic materials the surface energy $\gamma_{\mathrm{eff}}(v)$ can be an important contribution to rolling friction; see figure 55.

Let us consider the simplest and most fundamental case, where a hard and perfectly smooth cylinder is rolling on a smooth flat rubber substrate; see figure 56. Let m be the mass of the cylinder, and L its length. Assume that the rubber track is inclined at an angle θ to the horizontal. Thus, the change in the potential energy when the cylinder has rolled a distance x along the track will be $mgx\sin\theta$. Let us assume that this energy has been used to overcome surface adhesion effects (mainly consumed in the propagation of the opening crack at the trailing edge), though it is recognized that a small amount of the energy will be lost through sub-surface hysteresis. The energy necessary to roll the cylinder a distance x is given by

$$(\gamma_{\mathrm{eff}}^{\mathrm{open}} - \gamma_{\mathrm{eff}}^{\mathrm{close}})xL \approx \gamma_{\mathrm{eff}}^{\mathrm{open}} xL \equiv \gamma_{\mathrm{eff}} xL$$

where we have used the fact that usually $\gamma_{\mathrm{eff}}^{\mathrm{open}} \gg \Delta\gamma$ and $\gamma_{\mathrm{eff}}^{\mathrm{close}} \ll \Delta\gamma$. Thus we get

$$mgx\sin\theta \approx \gamma_{\mathrm{eff}} xL$$

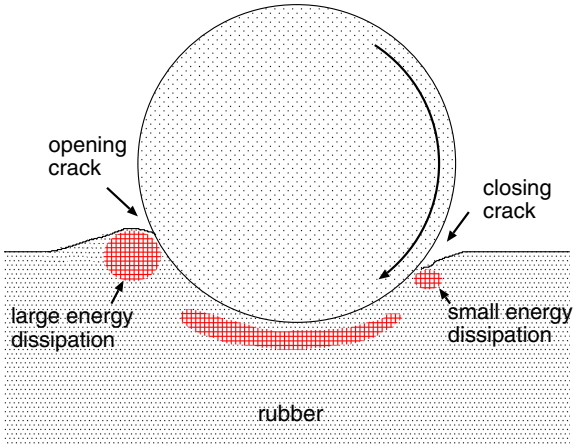

Figure 55. A hard cylinder or ball rolling on a flat rubber track. The region where most of the viscoelastic energy dissipation occurs is indicated by the red dashed areas.

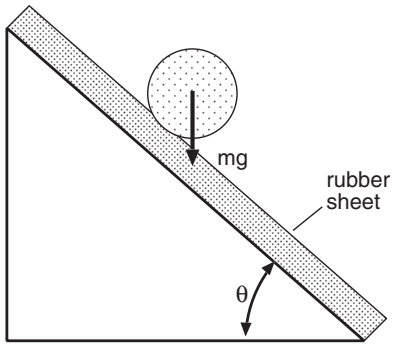

Figure 56. A rigid cylinder rolling down a rubber track. From the tilt angle θ, using (36) one can calculate the effective interfacial energy $\gamma_{\rm eff}$.

or

$$\gamma_{\rm eff} = (mg/L)\sin\theta. \tag{36}$$

Experimental results for glass cylinders rolling down smooth tracks of natural rubber and polychloroprene are shown in figure 57. The figure shows $\gamma_{\rm eff}(v)$ as calculated from (36), and plotted against the observed rolling velocity v of the cylinders. The different symbols correspond to different cylinder masses, which varied between 6 and 102 g. The fact that all the data points lies on the same curve shows that the contribution to the energy dissipation from the viscoelastic deformations of the rubber in the volume below the cylinder (the 'banana'-shaped dashed region below the cylinder in figure 55) is negligible compared to the contribution from the region close to the opening crack at the trailing edge. This important and non-trivial result can be understood as follows:

Following the argument presented in [62, 63], one can show that the bulk contribution to the dissipated energy after the cylinder rolls a distance x is of order

$$\Delta E \approx (r_0^2 L)\sigma_0^2\omega_0 T\,\mathrm{Im}\,\frac{1}{E(\omega_0)}$$

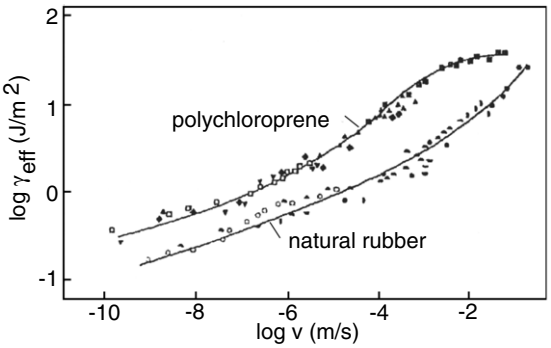

Figure 57. The logarithm (with 10 as basis) of the effective interfacial energy $\gamma_{\rm eff}(v)$ as a function of the logarithm of the crack-tip velocity v deduced from the rolling of glass cylinders down smooth plane rubber tracks. The different symbols correspond to different glass cylinder loads (0, 6, 18, 28 and 102 g) in such a way that (on average) increasing velocity corresponds to increasing load. For natural rubber and polychloroprene rubber tracks. Adapted from [44].

where T is the rolling time and r_0 the width of the contact region along the rolling direction (x-direction). Also, $\omega_0 = v/r_0$, where v is the rolling velocity. Since $vT = x$ we get

$$\Delta E \approx xLr_0\sigma_0^2 \,\mathrm{Im}\,\frac{1}{E(\omega_0)}.$$

Thus the ratio between the energy dissipated during crack opening ($\gamma_{\rm eff} xL$) and the bulk dissipation is

$$\gamma_{\rm eff} : r_0\sigma_0^2 \,\mathrm{Im}\,\frac{1}{E(\omega_0)}.$$

Assuming Hertzian-like contact we have $r_0 \approx R\sigma_0/E_0$, so that

$$\gamma_{\rm eff} : \left(\frac{\sigma_0}{E_0}\right)^3 R \,\mathrm{Im}\, E(\omega_0)$$

where we have used that $\mathrm{Im}\, E^{-1}(\omega_0) \approx (1/E_0)^2 \,\mathrm{Im}\, E(\omega_0)$. Using this formula one can show that for the rolling systems considered in figure 57 the contribution from the opening crack to the rolling resistance is about 10–100 times more important than the bulk contribution.

Consider, for example, the heaviest cylinder used in the experiments. In this case only relatively large rolling velocities were observed (filled squares and circles in figure 57) and $\gamma_{\rm eff} \approx 10\ \mathrm{J\,m^{-2}}$. Using $R = 2$ cm the ratio above

$$500\ \mathrm{Pa} : \left(\frac{\sigma_0}{E_0}\right)^3 \mathrm{Im}\, E(\omega_0).$$

One can estimate that for the heaviest cylinders used in the experiment the nominal pressure $\sigma_0 \approx 0.05$ MPa, and assuming $E_0 \sim 1$ MPa the ratio above is

$$4\ \mathrm{MPa} : \mathrm{Im}\, E(\omega_0).$$

The imaginary part of the viscoelastic modulus was not given by the authors of [44], but for the frequencies involved in the experiment $\mathrm{Im}\, E(\omega_0)$ should not be larger than perhaps 0.1 MPa. Thus, we conclude that the viscoelastic deformation below the cylinder was negligible in the experiments reported on in [44].

Note the increase in $\gamma_{\rm eff}$ by roughly a factor of 100 when the rolling velocity (which is the same as the crack-tip velocity) increases from 10^{-9} to 0.1 m s^{-1}; this strong increase is

due to the viscoelastic energy dissipation in the vicinity of the crack tip. The average slope of the curves in figure 57 is $\alpha \approx 0.25$, which is in accordance with the theory of section 3. Comparison between the results obtained for natural rubber and polychloroprene show that the latter gives higher crack propagation energy $\gamma_{\text{eff}}(v)$ in the studied velocity range. This is the expected result, because the glass transition temperature of polychloroprene (−44 °C) is about 26 °C higher than that of natural rubber. Application of the WLF rate–temperature transform suggests that this temperature difference should correspond to a rate difference of about two decades. The result in figure 57 is broadly consistent with this after having made an allowance of some 2 meV Å^{-2} for the difference in the surface energy between polychloroprene and natural rubber.

Roberts and Thomas also performed rolling friction studies using steel balls. Here we present a brief description of some of these results as they illustrate (qualitatively) the fundamental role of viscoelastic crack propagation in the ball dynamics. Using a surface freshly cleaned with isopropyl alcohol a ball with radius 0.4 cm took ∼50 min to travel the length down a track (25 cm) raised at $\theta = 10°$ above the horizontal. If the track was only raised $\theta = 0.5°$, the time taken was of the order of 10 days. Yet if the same track raised at 0.5° was powdered with French chalk the ball travelled its length in 5 s. Even more surprising, if the cleaned track was held at 90° to the horizontal the ball still took about 1 min to descend its length. During the 90° descent it was possible to turn the track right over, whereupon the ball remained stuck to the track for a while, but now underneath it.

6.4. Sliding friction for smooth surfaces

For certain conditions of sliding between soft rubber spheres and hard tracks, Schallamach [60] has shown that the relative motion between the surfaces is due to 'waves of detachment' crossing the contact zone. Between these waves there is no (detectable) slip between the rubber and the substrate. The waves were observed to move in folds in the rubber surface, their driving force being a tangential stress gradient. All gross displacement is solely associated with these waves, which originate from elastic instabilities due to the tangential compressive stresses in the contact zone. Thus the rubber buckled. Such instabilities have also been predicted theoretically [70].

Smooth flat substrate. Roberts and Thomas [44] have shown that the friction force which is measured when sliding occurs via the propagation of Schallamach waves can be attributed to the energy necessary to propagate the opening cracks associated with the detached regions. Thus, consider a rubber slab pulled at a velocity v_0 over a hard flat track by a tangential force F (figure 58). The Schallamach waves move with the velocity v and their spacing apart is λ. If $\gamma_{\text{eff}}(v)$ is the effective surface energy per unit area required to peel the rubber from the track, and if the energy dissipation in the bulk of the rubber can be neglected, then in steady state sliding, where the elastic energy of the rubber is not varying, the loss of energy is solely associated with peeling. During the time Δt the force does the work $F v_0 \Delta t$, which must equal the energy lost during peeling, which is $(A_0/\lambda)\gamma_{\text{eff}}(v) v \Delta t$, where γ_{eff} is the energy per unit area to propagate an opening crack (as before, we neglect the (negative) contribution from the closing crack as it is in general negligible). Thus we get the frictional shear stress $\sigma = F/A_0$:

$$\sigma = \gamma_{\text{eff}}(v)\frac{v}{v_0\lambda}.$$

Roberts and Thomas have shown that this equation gives frictional shear stresses in good agreement with experimental data. In one case, for a hard slider on a polyisoprene rubber track at the slip velocity $v_0 \approx 0.05$ cm s^{-1}, Schallamach waves was observed, propagating

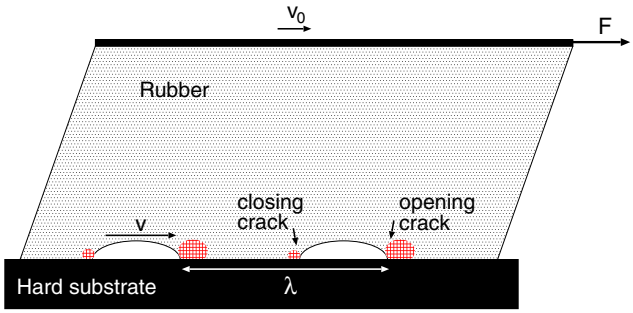

Figure 58. Generation of Schallamach waves at a rubber/hard track interface when one surface is sliding relative to the other. The red dashed areas indicate the spatial regions at the opening and closing crack tips where most of the bulk viscoelastic energy dissipation takes place.

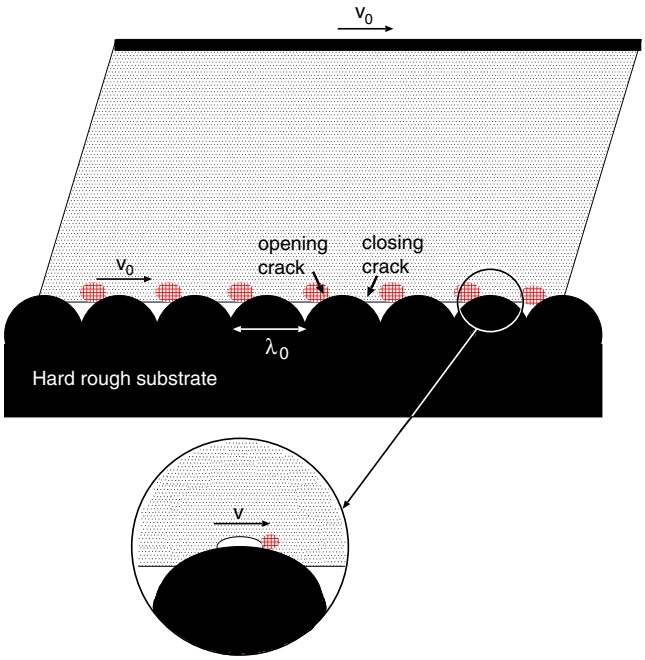

Figure 59. Opening and closing cracks at the interface between a smooth rubber surface and a hard wave substrate, when one surface is sliding relative to the other. The red dashed areas indicate the spatial regions at the opening crack tips where most of the bulk viscoelastic energy dissipation takes place. The inset illustrates that the sliding at the substrate asperity contact regions may occur via the propagation of Schallamach waves.

with the speed $v \approx 1$ cm s^{-1} and the spacing 0.1 cm. In this case $\gamma_{\rm eff}(v) \approx 0.7$ eV Å^{-2}, giving the shear stress $\sigma \approx 0.2$ MPa, in good agreement with the measured value.

Microscopically smooth but macroscopically wavy substrate. Let us now consider a rubber block sliding on a hard wavy substrate; see figure 59. We assume that there is no surface roughness on the substrate except for the waviness with wavelength λ_0. That is, if one of the asperities associated with the waviness is magnified, the surface remains perfectly smooth.

Assume that the rubber makes contact with the substrate asperities, but is not able to completely penetrate into the valleys. Assume that the area of real contact is A and that a frictional stress σ_f acts in the area of real contact during sliding. The origin of this frictional stress may be the propagation of Schallamach waves as indicated in the inset, or it may be due to shearing of a thin contamination layer; however, the exact mechanism behind σ_f is not important for what follows. In this case the frictional work $Fv_0\Delta t$ must equal $[\sigma_f A + (A_0/\lambda_0)\gamma_{\rm eff}(v_0)]v_0\Delta t$ so that

$$\sigma = \sigma_f \frac{A}{A_0} + \frac{\gamma_{\rm eff}(v_0)}{\lambda_0}. \tag{37}$$

This formula is only valid if the spatial size r of the dissipative region at the crack tips is smaller than the wavelength of the substrate waviness, λ_0. At low sliding velocity this will be the case even when $\lambda_0 \sim 1$ μm or less, but at high sliding velocity r may reach 10 μm or more, and then λ_0 must be relatively large in order for the theory to be applicable.

As an illustration, let us consider a styrene–butadiene copolymer rubber block sliding at $v_0 = 0.1$ m s^{-1}. In this case r will be several micrometres so the smallest possible λ_0 will be of the order of $\sim$10 μm. Assume that $\Delta\gamma \sim 10$ meV, which is the largest possible interfacial binding energy associated with a weak rubber–substrate interaction, and that the viscoelastic dissipation enhances the effective interfacial energy by a factor $E_\infty/E_0 \sim 10^3$ so that $\gamma_{\rm eff} \approx 10$ eV Å^{-2}. Thus, using (37) we get the maximal possible contribution from the asperity induced crack-opening to the shear stress $\sigma = \gamma_{\rm eff}/\lambda_0 \approx 10$ MPa. Recently it has been suggested that there will be an important contribution to rubber friction on randomly rough surfaces (e.g., road surfaces) from the mechanism described above [72]. However, it is not clear to us if this is indeed also the case when roughness occurs on many different length scales as in most practical applications. In addition, most practical situations involve contaminated rubber surfaces, which reduces the adhesive interaction. In fact, if a rubber ball is kept in the normal atmosphere it collects dust, which strongly reduces the adhesion to other solids.

6.5. Fatigue of rubber

On many occasions rubber materials are used in applications where they are loaded dynamically. Examples includes tyres, rubber springs and V-belts. An important property in such applications is the resistance to fatigue failure, which means the failure of a material or component when subjected to repeated loads below its short term ultimate strength.

Fatigue failure of rubber can be caused by two different mechanisms. In some cases damping (internal friction) causes a rapid temperature increase. The high temperature could produce deterioration in the material properties or lead to thermal breakdown. The risk of thermal failure increases with increasing frequency, strain amplitude and increasing part thickness.

In other cases failure occurs due to the nucleation and growth of one or several cracks. Usually these cracks are initiated from defects (pores, particle inclusion, impurities, surface defects) and grow initially at a low rate, but subsequently at an increased rate until the component separate into two or more parts or no longer fulfils its purpose. Here we consider this latter type of fatigue failure.

Consider a crack in a rubber block. Assume that an oscillating force act on the block. During a fatigue testing the crack length c is measured as a function of the number of cycles. From these data the crack growth rate per cycle, $\mathrm{d}c/\mathrm{d}N$ (where N is the number of cycles), is calculated. This is done at different amplitudes of the applied force, corresponding to different tearing or crack propagation energies $G_{\rm max}$ (see section 3.9), and the results are plotted in a

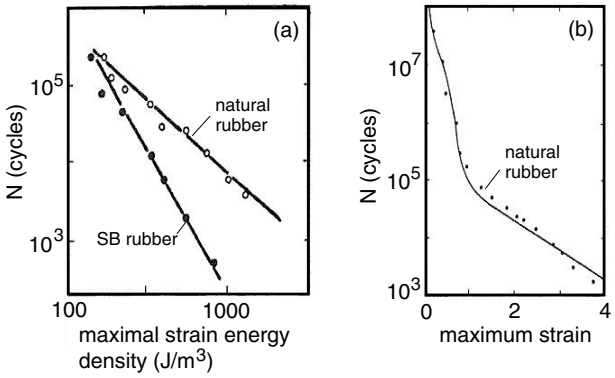

Figure 60. (a) The fatigue lifetime of natural rubber and styrene butadiene rubber. The solid lines are calculated from equation (22) assuming that the initial crack width $c_0 = 25$ and 56 μm for the natural rubber and the SB rubber, respectively. (b) Fatigue lifetime for unfilled natural rubber (minimum strain = 0). The solid line has been calculated from equations (20)–(23) assuming an initial crack size of 25 μm. Adapted from [55].

double-logarithmic diagram with G as a function of $\mathrm{d}c/\mathrm{d}N$. An example for unfilled natural rubber was given in figure 29.

Tearing energy diagrams, such as the one shown in figure 29, can be used to predict or estimate the lifetime of rubber components. We will illustrate this here with two applications involving natural rubber and styrene butadiene rubber.

Equations (20)–(23) can be used to calculate (or estimate) the fatigue lifetime of rubber components. Consider a rubber block and assume that the largest crack has the initial size c_0. If σ is the amplitude of the oscillating stress applied to the block then since $G \approx K^2/E_0$ with $K = \beta\sigma c^{1/2}$, where β is a number of order unity, we get $G \approx \beta^2\sigma^2 c/E_0$. We assume first that G is so large that the asymptotic formula (22) is valid. In the present case (22) gives

$$\frac{\mathrm{d}c}{\mathrm{d}N} = B'c^{\mu} \tag{38}$$

where

$$B' = B\left(\frac{\beta^2\sigma^2}{E_0}\right)^{\mu} \tag{39}$$

where B and μ depend on the material. For natural rubber $\mu \approx 2$ while for styrene butadiene rubber and many other rubbers which do not undergoes strain crystallization $\mu \approx 4$.

Integrating (38) gives the number of cycles at failure

$$N_{\mathrm{f}} = \frac{1}{B'(\mu-1)}\left(c_0^{1-\mu} - c_1^{1-\mu}\right) \approx \frac{c_0^{1-\mu}}{B'(\mu-1)} \tag{40}$$

where we have used that the crack size at failure $c_1 \gg c_0$. Thus, if the fatigue lifetime is plotted as a function of the strain energy density $\sim\sigma^2/E_0$ on a log–log scale, then one expects straight lines with the slope $-\mu$. This is indeed observed for natural rubber and styrene–butadiene rubber at medium to high strains, where (22) holds; see figure 60(a). In this case best agreement with experiment was obtained assuming the initial crack length to be 25 and 56 μm, respectively. In a more general case it may be necessary to use not the asymptotic formula (22) but the complete relation between $\mathrm{d}c/\mathrm{d}N$ and G as given by figure 29 for natural rubber, or approximately by equations (20)–(23). Figure 60(b) shows the comparison of the full theory (solid line) with experimental fatigue data for an unfilled natural rubber.

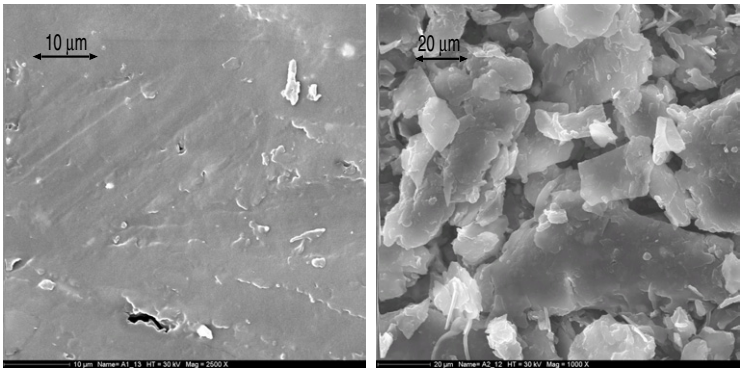

Figure 61. Rubber tread block surface before (left) and after (right) use. Courtesy of Bistac.

6.6. Rubber tyre wear

When a rubber block is sliding on a hard rough substrate, rubber particles will continuously be removed from the block. This wear process involves two different steps, namely (a) nucleation of crack-like defects and (b) propagation of the cracks, resulting in the detachment of rubber particles. The detached rubber particles are often very small, e.g., tyre tread block wear on road surfaces produces micrometre-sized rubber particles. In figure 61 we show the surface morphology of a new (not used) rubber tread block (left), and of a used tread block (right). Note the strong roughness of the used tread block on the length scale of the order of 10 μm. At some places sharp edges occur as expected if rubber particles have been removed by crack propagation, but which would not be expected if the rubber wear resulted entirely from thermal decomposition (pyrolysis) of the rubber surface region. Note also the layer-like structure, indicating that the rubber cracks have propagated along planar interfaces, separating the 'bulk' rubber from a thermally degraded surface layer.

We have shown above that crack propagation in rubber depends sensitively on the the viscoelastic modulus $E(\omega)$. Rubber materials with the viscoelastic peak centred at 'low' frequency will, in general, have a larger crack propagation energy G at low crack-tip velocities, and hence result in lower crack propagation velocities compared to rubber materials where the viscoelastic peak occur at higher frequencies. On the other hand, in most cases the rubber friction, and hence the shear stresses and (flash) temperatures at the rubber–substrate asperity contact regions, will increase if the viscoelastic loss peak is shifted toward lower frequencies. Since the nucleation of cracks is a stress-aided, thermally activated process, it follows that the crack nucleation rate will increase when the viscoelastic peak shifts to lower frequencies. Since rubber wear involves both the nucleation of cracks (process (a)) and the propagation of cracks (process (b)), it is not immediately obvious how the viscoelastic modulus $E(\omega)$ affects the wear rate. In fact, since the relative importance of (a) and (b) will depend on the nature of the substrate, e.g., road surface, and on the (background) temperature, there is no absolute wear strength for rubber materials, but the wear resistance and the rating (with respect to rubber wear) of different rubber materials will depend on the operational conditions. In the context of tyre tread wear this effect is well known: the rating of tyres with respect to tyre wear can change from one road surface to another.

Here we note that butadiene rubber has the viscoelastic peak centred at much higher frequencies than styrene–butadiene copolymer rubber. Thus, the tear strength of styrene–butadiene rubber for low crack-tip propagation velocities should be higher than for butadiene

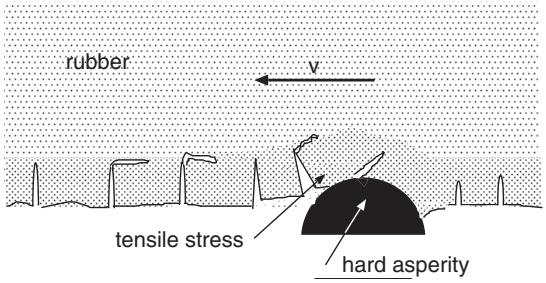

Figure 62. Rubber sliding over a substrate asperity. The tensile stress on the exit side leads to the formation of cracks in a thin layer at the rubber surface.

rubber. However, for the same reason, the rubber–substrate friction is higher for styrene–butadiene rubber, resulting in stronger shear stresses and higher temperatures in the rubber–substrate contact areas, and a higher rate of nucleation of crack-like defects. For tyre tread rubber the latter effect is very important, at least for truck tyres, which have larger tread blocks, resulting in more severe heating problems than for passenger car tyres. Thus truck tyres, where low rolling friction and high wear strength is more important than high tyre–road friction, are usually produced from blends of butadiene rubber and natural rubber, while passenger car tyres usually use mainly styrene–butadiene rubber in order to optimize the road–tyre friction.

6.6.1. General discussion. When a tyre is sliding on a road surface, tensile stress will develop on the exit side of the rubber–asperity contact regions. If the tensile stresses are high enough cracks can form and propagate in a thin layer of rubber; see figure 62. Finally, this may give rise to detachment of small rubber particles. The size of the rubber particles depends on the nature of the surface roughness but is typically of the order of a few micrometres for passenger car tyres on normal road tracks.

When discussing rubber wear one must distinguish between rubber wear on surfaces with very 'sharp' roughness, e.g., silicon carbide paper, and smoother surfaces such as a well used road asphalt surface. On surfaces with smooth surface roughness the wear is so slow that a modified (or degraded) rubber layer can continuously reform on the rubber surface (see below). In this case rubber wear occur by removing rubber particles from the thin modified surface layer. The wear rate is so slow (fatigue failure) that after removal of a rubber particle a modified surface layer can fully reform before a new rubber particle is removed from the same surface area. We believe that this mechanism of rubber wear is relevant to most personal car and truck tyres.

On the other hand, on surfaces with 'sharp' roughness, e.g., abrasive paper, or when a very soft (e.g., racer tyre) rubber compound is used even on surfaces with smoother roughness, the wear rate is so high that there may be no time for a modified rubber layer to be formed. In this case rubber particles are removed from a rubber surface layer with similar physical properties as the bulk rubber. This situation is clearly easier to describe theoretically. Thus Grosch and Schallamach [32, 33] have shown that for rubber sliding on silicon carbide paper the rubber wear rate as a function of the sliding speed and temperature obey the WLF transform, with the same shift factor a_T as determined from the bulk viscoelastic modulus. This shows that the dominant temperature and velocity dependence of the wear process are of viscoelastic origin, and determined by the bulk viscoelastic properties, rather than those of a modified rubber layer. The rubber wear particles have a typical diameter of about $\sim$40 μm, which is about 10 times larger than for tyre tread rubber on a road surface.

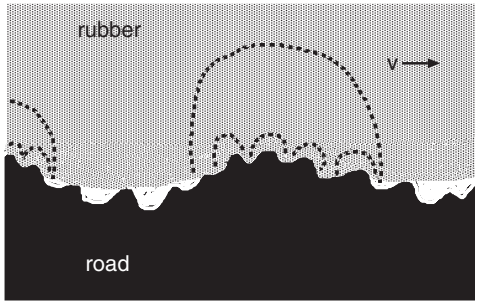

Figure 63. Hysteretic friction of a rubber block on a rough road surface. The road asperities exert pulsating forces on the sliding rubber block, leading to energy dissipation in the rubber via the rubber internal friction. Most of the energy dissipation occurs in the volume elements bounded by the dashed lines. The rubber viscoelastic deformations in the large volume elements are induced by the large road asperities, while the smaller dissipative regions result from the smaller asperities distributed on top of the large asperities. In general, in calculating the rubber friction, the viscoelastic energy dissipation induced by all the asperity sizes must be included, and the local temperature increase (flash temperature) in the rubber resulting from the energy dissipation should also be taken into account in the analysis.

Rubber wear does not only depend on the tear strength (or crack propagation energy), but also on the ability of the rubber to resist thermal and stress induced surface degradation (and degradation resulting from chemical reactions with foreign molecules, e.g., from the atmosphere). That is, the high temperatures (flash temperature) and stresses which occur in the tyre–road asperity contact areas will result in a thin layer of modified rubber at the rubber surface. At least for passenger car tyres, where the wear rate is relatively low, crack propagation and rubber particle removal is likely to occur within this thin (micrometre thick) layer of modified (degraded) rubber. Thus the wear rate is a product of two different processes: stress–temperature induced surface modification (and *nucleation* of crack-like defects), and particle removal by slow (fatigue failure) crack propagation.

6.6.2. Analysis of experimental data. The main contribution to rubber friction when a rubber block is sliding on a rough substrate, such as a tyre on a road surface, is due to the viscoelastic energy dissipation in the surface region of the rubber as a result of the pulsating forces acting on the rubber surface from the substrate asperities; see figure 63. Recently, one of us has developed a theory which accurately describes this energy dissipation process, and which predicts the velocity dependence (and, in a more general case, the time-history dependence) of the rubber friction coefficient [20, 31]. The results depend only on the (complex) viscoelastic modulus $E(\omega)$ of the rubber, and on the substrate surface roughness power spectra $C(q)$. Neglecting the flash temperature effect (the term *flash temperature* refers to a local and sharp temperature rise occurring in the tyre–road asperity contact regions during slip), the kinetic friction coefficient at velocity v is determined by [20]

$$\mu_{\mathrm{k}} = \frac{1}{2}\int_{q_0}^{q_1} \mathrm{d}q\, q^3 C(q) P(q) \int_0^{2\pi} \mathrm{d}\phi\, \cos\phi\, \mathrm{Im}\, \frac{E(qv\cos\phi)}{(1-\nu^2)\sigma},$$

where

$$P(q) = \mathrm{erf}\left(\frac{1}{2\sqrt{G}}\right),$$

with

$$G(q) = \frac{1}{8}\int_{q_0}^{q} \mathrm{d}q\, q^3 C(q) \int_0^{2\pi} \mathrm{d}\phi \left| \frac{E(q v \cos\phi)}{(1-\nu^2)\sigma} \right|^2,$$

where σ is the mean perpendicular pressure (load divided by the nominal contact area), and ν the Poisson ratio, which equals 0.5 for rubber-like materials.

The theory takes into account the substrate roughness in the range $q_0 < q < q_1$, where q_0 is the smallest relevant wavevector of order $2\pi/L$, where (in the case of a tyre) L is the lateral size of a tread block, and where q_1 may have different origins (see below). Since q_0 for a tyre tread block is smaller than the roll-off wavevector of the power spectra of most road surfaces, rubber friction is very insensitive to the exact value of q_0.

The large-wavevector cut-off q_1 may be related to road contamination, or may be an intrinsic property of the tyre rubber. For example, if the road surface is covered by small contamination particles (diameter D) then $q_1 \approx 2\pi/D$. In this case, the physical picture is that when the tyre rubber surface is covered by hard particles of linear size D, the rubber will not be able to penetrate into surface roughness 'cavities' with diameter (or wavelength) smaller than D, and such short-range roughness will therefore not contribute to the rubber friction. For rubber sliding over abrasive paper, the transfer of rubber degradation products to the substrate may result in 'smearing', which again would remove the contribution from short-wavelength roughness and hence act as a large-q cut-off. For perfectly clean road surfaces we believe instead that the cut-off q_1 is related to the tyre rubber properties. Thus, the high local (flash) temperatures during braking, and the high local stresses which occur in the tyre rubber–road asperity contact regions, may result in a thin (typically of the order of a few micrometres) surface layer of rubber with modified properties (a 'dead' layer), which would contribute very little to the observed rubber friction. Since the stresses and temperatures which develop in the asperity contact regions depend somewhat on the type of road (via the surface roughness power spectra $C(q)$), the thickness of this 'dead' layer may vary from one road surface to another, and some run-in time period will be necessary for a new 'dead' layer to form when a car switches from one road surface to another. Such 'run-in' effects are well known experimentally.

In the theory that one of us has developed, the thickness of the dead layer is determined by studying (via computer simulations) the temperatures and stresses which develop on the surfaces of the tyre tread blocks during slip.

We now apply this theory to a rubber block sliding on an asphalt surface and on a grit 180 sand paper. In figure 64 we show for both surfaces the logarithm (with 10 as basis) of the surface roughness power spectra as a function of the logarithm of the wavevector, as obtained from the measured height profiles. Note that the sand paper surface consist of particles with a diameter $D' \approx 0.14$ mm corresponding to the wavevector $q = 2\pi/D' \approx 4 \times 10^4\ \mathrm{m}^{-1}$. As can be seen in the figure, the slope of the power spectra for the sand paper surface indeed changes close to this wavevector. In the calculation of the rubber friction shown in figure 65 we have included surface roughness with wavevectors $q < q_1$, where $q_1 = 2.9 \times 10^5$ and $2.6 \times 10^6\ \mathrm{m}^{-1}$, for the asphalt and silicon carbide paper, respectively. The 'cut-off' wavevectors q_1 was determined as described above by studying the temperatures and stresses which develop in the rubber–substrate asperity contact regions during sliding. The calculations is for a standard rubber tread compound. Note that the friction coefficients shown in figure 65 have similar magnitude as observed experimentally.

In the present case, the thickness of the modified (degraded) layer on the rubber surface for sliding on the asphalt road is of order $1/q_1 \approx 3\ \mu$m. This value is typical for tread rubber sliding on road surfaces. It is also of similar size to the diameter of the rubber wear particles observed in huge amount on road surfaces. This is consistent with our basic picture: tyre rubber wear

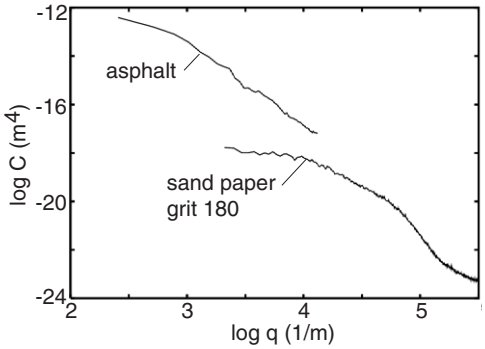

Figure 64. The surface roughness power spectra of an asphalt surface and of a grit 180 sand paper. The asphalt road has the *rms* roughness amplitude $\sigma = 0.26$ mm and the sand paper $\sigma = 0.037$ mm.

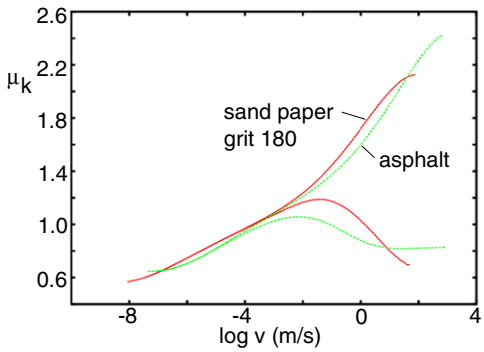

Figure 65. The kinetic friction coefficient for a standard tread rubber sliding on the asphalt and sand paper surfaces defined by the power spectra shown in figure 64. The lower and upper curves shows the friction coefficient with and without the flash temperature effect included in the calculation. For the asphalt $q_1 = 2.9 \times 10^5$ m^{-1}, while for the sand paper surface $q_1 = 2.6 \times 10^6$ m^{-1}.

occurs by the removal (by slow crack propagation–fatigue failure) of rubber particles from a thin modified (degraded) rubber layer on the tread block surfaces. The diameter of the rubber particles are similar to the thickness of the modified layer.

This picture is clearly not valid when rubber is sliding on surfaces with 'sharp' roughness such as abrasive paper. Thus, according to the calculations above the thin modified layer on the rubber block, when sliding on the 180 grit silicon carbide paper, is only $1/q_1 \approx 0.4$ μm, which is roughly $\sim$100 times smaller than the diameter of the rubber wear particles observed in this case. Hence, even if the thin modified layer may be important for the nucleation of the crack-like defects, it is clear that most of the crack propagation will occur in the bulk rubber. The size of the removed rubber particles on the abrasive paper is similar to the size of the silicon carbide particles, which is of the order of $\sim$100 μm.

Let us now present a simple analysis of tyre tread wear. We assume that the wear occurs by removal of rubber particles from a thin modified (degraded) layer of rubber at the tyre tread block surfaces. Let the modified layer have the typical thickness $d \sim 3$ μm and the wear particles the typical volume d^3. The wear results from the stresses the tyre surface is exposed to from the road asperities on the length scale $\lambda \sim 2\pi d \approx 10$ μm. At the magnification corresponding to the wavelength (or resolution) $\lambda = 10$ μm the tyre makes contact with the

road surface only at a few per cent of the nominal tyre–road foot print area, i.e., the contact area is $A \approx 1$ cm^2. Assume that a road asperity must slide N times over a particular surface area d^2 in order for a crack to propagate a distance d and detach a rubber particle. Thus, the number of generated rubber particles when the tyre has slipped the distance L is

$$n = \frac{A}{d^2}\frac{L}{d}\frac{1}{N}.$$

The volume of removed rubber is thus

$$V = nd^3 = AL/N$$

so that the wear volume per unit distance of slip

$$\frac{V}{L} = \frac{A}{N}. \tag{41}$$

Now, tyre wear typically results in the removal of $\sim$1 mm of rubber during 10^4 km of driving. Most of this wear will occur when slip occurs at the tyre–road interface (i.e., during acceleration, retardation and cornering). If we assume that the slip time period is a few per cent of the driving time, we get

$$\frac{V}{L} \approx \frac{0.001\ \text{m} \times 0.1\ \text{m} \times 1\ \text{m}}{10^5\ \text{m}} = 10^{-9}\ \text{m}^2.$$

Since $A \approx 10^{-4}$ m^2 we get $N \approx 10^5$. Note that since typically $d \approx 3\ \mu$m, on average the crack propagates only $d/N \approx 0.3$ Å during one stress cycle, i.e., the crack tip propagates on average by one atomic distance during ten stress cycles. In fact, the crack propagation is even slower in the initial stage, when the crack is much shorter than d, since the stress intensity factor at the crack tip depends on the crack length c as $\sim c^{1/2}$ and will vanish as $c \to 0$. Thus, tyre tread wear is due to fatigue and not due to catastrophic tear processes.

Let us compare this result with abrasion on sharp abrasives. Thus, in the study of Grosch and Schallamach, when a rubber block with 1 cm^2 side area was squeezed by 10 N against silicon carbide 180 paper, the wear $V/L \approx 3 \times 10^{-9}$ m^2. In this case the nominal pressure was 0.1 MPa, but the wear was found to be proportional to the load or nominal contact pressure, as expected because the area of real contact is proportional to the load as long as the nominal contact pressure is small compared to the (low-frequency) rubber elastic modulus. The rubber wear particles had a typical diameter of $D \approx 40\ \mu$m. The wear results from the stresses the tyre surface is exposed to by the substrate asperities on the length scale $\lambda \sim 2\pi D \approx 200\ \mu$m. At the magnification corresponding to the wavelength (or resolution) $\lambda = 200\ \mu$m, and for the nominal pressure 0.1 MPa, the calculation shows that the rubber makes about 3% contact with the substrate. Thus we obtain $A = 3 \times 10^{-6}$ m^2 and from (41) $N \approx 1000$. Thus this case too is likely to involve very slow crack propagation.

Let us analyse the factor N occurring in (41). Let us first assume that the fluctuating stresses are so large that (22) holds. In this case the fatigue lifetime is given by (40). If we assume the tread blocks are made from styrene–butadiene rubber, then (see section 6.5) $B = v_0 T G_0^{-\mu}$ so that

$$N_{\text{f}} = \frac{1}{v_0 T(\mu - 1)} c_a^{\mu} c_0^{1-\mu},$$

where the length parameter

$$c_a = \frac{E_0 G_0}{\beta^2 \sigma^2} \tag{42}$$

where β is a number of order unity, and where σ is the tensile stress at the exit of a rubber–road asperity contact area. The asperity–crack interaction time during one stress cycle is given by

$T \approx d/v_1$, where $v_1 \approx 0.1$ m s^{-1} is a typical slip velocity. As shown in [13], for SB rubber $\mu \approx 4$ so that

$$N_{\rm f} = \frac{1}{\mu - 1}\frac{v_1}{v_0}\frac{c_0}{d}\left(\frac{c_a}{c_0}\right)^{\mu} \approx \frac{1}{3}\frac{v_1}{v_0}\frac{c_0}{d}\left(\frac{c_a}{c_0}\right)^{4}. \tag{43}$$

Equation (43) is only valid when c_0 is larger than c_a (when this condition is not satisfied, we are no longer in the asymptotic region where (22) is valid). The time period where a crack-like defect has a size $c < c_a$ will be denoted by the crack nucleation time period. For tread rubber one typically has $G_0 \approx 60$ J m^{-2} and $E \approx 10$ MPa. The perpendicular pressure in the rubber–road asperity contact regions at the magnification ($\sim$100) relevant for the tyre wear is of the order of 15 MPa (this result follows from the assumption of 0.5 MPa nominal contact pressure and 3% actual contact) so that, assuming a friction coefficient of order unity, the tangential shear stress $\sigma \approx 15$ MPa. Substituting these values in (42) gives $c_a \approx 1$ μm. When the crack-like defect is below this size the standard crack propagation theory cannot be applied. Nevertheless, crack-like defects with size below $\sim$1 μm will grow by stress-aided thermally activated bond breaking processes, and by reaction with molecules from the surrounding media, e.g., ozone.

In a typical case we have $d \approx 10$ μm and for styrene–butadiene rubber at room temperature $v_0 \approx 10^{-9}$ m s^{-1}. Using these parameters, and assuming the initial crack length $c_0 \approx 1$ μm with $c_a \approx 1$ μm, (43) gives $N \approx 10^6$, which is a factor $\sim$10 larger than what is observed. However, it is likely that the high temperatures which occur in the rubber–road asperity contact regions will increase v_0 and hence decrease N.

7. Summary and outlook

In this paper we have considered crack propagation in viscoelastic solids. We have presented a qualitative discussion of how the viscoelastic energy dissipation in front of the crack tip and the bond-breaking processes at the crack tip combine to give the well known expression for the crack propagation energy $G(v, T) = G_0[1 + f(v, T)]$. We have also discussed the influence of the crack-tip flash temperature on crack propagation, and considered the limitations of the theory. Experimental results illustrate how the crack propagation energy depends on the cross-link density, the filler concentration, and the temperature. The theory is valid both for fast (catastrophic) crack propagation, and very slow crack propagation, as is usually involved in fatigue failure.

Several applications involving crack propagation in rubber were presented. We have shown how the rolling resistance and sliding friction between smooth surfaces can sometimes be understood from the dependence of the crack propagation energy on the crack-tip velocity. We have also discussed fatigue of rubber, and rubber wear when rubber is sliding on rough substrates. We have considered tyre tread wear in detail.

There are still many unsolved problems related to cracks in rubber. It is not understood in detail how strain crystallization modifies the $G(v)$-function, and no rigorous theory has been developed for crack propagation in rubber when the external driving force fluctuates in time. The latter is always the case in fatigue, which is not well understood in spite of its extreme practical importance.

Finally, we note that fracture mechanics in general is perhaps the central topic in the design of modern engineering structures. Most catastrophic breakdowns of engineering constructions are due to crack formation and crack propagation. In the construction of, e.g., nuclear reactors or aeroplanes, immense amounts of time and money have been invested in the development of new high-strength and high-toughness (high-fracture-energy, G) materials, and

in designing 'intelligent' structures that avoid stress concentration. Furthermore, during the use of engineering structures, e.g., aeroplanes, bridges or pressure vessels, the formation of cracks is usually monitored at regular intervals. When cracks are formed they are either removed or controlled, depending on their size and the type of application. This is well illustrated by the new A380 Airbus, which is the largest passenger aeroplane ever built. A large fraction of the aeroplane wings and main body is built from fibre (carbon or glass) strengthened (epoxy) polymers, which are relatively light materials with much higher strength and toughness than steel. About ∼400 sensors are distributed throughout the aeroplane body, which can detect the elastic waves emitted from fatigue cracks, and localize the cracks to within an area of radius 10 cm. In this way 'weak spots' in the aeroplane body can be detected early enough to be repaired, similar to the human body, where nerve cells locate the 'defect areas' in the body. In the A380 Airbus, cracks with a size up to ∼3 mm can be accepted in the wings and in the main body of the aeroplane, but no cracks are acceptable in the engines and the landing gears. Ironically, the breakdown of tyres because of catastrophic rubber crack propagation results in much higher loss of capital and life than aeroplane accidents, but there is little awareness of this, probably because such events are much less spectacular than a major aeroplane accident.

Appendix A. Crack stress field and relation between G and K

Here we present for the reader's convenience some simple arguments for two important results from the theory of elastic cracks. The exact derivations can be found in any standard text book on crack propagation, e.g., [22].

Let us consider the elastic displacement field u_y close to a crack tip. Assume that the crack edge is along the z-axis and that the crack opening occurs along the positive x-axis (i.e., the opposite direction as in figure 6). Thus, if the displacement of the upper crack surface is denoted by $u_y(x, 0^+) = u_1(x)$ then by symmetry we must have $u_y(x, 0^-) = -u_1(x)$ for the lower crack surface. In polar coordinates (r, ϕ) the crack-opening boundary condition can also be written as $u_y(r, \phi = 0) = -u_y(r, \phi = 2\pi)$. In the elastic continuum model, the displacement field satisfies a second order differential equation of the Laplace type

$$\nabla^2 u_y = 0. \tag{A.1}$$

The solution to (A.1) depends only on the polar coordinates r and ϕ and it is easy to show that

$$u_y = r^\alpha \cos(\alpha\phi)$$

satisfies (A.1) for any value of α. However, in order to satisfy the condition $u_y(r, \phi = 0) = -u_y(r, \phi = 2\pi)$ we must choose $\alpha = 1/2$. (Any other non-even multiple of $1/2$ would also satisfy the boundary condition. However, negative fractions such as $-1/2$ would result in a displacement field which diverged at the origin $r = 0$ and can be excluded. Positive numbers such as $3/2$ are possible and in fact usually occur in the expansion of the displacement field for small r, but can be neglected for small enough r as they correspond to finite (in fact vanishing) contributions to the stress field at the origin.) Since the stress is proportional to the strain, and since the strain is determined by the spatial derivative of the displacement, e.g., $\epsilon_{yy} = \partial u_y/\partial y$, we get immediately that the singular contribution to the crack stress field will be proportional to $r^{-1/2}$.

The relation (5) between the crack propagation energy G and the stress intensity factor K can be made plausible as follows: the condition for crack propagation is that the elastic energy stored in the solid must be large enough to propagate the crack. The stress in the vicinity of the crack tip $\sigma \sim Kr^{-1/2}$ (this equation defines K). The elastic energy stored in this stress

field will be proportional to $\sim\sigma\epsilon \sim \sigma^2/E \sim K^2/E$, where $\epsilon = \sigma/E$ is the strain. Thus we expect $G \sim K^2/E$.

Appendix B. The $G(v, T)$ function for viscoelastic solids

Here we present some simple rough arguments for how one can obtain the velocity dependence of the crack propagation energy $G(v)$. The full theory is presented in [13]. We also show how the viscoelastic contribution to $G(v)$ can be calculated effectively from the measured viscoelastic modulus $E(\omega)$.

The viscoelastic modulus $E(\omega)$ and the inverse $1/E(\omega)$ are causal linear response functions. For example, causality implies that the strain $\epsilon(t)$ in a solid at time t only depends on the stress $\sigma(t')$ it was exposed to at earlier times $t' \leqslant t$, i.e.,

$$\epsilon(t) = \int_{-\infty}^{t} \mathrm{d}t'\, C(t-t')\sigma(t'). \tag{B.1}$$

Defining the Fourier transform

$$\epsilon(\omega) = \frac{1}{2\pi}\int_{-\infty}^{\infty} \mathrm{d}t\, \epsilon(t)\mathrm{e}^{\mathrm{i}\omega t}$$

we get from (B.1)

$$\epsilon(\omega) = \sigma(\omega)/E(\omega)$$

where

$$\frac{1}{E(\omega)} = \int_0^{\infty} \mathrm{d}t\, C(t)\mathrm{e}^{\mathrm{i}\omega t}.$$

Since $\mathrm{Re}[\mathrm{i}\omega t] < 0$ for $t > 0$ and $\mathrm{Im}\,\omega > 0$ it follows that $1/E(\omega)$ is an analytical function of ω in the upper half of the complex frequency plane. Thus all poles and branch cuts of $1/E(\omega)$ will occur in the lower part of the complex ω-plane and we may write

$$\frac{1}{E(\omega)} = \frac{1}{E_\infty} + \int_0^{\infty} \mathrm{d}\tau\, \frac{H(\tau)}{1-\mathrm{i}\omega\tau} \tag{B.2}$$

where the *spectral density* $H(\tau)$ is real and positive. Using (B.2) one can easily prove the *sum rule*:

$$\frac{1}{E(0)} - \frac{1}{E(\infty)} = \frac{2}{\pi}\int_0^{\infty} \mathrm{d}\omega\, \frac{1}{\omega}\,\mathrm{Im}\,\frac{1}{E(\omega)}. \tag{B.3}$$

In a similar way one can show that

$$E_0 - E_\infty = \frac{2}{\pi}\int_0^{\infty} \mathrm{d}\omega\, \frac{1}{\omega}\,\mathrm{Im}\,E(\omega). \tag{B.4}$$

Using (B.3) and (B.4) we get

$$\frac{E_0}{E_\infty} = 1 - \frac{2}{\pi}E_0\int_0^{\infty} \mathrm{d}\omega\, \frac{1}{\omega}\,\mathrm{Im}\,\frac{1}{E(\omega)} \tag{B.5}$$

$$\frac{E_\infty}{E_0} = 1 - \frac{2}{\pi}\frac{1}{E_0}\int_0^{\infty} \mathrm{d}\omega\, \frac{1}{\omega}\,\mathrm{Im}\,E(\omega). \tag{B.6}$$

Thus the relation

$$\lim_{v\to\infty} G = G_0 E_\infty/E_0$$

can also be written as

$$\lim_{v\to\infty} G = G_0\left[1 - \frac{2}{\pi}E_0\int_0^\infty \mathrm{d}\omega\,\frac{1}{\omega}\,\mathrm{Im}\,\frac{1}{E(\omega)}\right]^{-1} \tag{B.7}$$

$$\lim_{v\to\infty} G = G_0\left[1 - \frac{2}{\pi}\frac{1}{E_0}\int_0^\infty \mathrm{d}\omega\,\frac{1}{\omega}\,\mathrm{Im}\,E(\omega)\right]. \tag{B.8}$$

Now, at a finite crack-tip velocity the highest deformation frequency in the rubber is $\omega = 2\pi v/a$, and we therefore tentatively use the following equations for finite v:

$$G(v) = G_0\left[1 - \frac{2}{\pi}E_0\int_0^{2\pi v/a} \mathrm{d}\omega\,\frac{1}{\omega}\,\mathrm{Im}\,\frac{1}{E(\omega)}\right]^{-1} \tag{B.9}$$

$$G(v) = G_0\left[1 - \frac{2}{\pi}\frac{1}{E_0}\int_0^{2\pi v/a} \mathrm{d}\omega\,\frac{1}{\omega}\,\mathrm{Im}\,E(\omega)\right]. \tag{B.10}$$

Note that $\mathrm{Im}\,E < 0$ so that (B.10) gives $G(v) > G_0$.

Neither of the results (B.9) and (B.10) is fully correct. The exact result is given by [13]

$$G(v) = G_0\left[1 - \frac{2}{\pi}E_0\int_0^{2\pi v/a} \mathrm{d}\omega\,\frac{F(\omega)}{\omega}\,\mathrm{Im}\,\frac{1}{E(\omega)}\right]^{-1} \tag{B.11}$$

where

$$F(\omega) = \left[1 - (\omega a/2\pi v)^2\right]^{1/2}.$$

The crack-tip radius a occurring in the equations above depends on the crack-tip velocity (and the temperature) and can be determined if one assumes that the stress at the crack tip takes some critical value σ_c. This gives [13]

$$a/a_0 = G/G_0, \tag{B.12}$$

where a_0 is the crack-tip radius for a very slowly moving crack. Equations (B.11) and (B.13) are equivalent to the equations given in section 3.2. In figure B.1 we compare the predictions of equations (B.9)–(B.11), using $a/a_0 = G/G_0$ and assuming a Kelvin model for the viscoelastic properties of the rubber. Note that the approximate result given by (B.10) differs rather little from the exact result (equation (B.11)). However, preliminary calculations using a more realistic viscoelastic modulus (measured experimentally) $E(\omega)$ show larger deviation between (B.10) and the exact result based on equation (B.11).

Since for 'high' crack velocities $G(v) \approx G_0E_\infty/E_0 \gg G_0$, the denominator in (B.11) (and (B.9)) must almost vanish, i.e., the integral term in the denominator must be nearly equal to unity (at high velocities it will be of the order of 0.999 if $E_\infty/E_0 \approx 1000$). If (B.11) is used directly this requires that $E(\omega)$ is accurately known for all frequencies which is nearly never the case in practical applications. However, it is possible to rewrite (B.11) in a form convenient for numerical calculations.

For practical calculations, where $E(\omega)$ has been measured experimentally, it is convenient to rewrite equation (B.11) as follows. From (B.5) we get

$$\frac{2}{\pi}E_0 = \left(1 - \frac{E_0}{E_\infty}\right)\left[\int_0^\infty \mathrm{d}\omega\,\frac{1}{\omega}\,\mathrm{Im}\,\frac{1}{E(\omega)}\right]^{-1}.$$

Substituting this in (B.11) and using that $G/G_0 = a/a_0$ gives

$$\frac{a_0}{a} = 1 - \left(1 - \frac{E_0}{E_\infty}\right)\frac{\int_0^{2\pi v/a}\mathrm{d}\omega\,\frac{F(\omega)}{\omega}\,\mathrm{Im}\,\frac{1}{E(\omega)}}{\int_0^\infty \mathrm{d}\omega\,\frac{1}{\omega}\,\mathrm{Im}\,\frac{1}{E(\omega)}}. \tag{B.13}$$

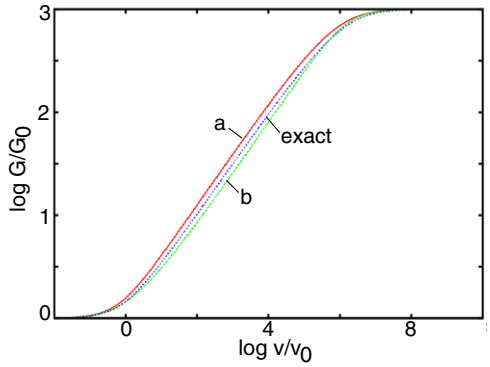

Figure B.1. The crack propagation energy (per unit area) G as a function of the crack-tip velocity for the approximations (B.9) (curve a) and (B.10) (curve b), and for the exact result (B.11).

In practical calculations $E(\omega)$ is not known for all frequencies but only for some finite range $\omega_0 < \omega < \omega_1$. In order to obtain an accurate result, ω_0 should be in the rubbery region so that $E_0 = E(0) \approx E(\omega_0)$ and ω_1 in the glassy region so that $E_\infty = E(\infty) \approx E(\omega_1)$. Thus we approximate $E_0/E_\infty \approx E(\omega_0)/E(\omega_1)$. Since the frequency range from ω_0 to ω_1 usually extends over many decades (typically 10 decades or more) it is not practical to perform the frequency integrals in (B.13) directly, but the integrals can be performed effectively if one substitutes

$$\omega = \omega_0 e^{\xi}.$$

Thus, for example, the integral in the denominator of (B.13) will be over $0 < \xi < \xi_1$, where $\xi_1 = \ln(\omega_1/\omega_0)$:

$$\int_{\omega_0}^{\omega_1} d\omega \frac{1}{\omega} \operatorname{Im} \frac{1}{E(\omega)} = \int_0^{\xi_1} d\xi \operatorname{Im} \frac{1}{E\left(\omega_0 e^{\xi}\right)}.$$

Equation (12) can be written as

$$\frac{a_0}{a} \approx 1 - \left(1 - \frac{E(\omega_0)}{E(\omega_1)}\right) \frac{\int_0^{\xi^*} d\xi \, F(\omega_0 e^{\xi}) \operatorname{Im}\left[1/E(\omega_0 e^{\xi})\right]}{\int_0^{\xi_1} d\xi \operatorname{Im}\left[1/E(\omega_0 e^{\xi})\right]}$$

where

$$F(\omega_0 e^{\xi}) = \left[1 - e^{2(\xi - \xi^*)}\right]^{1/2}$$

and

$$\xi^* = \ln\left(\frac{2\pi v a_T}{a\omega_0}\right)$$

where a_T is the temperature–frequency shift factor (which was not explicitly included in the formulae above).

Appendix C. Thermal degradation: stress-aided thermally activated bond breaking at the crack tip

The viscoelastic properties of rubber are determined by thermally activated processes involving flipping of polymer segments between different positions. The activation barriers separating the different configurations are typically of order ~0.2 eV. These barriers are much smaller

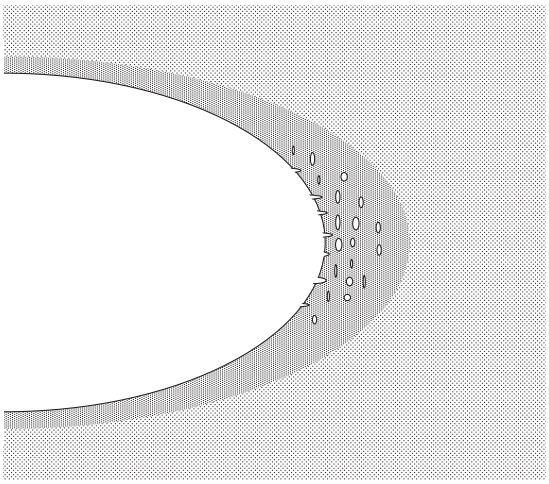

Figure C.1. In the crack-tip process zone crack-like defects occur. The average stress in the crack-tip process zone is of the order of the rupture stress σ_c but the local stress σ_c^* at the tips of crack-like defects may be high enough to break the strong chemical bonds in the hydrocarbon chains.

than the energy barriers involved in breaking the chemical bonds at the crack tip, which are of order $\Delta E \sim 1$ eV or more. Hence at not too high temperatures the main temperature dependence of crack propagation comes from the bulk viscoelastic deformations of the rubber in front of the crack tip. However, even if the temperature is not high enough to generate thermal fluctuations which are large enough to break the bonds at the crack tip, thermal effects are still important for the bond breaking process for slowly moving cracks for the following reason: during crack propagation, at the crack tip the polymer chains are stretched until they break. However, it is not necessary for the applied force to break the bonds alone, but it is enough to stretch the bond somewhat, i.e., to move the system some distance up toward the top of the barrier ΔE; the remaining part of the barrier can be overcome by a (large enough) thermal fluctuation. At high temperature this *stress-aided thermally activated process* will result in a strong reduction in the stress σ_c at the crack tip during (slow) crack propagation.

A simple analysis of the temperature and velocity dependence of the bond-breaking process at the crack tip is based on the following rate equation approach. Consider a polymer chain in front of a crack and assume that the crack tip arrives at the chain at time $t = 0$. The tensile stress acting on the chain at time t ($t < 0$) is *proportional* to (see figure C.1)

$$\sigma(t) \approx \sigma_c \left(\frac{a}{a - vt} \right)^{1/2}, \tag{C.1}$$

where a is the crack-tip radius and v the crack-tip velocity. Thus the chain is stretched already before the crack tip arrives at it, and the chain may break already for $t < 0$. Let $P(t)$ be the probability that the chain is not broken at time t. Thus

$$\frac{dP}{dt} = -w(t)P, \tag{C.2}$$

where the rate coefficient

$$w(t) = \nu e^{-\beta U(t)}, \tag{C.3}$$

where $\beta = 1/k_B T$ and where ν is a prefactor typically of order $\nu \approx 10^{14}$ s^{-1}, and where the barrier height (note $t < 0$)

$$U(t) \approx U_0 \left[1 - \left(\frac{\sigma_c}{\sigma_{c0}} \right)^2 \frac{a}{a - vt} \right],$$

where σ_{c0} is the yield stress at zero temperature, and where $U_0 = \Delta E$. The equations above give

$$\left(\frac{\sigma_c}{\sigma_{c0}} \right)^2 = 1 + \frac{k_B T}{\Delta E} \ln \left[\frac{v}{v_1} \frac{a_0}{a} \left(\frac{\sigma_c}{\sigma_{c0}} \right)^2 \right] \tag{C.4}$$

where

$$v_1 = a_0 \nu k_B T / \Delta E.$$

Equation (C.4) is valid as long as $k_B T/\Delta E \ll 1$. The weakest chemical bonds in rubber are usually multi-sulfur cross-links such as C–S–S–C, for which $\Delta E \approx 1.2$ eV. Single-sulfur cross-links have larger ΔE, and the energy to break a C–C bond in a hydrocarbon chain is much larger, of the order of 4 eV. In a typical case, for a slowly moving crack, $v_1 \approx 100$ m s^{-1}. Thus at room temperature with the crack velocity $v = 1$ μm s^{-1} one finds from (C.4) (with $\Delta E = 1.2$ eV) that $\sigma_c \approx 0.6\sigma_{c0}$.

In [14] we have performed calculations assuming that the rupture stress σ_c depends on the temperature and the crack-tip velocity according to (C.4). Since $\gamma_0 \sim \sigma_c^2$ this implies that

$$\frac{\gamma_0}{\gamma_{00}} = 1 + \frac{k_B T}{\Delta E} \ln \left(\frac{v}{v_1} \frac{a_0}{a} \frac{\gamma_0}{\gamma_{00}} \right) \tag{C.5}$$

where $\gamma_{00} = \gamma_0(v, 0)$.

When the thermally activated bond-breaking is taken into account, the increase of temperature at the crack edge is much smaller than when this effect is neglected [14]. Thus, the maximal temperature increase is in the range 630–840 °C, in good agreement with experimental results [71].

Appendix D. Experimental methods for the determination of $G(v)$

The amount of energy G required to advance a fracture plane by one unit area is a material property which can be measured using different experimental arrangements. The most common methods are illustrated in figure D.1. In most experiments either the loading force F is kept constant, or (part of) the external boundary is clamped and displaced and then kept fixed. In the latter case, as the crack propagates the loading force F will decrease with increasing time.

As an illustration, let us show how $G(v)$ can be obtained from the trouser test (figure D.1(b)) when the loading force F is constant. Let h denote the thickness of the rubber sheet and W the width of the trouser legs. If v denotes the crack-tip velocity, the energy necessary to increase the crack length with Δx is $G(v)h\Delta x$. The energy transfer from the external force to the rubber sheet is $2F\Delta x$. We assume that the elastic energy stored in the bent part of the rubber sheet is constant. However, since the length of the trouser legs has increased by Δx there will be an increase in the elastic energy by the amount $\Delta U_{el} = \Delta x h 2W\sigma^2/2E_0$. Here the tensile stress $\sigma = F/hW$. Thus we get the increase in the elastic energy equal to $\Delta x F^2/(E_0 hW)$. Energy conservation gives

$$2F\Delta x = G(v)h\Delta x + \Delta x F^2/(E_0 hW)$$

or

$$G(v) = 2F/h - F^2/(E_0 h^2 W). \tag{D.1}$$

In many cases it is possible to neglect the last term in this expression.

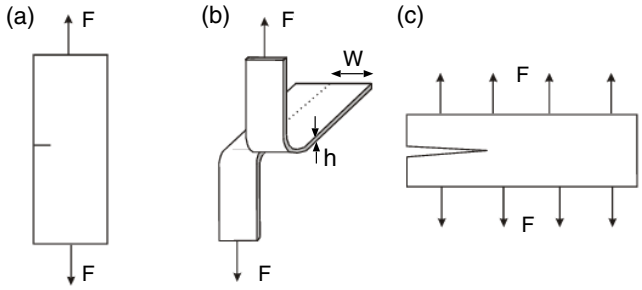

Figure D.1. Three standard methods to measure the crack propagation energy (per unit surface area) G.

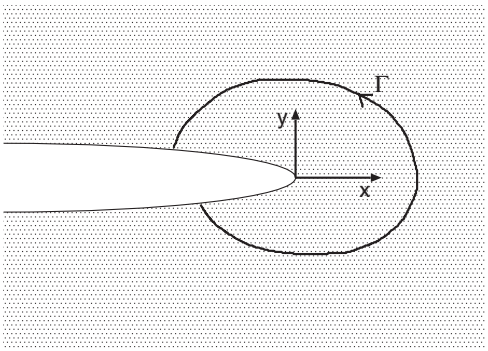

Figure D.2. Arbitrary contour around the tip of a crack.

Sometimes it is necessary to treat the rubber as a nonlinear elastic solid when calculating the change in the elastic energy. Rivlin [73] has proposed a simple model for the non-linear response of rubber. In this theory the force F necessary to maintain simple extension in a test-piece of cross section area (in the undeformed state) A_0 is

$$F = A_0\left(\lambda - \frac{1}{\lambda^2}\right)\left(C_1 + \frac{C_2}{\lambda}\right) \tag{D.2}$$

where C_1 and C_2 are two elastic constants, and where $\lambda = l/l_0$ is the ratio of the length l and l_0 of the stretched and unstretched block, respectively. The elastic energy stored in the block is

$$U_{\rm el} = \int_{l_0}^{l} {\rm d}l\, F = l_0 \int_1^{\lambda} {\rm d}\lambda\, F(\lambda). \tag{D.3}$$

Substituting (D.2) in (D.3) and performing the integral gives

$$U_{\rm el} = \frac{V_0}{2}\left[C_1\left(\lambda^2 + \frac{2}{\lambda} - 3\right) + C_2\left(\frac{1}{\lambda^2} + 2\lambda - 3\right)\right]$$

where $V_0 = A_0 l_0$ is the volume of the block. In our case $V_0 = 2hW\Delta x$ so that energy conservation gives

$$2F\Delta x = G(v)h\Delta x + hW\Delta x\left[C_1\left(\lambda^2 + \frac{2}{\lambda} - 3\right) + C_2\left(\frac{1}{\lambda^2} + 2\lambda - 3\right)\right]$$

or

$$G(v) = 2F/h - W\left[C_1\left(\lambda^2 + \frac{2}{\lambda} - 3\right) + C_2\left(\frac{1}{\lambda^2} + 2\lambda - 3\right)\right]. \tag{D.4}$$

We note that in some cases it may be impossible to measure $G(v)$ in some specific velocity range because of instabilities. One such type of instability was studied in section 3.6. In particular, if $G(v)$ is a decreasing function of the velocity v unstable crack propagation may occur. This is similar to sliding friction problems where instabilities (stick–slip motion) typically occur if the kinetic friction coefficient $\mu_k(v)$ is a decreasing function of the sliding velocity, and if the (relevant) elasticity of the system is small enough.

Appendix E. Nonlinear effects in fracture mechanics

Most materials exhibit linear elastic behaviour at low strain. In most cases the strain far away from a crack tip is small enough for the linear elastic theory to be valid. However, close enough to the crack tip non-linear elastic effects will always be important, even in ideal brittle materials. Usually, this region of space is considered as part of the crack-tip process zone and not studied in detail. However, any theoretical attempt to address the origin of the crack propagation energy $G(v)$ must involve studies of the highly nonlinear processes occurring close to the crack tip. In this context the so called J integral is of great importance. The J integral is defined by a contour integral [74, 75]

$$J = \int_\Gamma \left(U \mathrm{d}y - \sigma_{ij} n_j \frac{\partial u_i}{\partial x} \mathrm{d}s \right), \tag{E.1}$$

where U is the strain energy density, n_i are components of the unit vector normal to Γ, u_i are the displacement vector components, and $\mathrm{d}s$ is a length increment along the contour Γ. The elastic energy density

$$U = \int_0^{\epsilon_{ij}} \mathrm{d}\epsilon_{ij}\, \sigma_{ij}.$$

Rice [74] showed that the value of the J integral is independent of the path of integration around the crack. Furthermore, J is equal to the energy G necessary to propagate the crack per unit surface area. In the context of rubber (or polymer) physics, this quantity is sometimes also denoted as the tear energy T. Thus, $J = G = T$. Examples of experimental J integral estimations for unfilled and filled rubbers can be found in [78].

As an illustration of the use of (E.1), let us study the stress and strain field close to the crack tip in a material that obeys the following non-linear relation between the stress and strain:

$$\sigma + \alpha\sigma^n = E\epsilon, \tag{E.2}$$

where n is the so-called strain hardening exponent. In this case one can show that in order for J to remain path independent the product between the stress and strain must vary as $1/r$ near the crack tip [76, 77]. In particular, the stress $\sigma_{ij} \sim (J/r)^{1/(1+n)}$ and the strain $\epsilon_{ij} \sim (J/r)^{n/(1+n)}$. For a linear elastic material $n = 1$ and both the stress and strain are proportional to $\sim r^{-1/2}$, which is consistent with linear elasticity theory. However, for a strain hardening material, $n > 1$, which will result in a stress which diverges slower than $r^{-1/2}$ at the crack edge, and a strain which diverges faster than $r^{-1/2}$. For very large n the stress is nearly constant while the strain nearly diverges as $1/r$. However, further away from the crack tip the stress may be so small that the non-linear term $\sim\sigma^n$ in (E.2) can be neglected compared to the linear term, and in this region of space the standard $\sim r^{-1/2}$ divergence will be obeyed by both the stress and the strain.

References

[1] Heinrich G, Stuve J and Gerber G 2002 *Polymer* **43** 395
Coveney V A, Pritchard L and Johnson D E 2004 *Tire Technology International Annual Review* vol 122

[2] Creton C and Lakrout H 2000 *J. Polym. Sci.* B **38** 965
[3] Gent A N and Schultz J 1972 *J. Adhes.* **3** 281
[4] Maugis D and Barquins M 1978 *J. Phys. D: Appl. Phys.* **11** 1989
[5] Gent A N 1996 *Langmuir* **12** 4492
[6] Guillement J, Bistac S and Schultz J 2002 *Int. J. Adhes. Adhesives* **22** 1
Guillement J and Bistac S 2001 *Int. J. Adhes. Adhesives* **21** 77
Bistac S 1999 *J. Colloid Interface Sci.* **219** 210
[7] de Gennes P G 1996 *Langmuir* **12** 4497
[8] Schapery R A 1975 *Int. J. Fract.* **11** 141
Schapery R A 1975 *Int. J. Fract.* **11** 369
Schapery R A 1989 *Int. J. Fract.* **39** 163
[9] Greenwood J A and Johnson K L 1981 *Phil. Mag.* A **43** 697
[10] Barber M, Donley J and Langer J S 1989 *Phys. Rev.* A **40** 366
[11] Baney J M and Hui C Y 1999 *J. Appl. Phys.* **86** 4232
Hui C Y, Baney J M and Kramer E J 1998 *Langmuir* **14** 6570
[12] Hui C Y, Jagota A, Bennison S J and Londono J D 2003 *Proc. R. Soc.* A **459** 1489
[13] Persson B N J and Brener E 2005 *Phys. Rev.* E **71** 036123
[14] Carbone G and Persson B N J 2005 *Eur. J. Phys.* E **17** 261
[15] Knauss W G 1974 *Deformation and Fracture of Polymers* ed H H Kausch, J A Haswell and R I Jaffe (New York: Plenum) pp 501–41
[16] Knauss W G 1976 *Mechanics of Fracture* (*AMD* vol 19) ed F Erdogan (New York: ASME) pp 69–103
[17] McCartney L N 1977 *Int. J. Fract.* **13** 641
[18] McCartney L N 1988 *Int. J. Fract.* **37** 279
[19] Williams M L, Landel R F and Ferry J D 1955 *J. Am. Chem. Soc.* **77** 3701
[20] Persson B N J 2001 *J. Chem. Phys.* **115** 3840
[21] Griffith A A 1920 *Phil. Trans.* A **221** 163
[22] Freund L B 1998 *Dynamic Fracture Mechanics* (Cambridge: Cambridge University Press)
[23] Anderson T L 1995 *Fracture Mechanics: Fundamentals and Applications* (Boca Raton, FL: Chemical Rubber Company Press)
[24] Fineberg J and Marder M 1999 *Phys. Rep.* **313** 1
[25] Dion M, Rydberg H, Schroder E, Langreth D C and Lundqvist B I 2004 *Phys. Rev. Lett.* **92** 246401
Dudiy S V, Hartford J and Lundqvist B I 2000 *Phys. Rev. Lett.* **85** 1898
[26] Barenblatt G I 1962 *Adv. Appl. Mech.* **7** 55
[27] Greenwood J A 2004 *J. Phys. D: Appl. Phys.* **37** 2557
[28] Deegan R D, Petersan P J, Marder M and Swinney H L 2002 *Phys. Rev. Lett.* **88** 014304
Petersan P J, Deegan R D, Marder M and Swinney H L 2004 *Phys. Rev. Lett.* **93** 015504
[29] Freund L B 1990 *Dynamical Fracture Mechanics* (Cambridge: Cambridge University Press)
[30] Marder M 2005 *Phys. Rev. Lett.* **94** 048001
[31] Persson B N J and Volokitin A I 2002 *Phys. Rev.* B **65** 134106
[32] Schallamach A 1968 *Rubber Chem. Technol.* **41** 209
[33] Grosch K A and Schallamach A 1968 *Rubber Chem. Technol.* **39** 287
[34] Heinrich G, Rennar N and Dumler H 1996 *KGK Kautschuk Gummi Kunstoffe* **49** 32
[35] See, e.g., table 4–1 in Haney P 2003 *The Racing High-Performance TIRE* co-published by TV MOTERSPORT and SAE (ISBN 0-9646414-2-9)
[36] Ahagon A, Gent A N, Kim H J and Kumagai Y 1976 *Rubber Chem. Technol.* **48** 896
[37] Klüppel M and Heinrich G 1994 *Macromolecules* **27** 3596
[38] Heinrich G, Rennar N and Stähr J 1992 *KGK Kautschuk Gummi Kunstoffe* **45** 442
[39] Herrmann V, Unseld K, Fuchs H-B and Blümich B 2002 *Colloid Polym. Sci.* **280** 758
[40] Grosch K A 1963 *Proc. R. Soc.* A **274** 21
[41] Johnson K L, Kendall K and Roberts A D 1971 *Proc. R. Soc.* A **324** 301
[42] Westergaard H M 1939 *Trans. Am. Soc. Mech. Eng.* **61** A49
[43] Johnson K L 1985 *Contact Mechanics* (Cambridge: Cambridge University Press)
[44] Roberts A D and Thomas A G 1975 *Wear* **33** 45
[45] Carbone G and Mangialardi L 2004 *J. Mech. Phys. Solids* **52** 1267
[46] Southern E and Thomas A G 1972 *J. Appl. Polym. Sci.* **16** 1641
[47] Gdoutos E E, Schubel P M and Daniel I M 2004 *Strain* **40** 119
[48] South J T, Case S W and Reifsnider K L 2002 *Mech. Mater.* **34** 451–8
[49] Tsunoda K, Busfield J J C, Davies C K L and Thomas A G 2000 *J. Mater. Sci.* **35** 5187

[50] See Kawahara S *et al* 2000 *Polymer* **41** 7483
[51] Tosaka M, Murakami S, Poompradub S, Kohiya S, Ikeda Y, Toki S, Sics I and Hsiao B S 2004 *Macromolecules* **37** 3299
Poompradub S, Tosaka M, Kohjiya S, Ikeda Y, Toki S, Sics I and Hsiao B S 2005 *J. Appl. Phys.* **97** 103529
[52] Mitchell J C and Meirer D J 1968 *J. Polym. Sci.* A-2 **6** 1689
[53] See chapter 2 in Gent A (ed) 1992 *Engineering with Rubber, How to Design Rubber Components* (Munich: Carl Hanser Verlag)
[54] Lindley P B 1973 *Int. J. Fract.* **9** 449
[55] Selden R 1995 *Prog. Rubber Plast. Technol.* **11** 56
[56] Becker A, Dorsch V, Kaliske M and Rothert H 1998 *Tire Sci. Technol.* **26** 132
[57] Lindley P B 1974 *Rubber Chem. Technol.* **47** 1253
[58] Mars W V and Fatemi A 2003 *Rubber Chem. Technol.* **76** 391
[59] Fox P G and Soria-Ruiz J 1970 *Proc. R. Soc.* **317** 79
[60] Schallamach A 1971 *Wear* **17** 301
[61] Creton C, Hooker J and Shull K R 2001 *Langmuir* **17** 4948
[62] Persson B N J 2000 *Sliding Friction, Physical Principles and Applications* (Berlin: Springer)
[63] Persson B N J 1998 *Surf. Sci.* **401** 445
[64] Gent A N and Lindley P B 1958 *Proc. R. Soc.* A **249** 195
[65] Gay C and Leibler L 1999 *Phys. Rev. Lett.* **82** 936
[66] Persson B N J, Albohr O, Creton C and Peveri V 2004 *J. Chem. Phys.* **120** 8779
[67] Peressadko A G, Hosoda N, Persson B N J and Albohr O 2005 *Eur. Phys. J.* E submitted
[68] Perutz S, Kramer E J, Baney J and Hui C Y 1997 *Macromolecules* **30** 7964
[69] Fuller K N G and Tabor D 1975 *Proc. R. Soc.* A **345** 327
[70] Persson B N J 2001 *Phys. Rev.* B **63** 104101
[71] Fuller K N G, Fox P G and Field J E 1975 *Proc. R. Soc.* A **341** 537
[72] Le Gal A, Yang X and Klüppel M 2005 *J. Chem. Phys.* **123** 014704
[73] Rivlin R 1948 *Phil. Trans. R. Soc.* A **241** 379
[74] Rice J R 1968 *J. Appl. Mech.* **35** 379
[75] Rice J R 1968 *Fracture: An Advanced Treatise* vol 2 *Mathematical Fundamentals* ed H Liebowitz (New York: Academic) pp 191–311
[76] Rice J R and Rosengren G F 1968 *J. Mech. Phys. Solids* **16** 1
[77] Hutchinson J W 1968 *J. Mech. Phys. Solids* **16** 13
[78] See article by Grellmann W, Heinrich G and Caesar T 2001 *Deformation and Fracture of Polymers* ed W Grellmann and S Seidler (New York: Springer)